Deutsches Zentrum
für Luft- und Raumfahrt
German Aerospace Center

FH AACHEN
UNIVERSITY OF APPLIED SCIENCES

Aachen University of Applied Sciences
Campus Jülich

Faculty 10: Energy Technology
M.Sc. in Energy Systems

Techno-economic Assessment of Hybrid Photovoltaic/Solar Thermal Power Plants: Modeling and Potential for Synergies

Master Thesis by

Ricardo Alexander Chico Caminos

Cologne, Germany
October 2017

This thesis is my own independent work and is the result of my sole efforts.
Only the cited sources and references have been used.

_____

Ricardo A. Chico Caminos, B.Eng.
Cologne, October 20th 2017

This master thesis has been supervised by:

Prof. Dr.-Ing. Ulf Herrmann

Fachhochschule Aachen
University of Applied Sciences
Faculty 10 – Energy Technology

Dipl.-Ing. Dipl.-Wirt.Ing. Simon Dieckmann

Deutsches Zentrum für Luft- und Raumfahrt
(German Aerospace Center)
Institute of Solar Research

Acknowledgements

This master thesis was carried out at the Institute of Solar Research of the German Aerospace Center (DLR) in Köln Porz, Germany. I would like to thank the DLR, for having allowed me to work at one of the top German research institutions.

I would like to express my deepest gratitude to Simon Dieckmann and Dr. Jürgen Dersch for their guidance and support during the course of this thesis, but especially for the trust they put in me to complete this project. All our conversations during the course of this project have helped me widen my knowledge on this subject. I would also like to thank Prof. Dr.-Ing. Ulf Herrmann for the interest shown in this work and for all his guidance during the course of my studies.

My most sincere gratitude goes to all my colleagues at the Institute of Solar Research, for the awesome working environment, especially to my working group and friends that I made over the past six months. Last but not least, my most sincere thanks to my family and friends in Jülich and El Salvador, because this thesis is a product of their constant support and motivation.

Abstract

In this master thesis a hybrid photovoltaic / solar thermal power plant was modeled for a high irradiance location. The selected location was Chile's northern region. For the evaluation the software *greenius* was used, a program being continuously developed at DLR since 1999. This program did not possess a storage function for PV simulations. Therefore one of the aims of this thesis was firstly to analyze the accuracy of the PV model and subsequently develop and implement a battery model to evaluate the financial viability of standalone PV systems. For this reason the *greenius* model was compared with PVWatts and PVSyst photovoltaic models. Additionally, an electric storage element based on a charge balance model was implemented in the system. This model proved to accurately depict the performance of batteries without the need for many parameters. The second aim of this thesis was to optimize and evaluate the financial feasibility of hybrid power plants with a high capacity factor (> 90%). The designed plants were based on the published specifications of Cerro Dominador, Chile for two main reasons. On one hand, this is going to be the first hybrid PV/CSP plant to be commissioned in South America (2019). Therefore it is going to be the benchmark for hybrid solar power plants in the future. On the other hand, Chile's climate is perfect for solar projects. Thus it was important to assess the profitability of a sample plant in this region for future projects to be developed. The calculations were performed with the latest PV benchmark costs of 2017, which have decreased by 21% compared to 2016. The results showed that hybrid solar plants are more cost-efficient for base-load electricity supply than standalone CSP plants in high-irradiance regions. The hybrid CSP+PV plant has 1.7% lower LCOE than the standalone CSP plant (86 vs. 84 €/MWh). However, the main advantage of CSP+PV plants is that they can achieve 3.5% higher capacity factors than CSP at the same LCOE. While the highest annual capacity factor achieved by the hybrid power plant for this location is 98%, the pure CSP plant cannot achieve capacity factors larger than 95%. Photovoltaic power plants with battery storage can be competitive starting 2032, since the results show an LCOE reduction from 158 to 69 €/MWh between 2017 and 2032.

Keywords: Hybrid solar, CSP, PV, Battery model, PV model, Greenius

Table of Contents

Nomenclature

List of symbols

Symbol	Description	Unit
DOD	Depth of Discharge	%
E	Irradiance	W/m^2
I	Current	A
I_{mpp}	Current at maximum power point	A
I_{sc}	Short-circuit current	A
Q	Charge	C
R	Resistance	Ω
SOC	State of charge	%
T	Temperature	K
V	Voltage	V
V_{mpp}	Voltage at maximum power point	V
V_{oc}	Open-circuit voltage	V
γ	Diode quality factor	-
η	Efficiency	%

List of abbreviations and acronyms

Abbreviation	Description
a	year
AC	Alternating current power
a-Si	Amorphous Silicon cells
CAPEX	Capital expenditure
CCS	Carbon Capture and Storage
CdTe	Cadmium-Telluride PV cells
CIEMAT	Centro de Investigaciones Energéticas, Medioambientales y Tecnológicas (Research Centre for Energy, Environment and Technology)
CIS	Copper- Indium-Gallium-Selenide solar cell
CNE	Comisión Nacional de Energía (Chilean national energy commission)
CO_2	Carbon Dioxide
CSP	Concentrated Solar Power
DC	Direct current power
DHI	Direct horizontal irradiance
DLR	Deutsches Zentrum für Luft- und Raumfahrt (German Aerospace Center)
DNI	Direct normal irradiance
GHI	Global horizontal irradiance
GT	Gas turbine
HTF	Heat transfer fluid
IEA	International Energy Agency
IRENA	International Renewable Energy Agency
IRR	Internal rate of return
LCOE	Levelized cost of electricity
Li-ion	Lithium-ion batteries
MENA	Middle East and North Africa region

Mono-Si	Monocrystalline Silicon cells
NOCT	Normal operating cell temperature
OECD	Organization for Economic Cooperation and Development
Poly-Si	Polycrystalline Silicon cells
PPA	Power purchase agreement
PTC	Parabolic trough collector
PV	Photovoltaic
Si	Silicon
SING	Sistema interconectado del norte grande (Chilean northern interconnected grid)
SM	Solar Multiple
STC	Standard test conditions
STE	Solar Thermal Energy
SWEC	Spanish Weather for Energy Calculations
TES	Thermal energy storage
We	Watt-electric
Wp	Watt-peak
Wth	Watt-thermal

List of figures

List of tables

1 Introduction

Climate change, energy efficiency, global warming, radioactive waste are all terms that have resonated globally over the past few decades. There is a trend towards cleaner energy systems. The technologies to achieve a meaningful transition have surpassed the developing phase and many are already commercially available. Therefore, one of our society´s primary challenges of this century is the implementation of those clean energy systems at large scale in order to make this transition happen. Although there are new technologies, such as carbon capture and storage (CCS) currently being developed, which can certainly counter the adverse effects of fossil fuels, there is a need for new renewable energy technologies. It is fundamental to identify which resources can be exploited in a sustainable manner in order to ensure a secure energy generation to cover the different sector demands. The technology must also be cost-competitive with other conventional energy generation systems. For this reason there are many tools that provide guidance on which technology is most suitable for a specified application and location.

The software *greenius* was used and expanded during the course of this thesis. The Institute of Solar Research of the German Aerospace Center (DLR) developed this tool in 1999 and has been upgrading it ever since. With the help of this tool annual yield calculations of renewable energy technologies can be performed, which are of significant importance for project planners, investors, and researchers.

The main focus on this thesis is PV and CSP. Both technologies use the solar radiation to its advantage in a unique way. CSP plants transform the solar energy into thermal energy and therefore one of the main advantages is its cheap thermal energy storage. This makes CSP plants able to generate dispatchable power at times when there is a higher demand. On the other hand, PV transforms solar radiation directly into electrical energy thus avoiding the use of large mechanical equipment. However storing electrical energy is more expensive than thermal energy. Therefore a hybrid PV/solar thermal power plant could represent a cost-efficient option to replace conventional fossil fuel plants to ensure a base-load power generation. By integrating PV modules in a hybrid system, the CSP heliostat field is designed smaller. Since the costs for PV have declined significantly in the last decade, the cost savings in the heliostat field are potentially larger than the costs of the installed PV system.

Moreover, energy storage is a critical issue that must be addressed. Since the solar resource is limited by daytime and clear sky conditions, the generated power must be stored in an efficient way. Batteries have not been exploited in utilities-scale due to their elevated costs. A decrease in costs is making now companies and utilities start using batteries as energy storage for peak and hourly demand respond, as well as voltage and frequency control. Therefore the challenge is combining the synergies between these different types of technologies to ensure a reliable energy transition.

A description of how solar technologies work is presented in chapter 2. The main components and configurations are shown for standalone and hybrid systems, as well as the economic boundaries and current studies on their performance. In chapter 3 different photovoltaic models are discussed and compared. In chapter 4, a battery model is developed to be integrated in *greenius*. Since the program only had the option to feed in the solar energy produced by the PV panel in the grid, it was needed to include a battery model to correctly analyze the benefits and drawbacks of storing energy in either thermal or electrical form. Finally, in chapter 5 the parametrization of an optimized hybrid power plant

is made based on a reference plant in Chile: Cerro Dominador, a 110 MWe CSP and 100 MWp PV plant. The financial feasibility of the hybrid power plant is compared to the standalone CSP and PV configurations. Special attention was also paid to the battery cost evolution for the following years and the economic viability of PV plants with electrical storage compared to CSP.

2 State of the Art

Solar energy is commonly associated with photovoltaic power generation; however, the sun irradiance also delivers its energy in the form of heat. Researchers have been able to observe this effect and use the solar heat since decades warming up either water or different passive environments, such as greenhouses. Concentrated solar power plants use the heat to produce power. The power sector is thus a market for both PV and CSP technologies.

2.1 Global energy market

In the past 10 years there has been an expeditious increase in CO_2 levels. Coal combustion was responsible for 46% of the global CO_2 emissions and 31% alone was from coal-fired power plants, according to data of 2013 [1]. The concentration of carbon dioxide in our atmosphere has surpassed 400 ppm [2]. The effects of increasing CO_2 levels have a global reach and many countries are already taking actions on this matter. In Europe efforts have been made towards a cleaner environment. These are listed under the European Union's (EU) "20-20-20" targets [3], which are namely:

- Reducing the greenhouse gas emissions by at least 20% by 2020 compared to 1990 levels.
- Increasing the renewable energy share in the total energy consumption to 20% by 2020.
- Improving the energy efficiency by 20% by 2020.

However, Europe alone cannot solve a global issue; especially when OECD countries do not have as big of an impact as non-OECD nations. According to the U.S. EIA's International Energy Outlook 2016 [4] it was projected that the energy demand in developing countries would strongly increase by 71% between 2012 and 2040. Therefore it is really important to ensure a low-emission energy supply for these countries. Interestingly, a majority of developing countries have an abundant potential for renewable energies. It can be observed in Fig. 1 that especially the Middle East and North Africa (MENA) region, Central and South Africa, as well as Central and South America have the biggest share of all renewable energy sources [2].

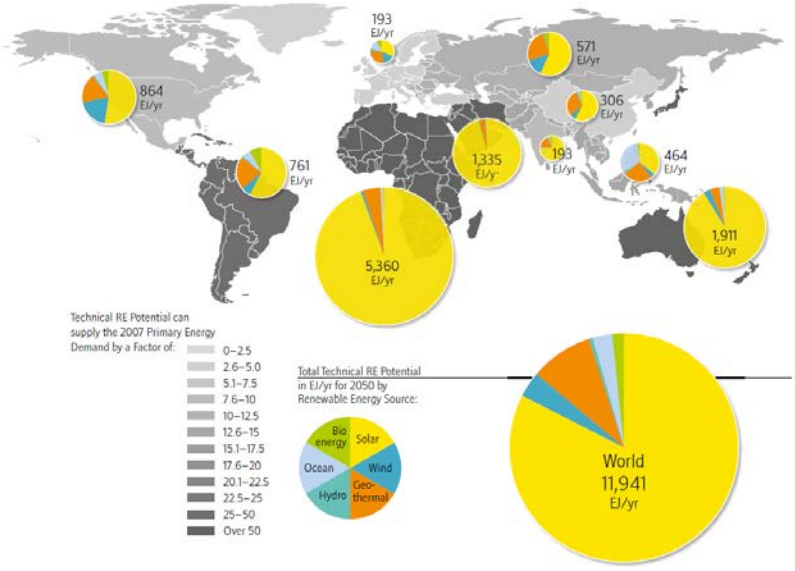

Figure 1: Solar energy potential in 2050 [2]

Renewable energy generation is increasing globally at a rate of 2.9%/a and is the fastest growing source of electric power generation. India and China have adopted also several targets regarding solar energy generation that support this growth [4]. The installed solar PV global capacity by the end of 2015 reached 227 GWe and is increasing exponentially [5]. Costs are no longer an issue, since many countries around the world have already reached grid parity [5]. Meanwhile, CSP is also a growing market, especially in countries like Morocco, Chile and South Africa. Remarkably, CSP is reaching also other industries, such as the oil and gas sector, with a 1 GWth solar plant being constructed in Oman [5].

2.2 Concentrated solar power

Solar thermal energy is not only used in small collectors for heating water or solar stoves. It can be used also to supply electricity and heat demand at high temperatures. Concentrated solar power plants are high temperature systems.

2.2.1 Types of CSP plants

CSP technology for commercial applications can be present in four different configurations:

- Parabolic trough plants
- Linear Fresnel plants
- Central Receiver or solar tower
- Parabolic dish

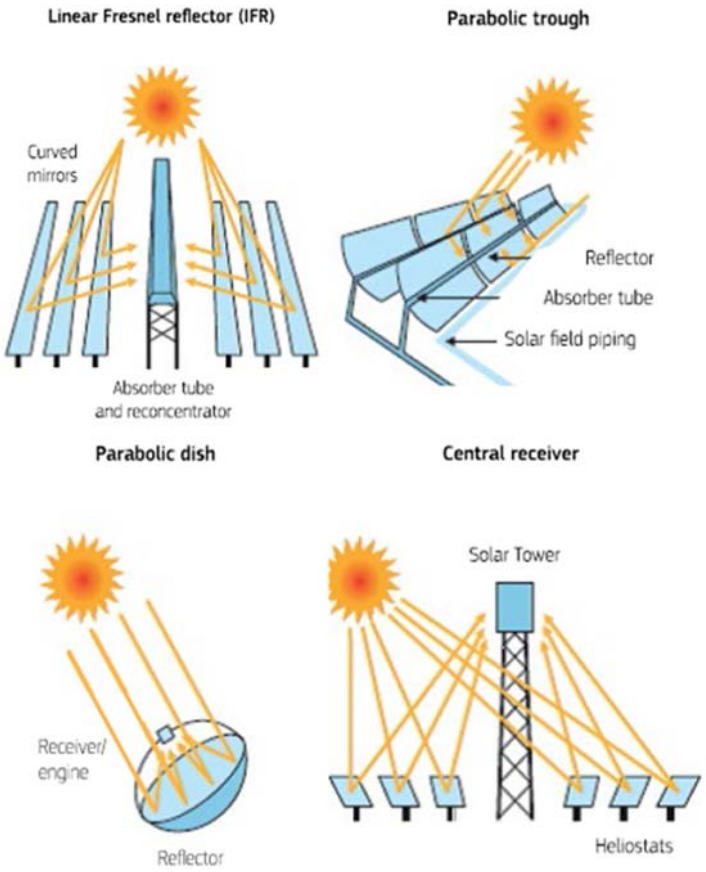

Figure 2: Line and point focus CSP technology types. Modified from [6]

Parabolic trough collectors and linear Fresnel plants can be classified in a single group: Line focus systems. The reason for this is that the concentration occurs in one axis only. The incoming irradiance is focused onto a tubular absorber where the heat transfer fluid (HTF) flows. The HTF is continuously pumped through a set of heat exchangers, where the evaporator and superheater are located. Steam is produced this way and transported to a steam turbine, where electricity can be generated [7]. This whole process resembles a traditional coal-fired plant process. It is indeed, an application of the Rankine cycle; however the supplied energy is the sun irradiation and not a fossil fuel.
Parabolic trough plants consist of several arrays of parabolic-shaped curved mirrors that serve this focusing purpose. Fresnel plants operate in a similar way, but the mirrors are flat and aligned in such a way that they reflect the incoming radiation on a single receiver tube above the reflectors. Central receiver plants and parabolic dishes are also grouped in so-called point focus systems. A central receiver plant, also called solar tower plant, has a large field of mirrors, which are called heliostats. The heliostats are controlled in two-axis so that they reflect the sunlight into a single point, hence the name central receiver. The receiver sits on top of a high-standing structure [7] [5]. Parabolic dishes, on the other hand, concentrate the irradiation via a single parabolic dish to a focal point. Commonly, each of the dishes has a Stirling engine at this point, so that power can be generated at each individual dish [5]. This technology however, is not yet commercially viable.

Parabolic trough plants

This type of plant is considered a medium temperature technology, with working fluid temperatures of up to 400°C. The parabolic-shaped collector arrays are ordered in a north-south configuration and possess a 1-axis tracking unit [8]. The HTF is predominantly a eutectic mixture of 73.5% diphenyl oxide and 26.5% biphenyl, with operating temperatures between 290 °C and 390 °C [9]. The typical storage is based on a 2-tank system with the storage medium being a eutectic mixture of KNO_3 and $NaNO_3$. This storage medium has proven to be a more cost-effective solution than thermal oil and its operation temperature can reach up to 550 °C in contrast to the 400 °C thermal oil limit [9]. For this reason salt is competing with thermal oil in order to be used as the HTF; however the obstacle is that this mixture freezes at 238 °C [9]. Therefore it must be ensured that the temperatures do not fall below this limit as severe damages in the tanks and pipelines might occur. There are other types of systems, for example direct-steam generation plants, where water/-steam is used as HTF. Fig.3 shows a parabolic trough plant with thermal oil as HTF and two-tank storage with molten salt.

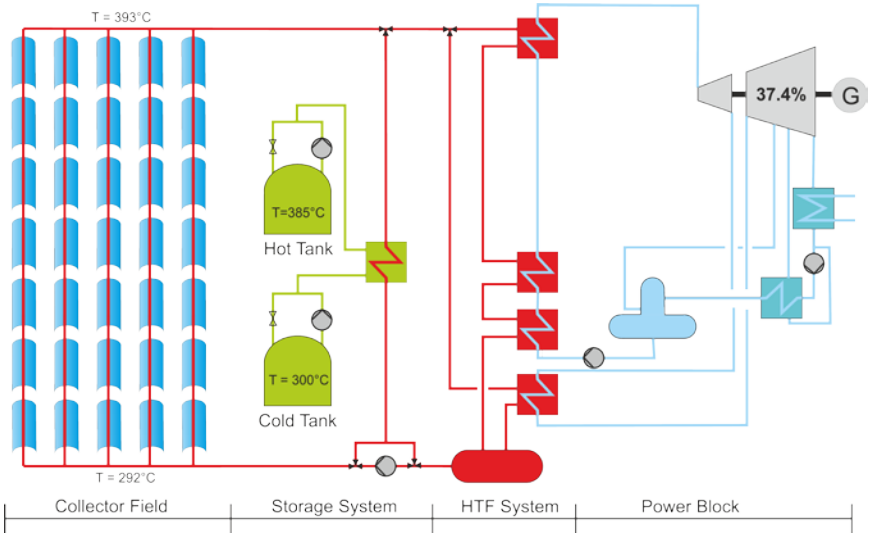

Figure 3: Example of parabolic trough plant with two-tank molten salt storage

Central receiver plants

Central receiver plants are a high temperature technology with temperatures that can reach up to 1000 °C on the receiver side. As explained before the radiation is focused into the receiver by means of heliostats. The concentration factor achievable by this technology is around 1000, meaning a 10x higher concentration factor than in line focus systems [9]. There is a wide range of technologies available or being researched. There are some plants around the world with a molten-salt receiver type, like Gemasolar in Spain or Crescent Dunes in Nevada, US. The advantage hereof is the direct storage possibility [10]. Particle receivers represent a technology which might be implemented in the future due to their ability to handle temperatures higher than 1000 °C, which is a great advantage over molten salts, as well as absence of any freezing issues [10]. Another technology is the high-temperature gas-based receivers. These include the volumetric air receivers, where the concentrating beams are focused onto a porous structure, where air is sucked in and transferred to a heat exchanger where it can heat up a water-steam fluid in a Rankine cycle or be used directly in a gas turbine [10]. When the air is used in an open-loop it is called an open volumetric receiver. On the other hand, when gas turbine cycles are preferred, pressurized closed-loop receivers are used [10]. Passive solid material storage is a possible way to store thermal energy from the hot air flowing from the receiver. Fig. 4 shows an example of a solar tower plant with molten-salt receiver and direct two-tank storage.

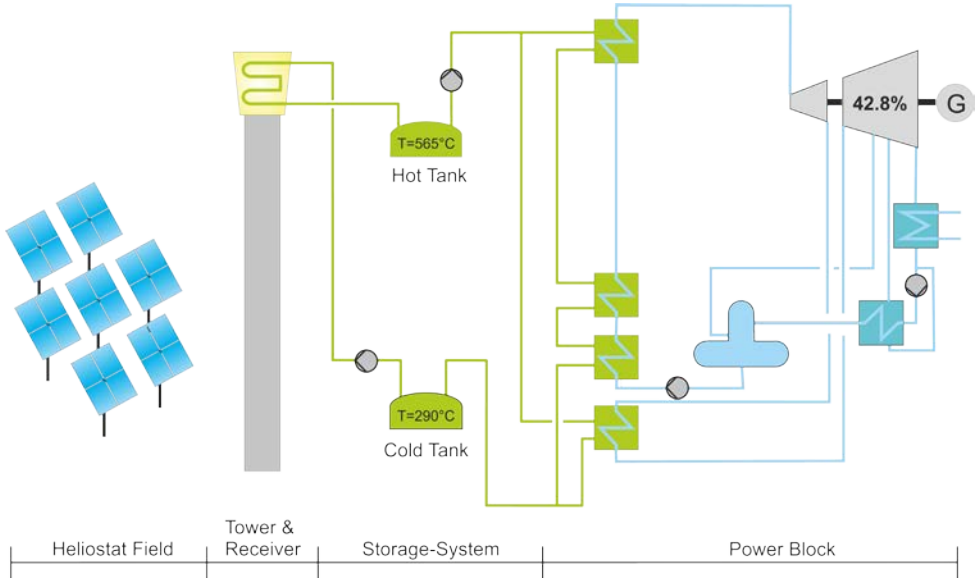

Figure 4: Example of a central receiver power plant with direct two-tank storage

2.2.2 Economic framework

Spain and the United States are both the countries that have the highest number of CSP installed capacity in the world, with the US being pioneers in erecting the Solar Energy Generating Systems (SEGS) between 1985 and 1990 [5]. Starting in 2007 there has been a rapid growth in this market, especially for parabolic trough plants. They account for the 85% of the total capacity worldwide, however a high amount of central receiver plants are being planned or constructed at the moment. CSP plants with integrated thermal storage offer lower levelized costs of electricity (LCOE) than without it. Between 2012 and 2014 the LCOE sank from >300 $/MWh into the 200 $/MWh region [5], with projects in 2017 acquiring PPA of less than 100 $/MWh, such as in Dubai or Chile. According to a

study from the international renewable energy agency (IRENA) the weighted average costs for CSP in 2015 was between 150 and 190 $/MWh. The LCOE could be between 80 and 120 $/MWh in 2025 [11].

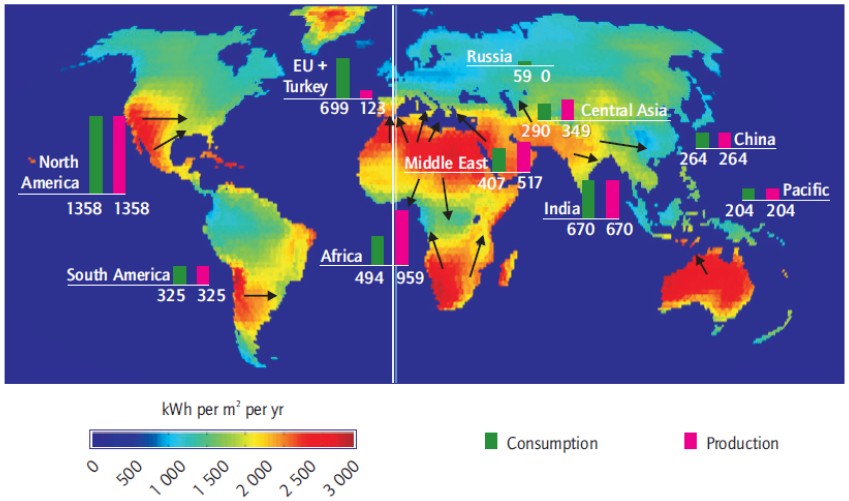

Figure 5: 2050 IEA CSP scenario. Arrows indicate CSP electricity transport. Consumption and Production in TWh [12]

The global installed capacity in 2015 was 5 GWe [5] [11]. In the Blue map scenario from the IEA it is projected that CSP could supply 11.3% of the global electricity demand by 2050, i.e. 1000 GWe [12], given that this technology receives the appropriate political support. This market is receiving at the moment investments of more than $2 billion. Under this scenario the investment would almost reach the $100 billion mark in 2050 [5].

2.3 Photovoltaic energy

Photovoltaic energy systems are present in different sizes thanks to their modular nature. PV cells are able to convert solar radiation directly into electrical energy for small applications in pocket-size devices up until large scale utilities without any moving parts. Regarding the solar resource the main difference between CSP and PV is that photovoltaic panels make use of the whole solar irradiance, i.e. the direct irradiance beams (DNI) and the diffuse irradiance, which is the irradiance scattered through the atmosphere possessing no unique direction. The reflected irradiance from the ground is also used by the PV panels. This means that photovoltaic panels are also able to produce energy during cloudy days, in contrast to CSP plants, which can only collect and make use of the direct irradiance.

2.3.1 Basics of photovoltaics

The simplest unit of a photovoltaic power plant is the photovoltaic cell, also called solar cell. A PV cell works based on the photoelectric principle. The energy provided by a photon can cause a material's electron to jump from one energy band (valence band) to a higher energy one, i.e. the conduction band. This effect occurs in semiconductors, since the energy gap between the two bands is small enough, so that when an external energy is supplied (photon energy) the electrons can move from one band to the other [7]. If a load is connected and a circuit is made the electrons can move, thus creating an electric current. There are different types of cells, the most important at the moment are:

- Monocrystalline (Single-crystalline) Silicon
- Polycrystalline (Multi-crystalline) Silicon
- Thin film PV cells

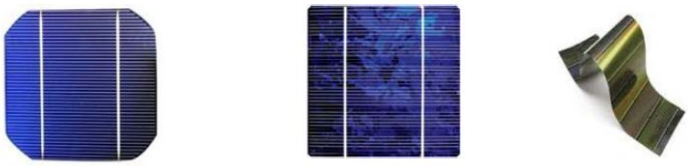

Figure 6: Types of solar cells: From left to right: Mono-Si, Poly-Si, thin film cell (Amorphous Silicon). Modified from [5]

Monocrystalline Silicon (Mono-Si) cells have the highest efficiency of the three of them with 21%, whereas polycrystalline (Poli-Si) have efficiencies of around 17% [13]. Thin-film cells describe cells of different elements, such as amorphous Silicon, Copper-indium/gallium (CIGS) or Cadmium-telluride (CdTe). These cells have 10%, 14% and 12% average efficiency accordingly [13]. Cells can be mounted into a unit called module or panel, which can be then interconnected in parallel or series to reach the desired voltage and power output. Photovoltaic module manufacturers provide information about the efficiency of their systems. This efficiency is tested under a standard set of surrounding conditions. These conditions are achieved in testing facilities, where all the single cells and modules can be uniformly tested. These are the Standard Test Conditions (STC). The STC are defined as [14]:

- Irradiance: 1000 W/m^2
- Spectrum: 1.5 Air Mass (AM)
- Cell temperature: 25 °C

In operational conditions however, the efficiency is not as high as in STC. Irradiance, spectrum and cell temperature are all dependent on the location, meteorological conditions and the state of the module itself (cleanliness, plane tilt, etc.).

2.3.2 Photovoltaic plants

A typical configuration of a PV plant consists of many arrays of PV panels fixed to a mounting rack or in few cases built with a 1- or 2-axis tracking system. These are connected together to an inverter, which transforms the DC power into AC in order to feed it into the grid. The DC line losses should ideally be kept at a maximum of 1%, for a correctly sized system it should not surpass 3% [15] [16].

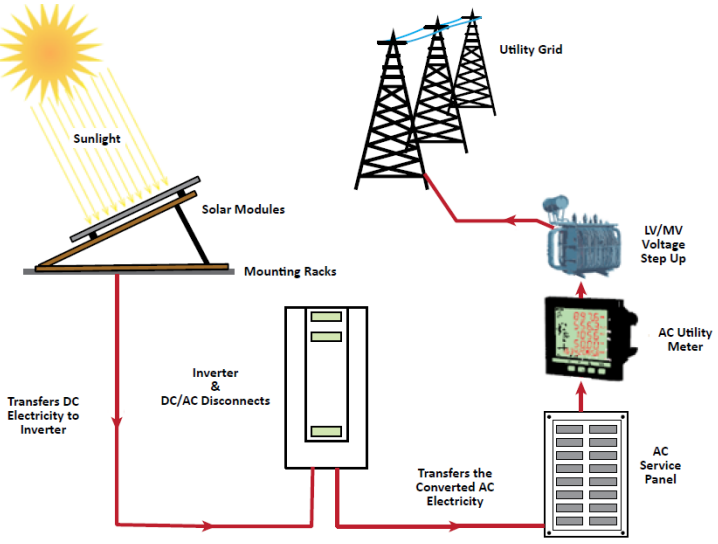

Figure 7: Grid-connected battery system without storage [16]

The AC lines are typically smaller than DC and even more for central inverter system. The AC current is then measured in a utility meter and transformed up to a higher voltage to reach the grid's voltage level. This normally occurs at a distribution level higher than 11 kV [16].

The individual PV modules are connected in series to form a string. A PV array consists of several strings connected in parallel to a central inverter. This is the most typical configuration for medium- and large-scale PV power plants, due to its simple installation and high reliability [16]. However, there is the possibility to use a string inverter configuration. In this case an inverter is connected after every string, hence being able to track the maximum power point (MPP) individually for each string and reduce the overall mismatch and shading loss effects, but at a higher cost. The MPP is the optimal operation point, where it generates the maximum possible power at all irradiance and temperature conditions. The string inverter configuration might prove to be more effective in rather small applications in areas where shading from nearby buildings are a problem, modules have a different orientation or simply modules with different specifications are used [16]. The inverter does not always have the same nominal rating as the PV module rating. The power ratio is defined as the ratio between the inverter DC rated power and PV peak power [16]. According to [16] the Power Ratio is dependent on each plant design specifications and reactive power regulations. It varies between 0.8 and 1.2. Most commonly however, inverters are efficiently designed with a power ratio less than 1.0 [16]. In such case the inverter clips power spikes that are near the panel's peak power. This does not have a significant impact on the total efficiency, since these peak power moments (near STC) are rare [17]. Normally, inverters work at a voltage of 300 V to 450 V. Thus the voltage at the panel side is normally below 1 kV, as Fig. 8 shows.

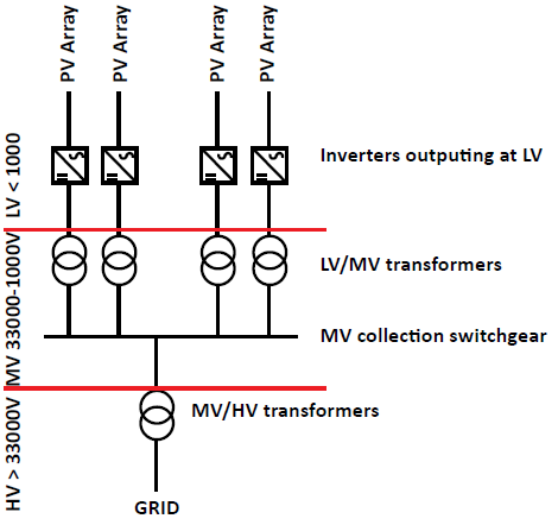

Figure 8: Voltage level of a typical PV grid-connected plant [16]

The aforementioned configuration is a common arrangement for grid-connected utility-size PV systems without storage. The use of batteries has been commonly attributed to residential PV. Nonetheless, as battery costs sink the application of batteries for PV power plants is becoming more feasible. The layout for a PV system including a battery bank is shown in Fig. 9. In this case a charge controller is used, which limits the battery current intake and output to protect the battery and to regulate the power being fed in the grid.

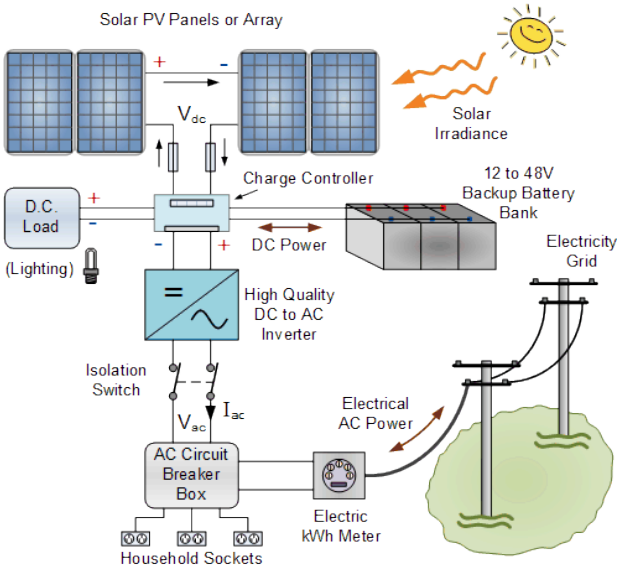

Figure 9: Grid-connected residential PV system with battery. [18]

Battery-coupled DC configuration:

For many applications, the battery is used on the DC side of the arrangement. This requires less DC-AC transformers. There are two modes of operation presented by Sauer [19], MPP-Tracker operation and direct coupling between PV generator and battery.

The main function of an MPP tracker is to maintain the PV module at its maximum power point at all operation conditions. The MPP tracker is a high frequency DC-DC converter [20], which converts the DC output from the PV panel to a desired DC voltage and current. The voltage at the input side of the DC-DC converter is kept at the maximum power point. Meanwhile, the voltage at the output side is set congruently with the battery operational voltage. The charge controller can include this MPP tracking function. Parra et al [21] used this mode of operation in their own study. It is also described in Weniger et al [22], where it is used for a DC-coupled residential PV battery system.

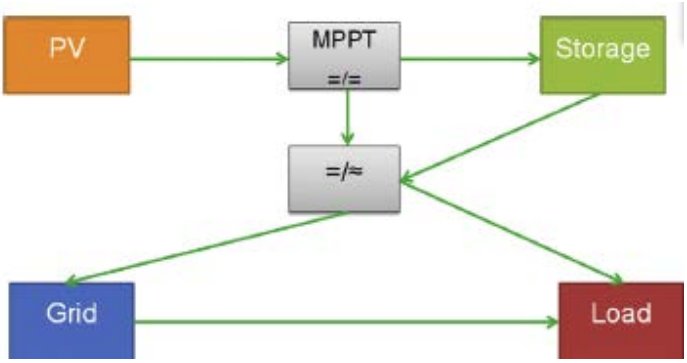

Figure 10: DC- coupled PV-battery system with MPP tracker [22]

The main disadvantage of the MPP tracker is the transformation loss that occurs in the DC-DC converter. In some few cases it is more beneficial to operate the system with the battery directly dictating the voltage at the PV module output [19]. Although the system does not generate the maximum power it is compensated by not having the additional losses from the MPP tracker.

Battery-coupled AC configuration:
The battery can also be installed on the AC side of the PV system arrangement, as in Fig. 11:

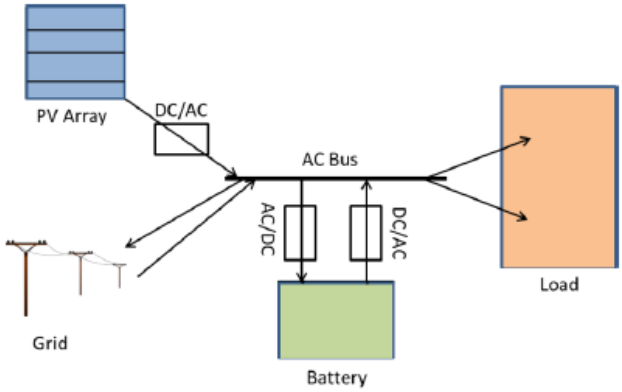

Figure 11: AC-coupled PV-battery system [23]

The efficiency of DC and AC configurations depends strongly on the size, charging strategies and grid boundary conditions, as indicated by Weniger et al [24]. AC configurations are especially suitable for retrofitting existing PV systems [25].

2.3.3 Economic framework

Photovoltaic energy covered in 2015 1% of the total worldwide electricity demand. The total installed power was 227 GWe [5]. The largest PV markets globally are Germany, Italy, Japan, Spain and France [4]. China and the Unites States are also playing an important role in the development of PV. According to the rather optimistic solar photovoltaic roadmap scenario from IEA it is expected that by 2050 the installed capacity could reach 3000 GWe, making 11% of the total global demand [13]. The prices for PV modules have declined steeply in the last decade, falling by 79% between 2007 and 2014 [5]. The most recent study from IRENA states that the average LCOE in 2015 was 130 $/MWh and in 2025 it will be 60 $/MWh [11]. Starting this decade, another study projected the average LCOE to sink from $ 105/MWh in 2020 to $ 45/MWh in 2050 [13]. The market is however currently highly competitive and in some regions this mark was already surpassed, reaching the record-breaking price of 27 $/MWh for a project in Mexico [26].

2.4 Energy storage

There are two main reasons why energy storage is such an important issue nowadays. The first aspect is that energy production has to meet the demand. Energy demand is variable and the energy infrastructure must be able to deliver electricity according to the flexible demand at all times [27]. On the other hand, renewable energy sources are dependent on meteorological conditions, which can be extremely variable too. The second reason is that energy is sometimes produced in places far away from where it is consumed, e.g. off-shore wind parks or solar plants in sunny regions, where it is necessary to transport the electricity generated to other regions [27]. In the case that new transmission networks cannot be built, hydrogen storage could represent a suitable solution. For the expansion of renewable energies it is therefore required that electricity is stored in an efficient and reliable way.

2.4.1 Types of energy storage

Energy storage can be classified under two different criteria, i.e. according to the form of energy used and to the duration of use [27]. These are shown in Fig.12 and 13.

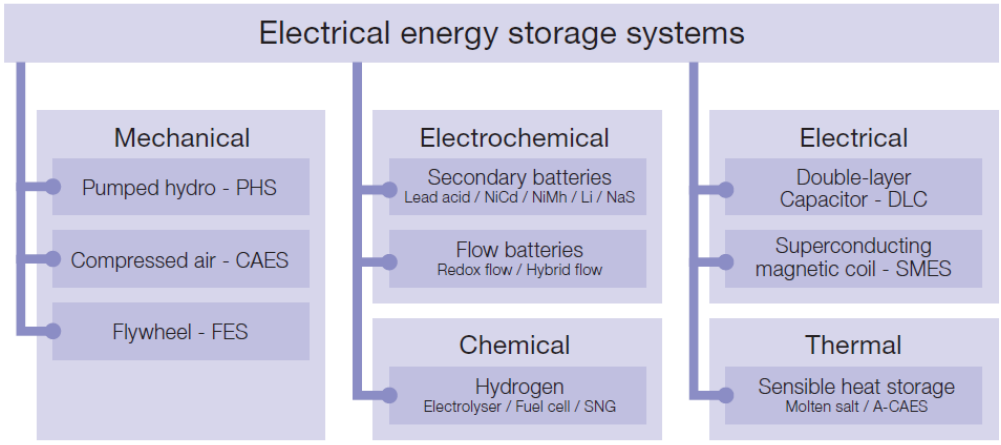

Figure 12: Types of energy storage according to energy form [27]

Hydrogen storage is thought to be the best technology for renewable energies to level the load over long periods of time and batteries are the best option to stabilize the grid during peak loads, due to their power range being between 1 kW to MW scale [21]. Besides these two technologies thermal storage has great potential to store energy before converting it into electricity when needed.

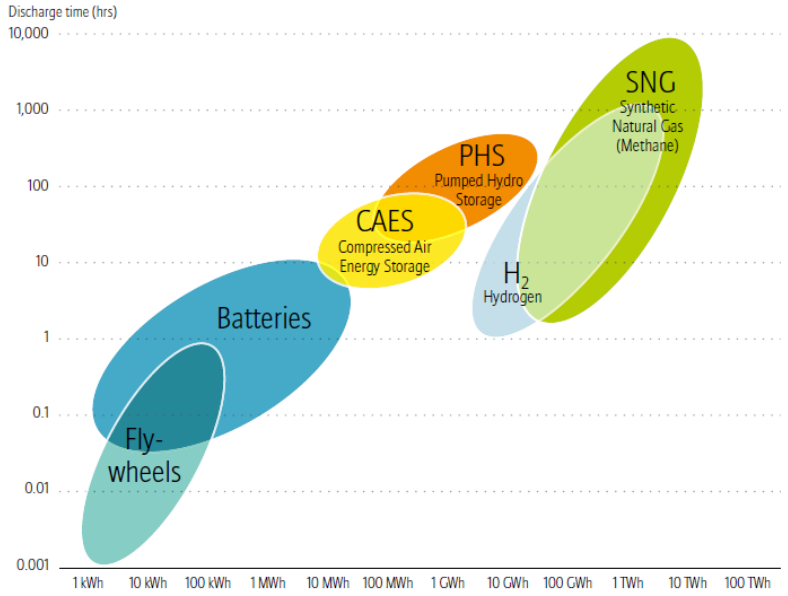

Figure 13: Energy storage systems according to their duration and amount of energy possible to store. Flywheels, CAES and PHS: Mechanical energy capacity; Batteries: Electrical energy capacity; SNG and H_2: Chemical energy capacity. [2]

Thermal energy storage (TES) is normally integrated to CSP plants to ensure an optimal power dispatch for several hours after sunset. There are different types of TES. It can be split in three main groups [28]:

- Sensible heat storage
- Latent heat storage
- Chemical heat storage

Sensible heat storage is based on the physical principle of storing and releasing energy from a medium by a temperature difference. Latent heat storage makes use of a material's enthalpy of transition, and chemical heat storage is the use of reversible endothermic chemical reactions [28].
An example of sensible heat media is steam, mineral oils or molten salts, which are the most mature technology for CSP. Whereas latent heat media can be paraffins, fatty acids or hydrated salts [28]. Sensible heat storage technology is mainly used in the form of active storage systems. This means that the storage media stores and releases the heat through forced convective heat transfer [28]. There are however, passive storage systems, where the heat transfer fluid gives away its heat energy to a stationary solid material acting as storage. It can be regained afterwards by recirculating in the opposite direction. An example of this technology is the ceramic storage system in the solar tower Jülich, Germany.

Batteries can be classified into 3 main categories [29]

- Primary batteries.
- Secondary batteries.
- Reserve batteries

Secondary batteries are also known as rechargeable batteries. Primary batteries are not able to be recharged. A rechargeable battery is capable of transforming electricity into the form of chemical energy in order to store it and using that chemical energy again to regain the electrical energy. This process is enabled by an electrochemical redox reaction [29]. More information about batteries is presented in Chapter 4.1.

2.4.2 Economic framework

Companies are looking into batteries as an increasingly growing market. In the US, the California Public Utilities Commission aims to install 1.3 GW of energy storage in the state by 2020 [30]. In Germany, on the other hand, there were until 2016 about 25.000 domestic battery installations for PV systems, with a total capacity of 160 MWh. It is estimated that the amount will reach 150.000 in 2020 [31]. According to the World Energy Council, the total installed capacity of large batteries was 750 MW before 2016 and could reach 250 GW by 2030 [31].
Until 2014 the most utilized types of batteries in the power sector were [32]:

- Sodium Sulphur batteries
- Lithium-ion batteries
- Advanced Lead-acid batteries
- Redox flow batteries.

Even though sodium Sulphur batteries had the highest share on worldwide installed capacity until 2014, it is not expected that this technology will remain as the benchmark for this industry. Rather, the Li-ion batteries and advanced Lead-acid batteries are trending to become the favorite technology [32]. Lithium-ion (Li-ion) batteries have been extensively researched in the last years, due to their application in mobile applications and most recently in the electric car industry. The currently most used batteries for electric cars are namely, lithium-nickel-cobalt-aluminum (NCA), lithium-manganese oxide spinel (LMO), lithium-nickel-manganese-cobalt (NMC), lithium-iron phosphate (LFP) and lithium titanate (LTO) [33]. Lead-Acid batteries have been used in large-scale storage systems since many decades now. In 1988 the world's largest energy storage battery facility was made of Lead-Acid batteries and was located in California, US. It consisted of a 40 MWh system, being able to feed in 10 MW of electricity in the grid at 2 kV and 8 kA 4 hours long [29]. Nowadays there are larger battery

systems [32], including an 800 MWh facility being planned in Asia [34]. Japan and USA have the largest installed capacity of batteries [32]. On the other hand, Germany has been increasing its efforts to store energy, due to the nuclear power phase-out**.** Until 2016 there were the following projects either on planning or installation [32]:

- 5 MW/ 5 MWh li-ion battery park in Schwering
- 10 MW li-ion battery park in Feldheim
- 5 MW hybrid li-ion and lead-acid battery park in Aachen.

Lithium-ion batteries will have a significant rise in the energy market, transitioning from being mostly used in the consumer sector in 2013 to presumably have the grid & renewable energy storage market as top client in 2020 [34]. A study from 2014 estimated the specific costs for lithium-ion batteries at 575 €/kWh plus 160 €/kW [35].

In regard to lead-acid batteries, in 2017 the German company Innogy acquired Belectric. This company sells the Energy Buffer Unit that can be either made of lead acid or lithium ion batteries. It stores 10 MW and serves for grid stability, peak shaving and ramp rate control purposes [36]. The specific costs of lead-acid batteries were 200 €/kWh and 160 €/kW, according to a study of 2014 [35]. Furthermore, there are some commercial batteries in the market already, especially made for utilities purposes, e.g. the Tesla Powerpack and the Eos Aurora.

Table 1: Comparison of commercial batteries for utilities, data from [37] [38]

	Tesla Powerpack	**Eos Aurora 1000 | 6000**
Technology	Li-ion	Zinc
Efficiency	92%	75%
No. of cycles	5000	10000
Price	$445/kWh	$160/kWh

The Eos Aurora DC battery system is being offered for $ 95 per usable kWh for shipment in 2022 (this includes battery modules, battery management system and outdoor-rated enclosure), thus becoming the first one to go below the 100 $/kWh threshold [39]. The company made this announcement in April, 2017. These batteries will be supplied as standardized 250 kW/ 1 MWh building blocks [39]. Tesla on the other hand, has already commissioned several projects of its Powerpack product. Although it was initially announced to be offered at 250 $/kWh, it has a sale price of 445 $/kWh [38]. The Powerpack has a nominal capacity of 210 kWh AC and 50 kW AC power [40]. Another competitor is Fluence, a joint venture founded by Siemens and AES and announced in July, 2017 to provide lithium-ion battery storage solutions [41].

2.5 Hybrid PV/CSP

CSP has proven in the last years to offer storage options in a more cost-efficient manner than PV plants with integrated batteries. CSP can therefore to cover the demand during sunset when there is an increasing electricity demand. The advantage of CSP plants are the storing capabilities during daytime and low-cost thermal storage for more than 12 hours. CSP average LCOE in 2015 was between 150 and 190 $/MWh. On the other hand, PV systems have become very cost efficient in the last years generating electricity at an average LCOE of 130 $/MWh in 2015. In addition to this, in the utility sector PV power plants have become even cheaper to install, with the lowest PV price being 27 $/MWh in Mexico. Therefore using PV-generated energy at day time and the thermal storage

advantages of CSP a cheap baseload supply could be achieved. A hybrid concept was made available for commercial applications by the company SolarReserve [42]. This is shown in Fig. 14 and 15.

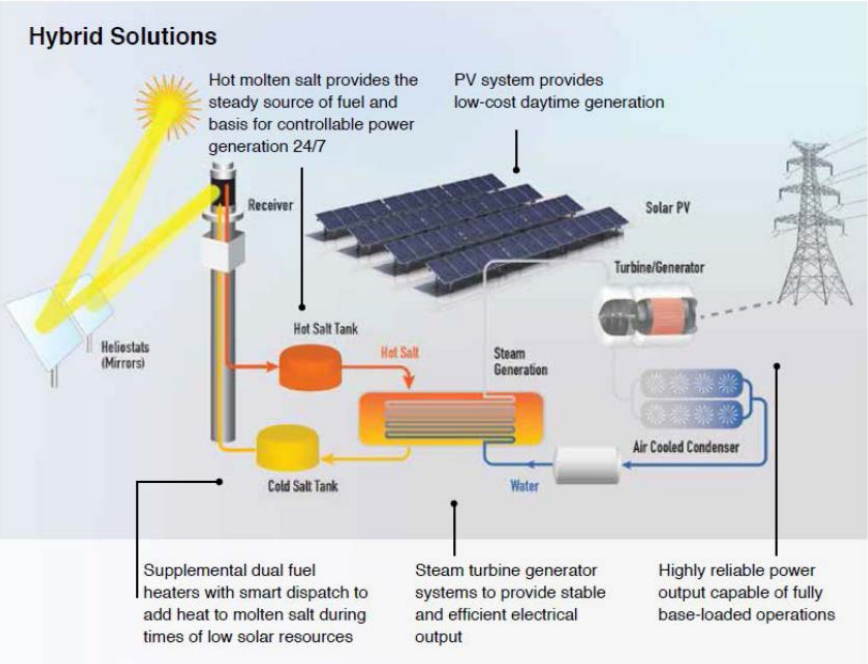

Figure 14: Hybrid solutions from the company SolarReserve [42]

They included this type of hybrid solutions in their catalog for suppling energy requirements of the mining industry in sunny regions. M-class and S-class solutions are the commercial names for different types of CSP plants with salt TES. M-class are central receiver plants with a half-cylindrical receiver and 180° heliostat field, being able to produce 200 to 400 GWh/a. S-class on the other hand are suitable for bigger mines requiring more electricity. It consists of a central receiver with full 360° heliostat field and producing 500 to 700 GWh/a.

Combining these CSP plants with PV and backup fuel generators it is possible to reach high capacity factors (> 90%), according to SolarReserve.

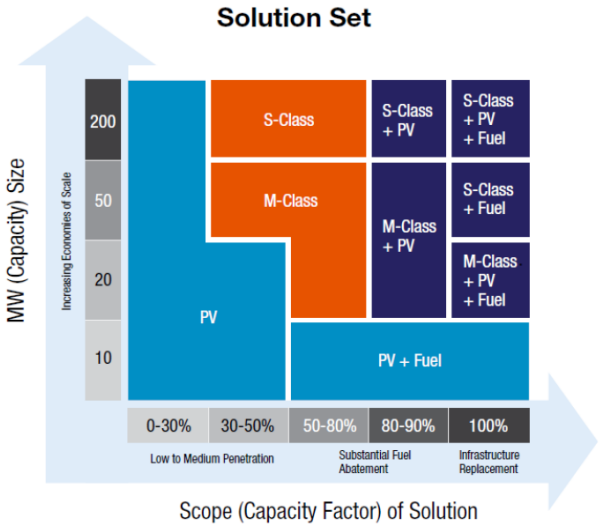

Figure 15: Solution set of solar technologies from the company SolarReserve [42]

2.5.1 Projects worldwide

Starting 2015 Chile has received much attention in the solar thermal segment. SolarReserve and Abengoa, from USA and Spain respectively, announced their plans to construct a CSP/PV hybrid power plant each: Copiapó and Atacama 1 [43]. Together with these two plants there have been other projects being planned but they are in the development phase. A short introduction of all the projects is presented, and subsequently a comparison with many of their technical and economical specifications.

Copiapó, Chile

Copiapó originally consisted of two 130 MWe solar towers with 14 h thermal storage, alongside a 150 MW PV plant. A hybrid operation would allow the PV plant to supply the necessary energy during the day, while the CSP plant would offer energy supply at night thanks to its storage capabilities, hence providing base-load power [43]. The hybrid project was granted the necessary environmental permits in 2015 [44, 45] and the company was waiting for a suitable PPA [44]. In August 2016 SolarReserve´s management opted to bid its plant at 0.063 $/kWh. This is the lowest price of CSP that has been recorded [46]. Interestingly the company did not bid for the hybrid CSP-PV configuration, but rather for only the two standalone CSP plants [46]. The reason behind this is that PV spot prices in northern Chile are currently so low, that it has become less valuable to dispatch PV power [46]. There is a lacking infrastructure between Chile´s central and northern grid, which results in the unavailability of transmitting the surplus solar power to the rest of the country [47]. There were 113 days by April 2016 when the solar electricity prices dropped to zero due to overcapacity [47].

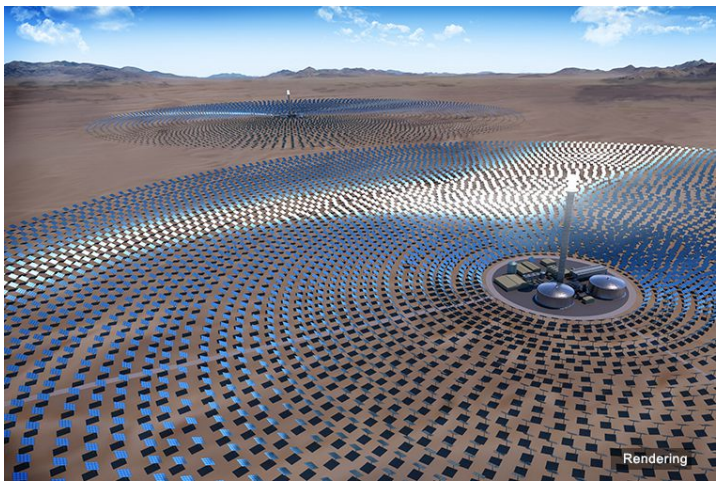

Figure 16: Copiapó most recent configuration with two solar towers (Rendering) [48]

The permit for the Copiapó project was granted for the CSP as well as the PV plant and according to SolarReserve's director the possibility of including the PV plant exists, only if the economic scenario for PV improves [46]. The reason for such low costs is on one hand the climate conditions. The DNI in Chile's desert is as high as 3800 kWh/m^{2}a. On the other hand SolarReserve has already gained experience from Crescent Dunes project in the US. They reduced the CAPEX in Redstone project in South Africa by 30% [49]. These technology advancements are the key to understand this low price for Copiapó. Furthermore, the supply costs were improved, by using a lot of Chile's local components for the plant such as Steel, concrete, glass, piping, valves, mechanical and electrical equipment and the thermal storage salts. For comparison reasons the original hybrid set-up is considered for this study.

Cerro Dominador, Chile

Abengoa started building the Cerro Dominador plant in Antofagasta, Chile. The project consists of a CSP and PV plant: A 110 MWe solar thermal tower and a 100 MW PV [50].

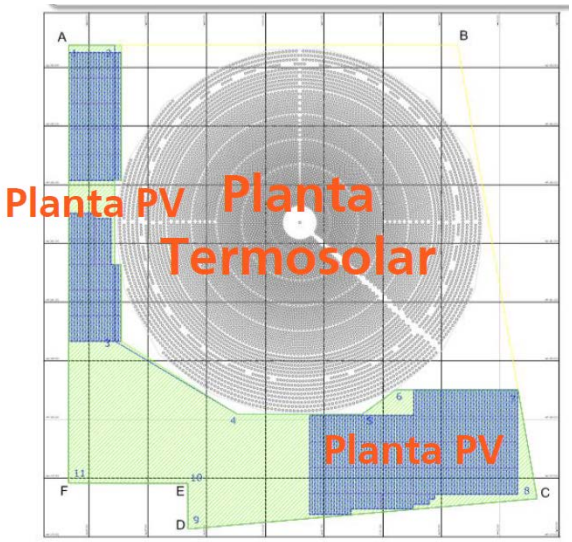

Figure 17: Cerro Dominador site layout with CSP tower plant and two PV parks [50]

The combination of the two plants should dispatch energy into the Chilean grid 24 hours a day, being able to respond during industry and household high demand times [51] [52]. The Cerro Dominador CSP plant together with the Maria Elena PV project was originally called Atacama 1 [43]. Now it is only called Cerro Dominador. After being owned and developed by Abengoa this project was sold to EIG Global Energy Partners [53] and after several delays the CSP plant shall start operations in 2019 and the PV park in 2017. More information about this plant is discussed in Chapter 5.

Redstone CSP, South Africa

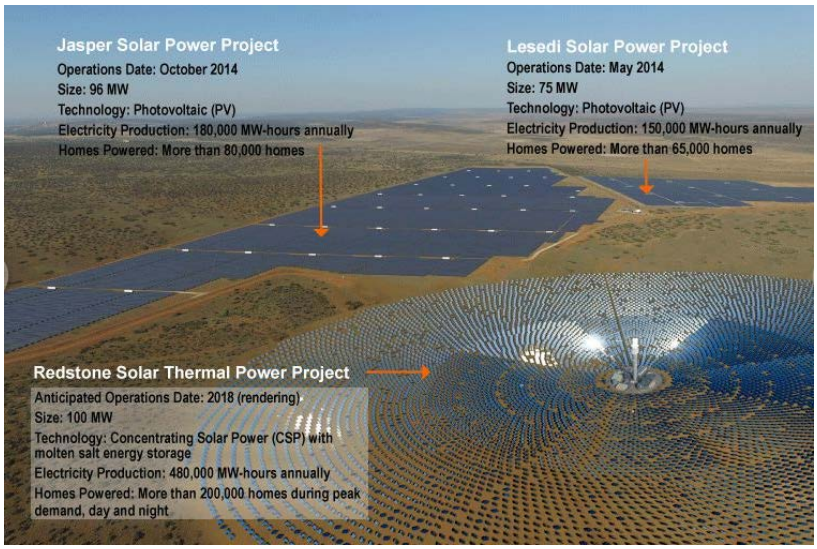

Figure 18: Redstone CSP and Lesedi and Jasper PV plants (Rendering) [48]

Redstone is a co-located PV and CSP power plant. It is a CSP project to be installed together with the two PV parks already built by SolarReserve in Postmasburg, South Africa (Lesedi and Jasper) [54]. The total installed capacity of the 3 plants combined will be 271 MWe. This project has been developed in the framework of the Renewable Energy Independent Power Producer Procurement Program (REIPPPP) [48]. Under this program there are currently about 2 GW of PV capacity and 600 MWe of CSP under planning or construction [55].

Bokpoort II, South Africa

Bokpoort II was originally a co-located PV/CSP project consisting of 4x75 MW PV facilities together with 2x100 MWe CSP parabolic trough or tower to have a total 500 MW capacity [56] [57]. It is now being planned to be 2x75 MW PV plus 150 MWe CSP tower to a total of 300 MWe [58]. However, there is not sufficient available information to date on the project status. It is supposed to be an extension of Bokpoort I, which is a CSP plant owned by ACWA Power Africa Holdings and located in Groblershoop, South Africa [57].

Ashalim, Israel

Ashalim power plant originally consisted of 2 CSP power plants and one co-located PV [56]. It was firstly announced in 2008 [59], but there is not enough information available about the status of this project.

Mendoza, Argentina

In 2016 a pre-contract was signed by the Dutch company Gigawatt Global to build a 100 MW PV plant and a 110 MWe solar thermal power plant in Mendoza, Argentina. The PV plant is valued in $220M and $520M is the estimated investment for the CSP plant, totaling a $740M [60] [61]. It is still being planned and there is no information about the operation strategy of these two plants.

Noor Midelt, Morocco

The plant Noor Midelt will consist of an 800 MWe hybrid PV/CSP power plant. For the phase I two hybrid plants are being tendered by MASEN (Moroccan Agency for Solar Energy). The CSP capacity of each plant should be between 150 MWe and 190 MWe [62]. A full time connected capacity of 400 MWe is wanted for each project, irrespectively of the total installed capacity [63].

Until the second quarter of 2017 there were 5 consortia prequalified on the bidding process. The winner is expected to be announced in 2017. According to [64], the CSP technology must be either a thermal oil parabolic trough plant with storage or a molten salt tower with storage. All Noor projects are part of Morocco’s initiative to produce 2000 MWe solar energy by 2020 and ensure 52% of its energy mix to from renewable sources by 2030 [65].

Table 2 shows an overview of the main features of the three hybrid power plants being under development or construction as of 2017.

Table 2: Overview of the main hybrid photovoltaic/solar thermal power plants

Description	Units	Copiapó Original Hybrid Project	Ref.	Cerro Dominador (ex Atacama 1)	Ref.	Redstone CSP + Lesedi & Jasper PV	Ref.
Total Capacity	MW	410	[54]	210	[50]	271	[66]
CSP Capacity	MW	2x130	[54]	110	[50]	100	[66]
PV Capacity	MW	150	[54]	100	[50]	171	[66]
Baseload power output	MW	260	[44]	N/A	[50]	N/A	
Location	-	Copiapó, Chile	[49]	Antofagasta, Chile	[67]	Postmastburg, South Africa	[68]
Heliostat area	m^2	115	[54]	140	[69]	N/A	
No. of heliostats	-	20,000 – 35,000	[54]	10,600	[69]	N/A	
Field aperture	m^2	2,656,000	[54]	1,484,000	[54]	N/A	
Tower height	m	N/A		250	[51]	N/A	
Storage capacity	h	2x14	[49]	17.5	[70]	12	[66]
Storage type	-	2-tank direct molten salt	[71]	2-tank direct molten salt	[69]	2-tank direct molten salt	[66]
Storage temperatures	°C	N/A		290 – 565	[51] [72]	288 - 566	[71]
No. of PV panels	-	N/A		392000	[67]	602992	[68]
PV Tracking	-	Fixed tilt	[54]	One-axis	[73]	Fixed tilt	[54]
Net electricity output	GWh	1800	[71]	950 (15a PPA)	[51] [50] [74]	810 (480 CSP only)	[48] [68]
PPA Tariff Rate	$/kWh	0.063 (CSP only)	[49]	0.114	[74]	0.124 (CSP only)	[66]
CAPEX	$Million	2000	[54]	1300	[70] [72]	1100	[68] [75] [76]
Operations start	-	2019 (CSP only)	[45]	2019 (PV operates already)	[53]	Early 2018 (PV operates already)	[66]
Lifespan	a	N/A		30	[72]	N/A	
Status	-	Under development (CSP only)	[71]	Under construction	[69]	Under development	[71]
Back up fuel	-	No	[43]	N/A		No	[66]
Battery	-	LTO ramping support, frequency regulation	[54]	Li-NMC spinning frequency regulation (12 MW, 4MWh)	[77]	N/A	

2.5.2 Studies on hybrid solar systems and economic perspectives

There have been some studies in the last years regarding the hybridization of photovoltaics / solar thermal power plants and their economic and technical feasibility for different locations or different tariff schemes. Larchet [54] investigated the economic advantage of a hybrid solar plant for baseload operation against standalone CSP and PV-diesel in Chile. PV-Diesel is the least economic option, since the diesel generator must cover about 60% of the total annual generation. Besides during the optimization of the CSP hybrid plant it was shown it is more cost-effective to have a natural gas backup rather than an additional PV component. The problem is that the information related to the backup gas legislation was not available; therefore it wasn't possible to conclude to which extent it is possible to implement natural gas backup boilers in CSP plants in Chile. The optimal hybrid configurations has an LCOE of 0.11 $/kWh [54].
Dominio [56] investigated the optimal hybrid configuration to meet intermediate and peak load demands under a specific tariff scheme in South Africa. The optimum solar multiple is SM = 1 and 5 hours storage time for both CSP standalone and PV/CSP. Higher solar multiples are instead suitable for baseload operation. The most economical plant for this price scheme however is the standalone CSP plant, since it is more flexible to lower its output during non-peak time. The hybrid plant however shows a better base-load capability and higher capacity factors [56]. This 120 MW plant has an LCOE of 0.185 $/kWh.
Castillo [78] also studied the performance of this type of plants under different schemes for the South African location. He states that the CSP plant when operating solely during high demand periods has a higher LCOE due to the increase in needed capacity. The CSP and PV single configurations resulted in a lower LCOE than the hybrid option. The only benefit of the hybrid is again the higher capacity factor [78]. Moreover, Pan and Dinter [55] presented a study where they combined a 100 MWe CSP central receiver power plant with a 100 MW PV plant to supply a constant baseload of 100 MW. This study also focused on South Africa. Their results are that for a CSP alone it is possible to supply an almost constant load 24 hours a day with a solar multiple (SM) higher than 3.5 and more than 18h of TES. For a hybrid system the SM reduced to 2.5 and the TES to 16h. This is shown in Fig. 19.

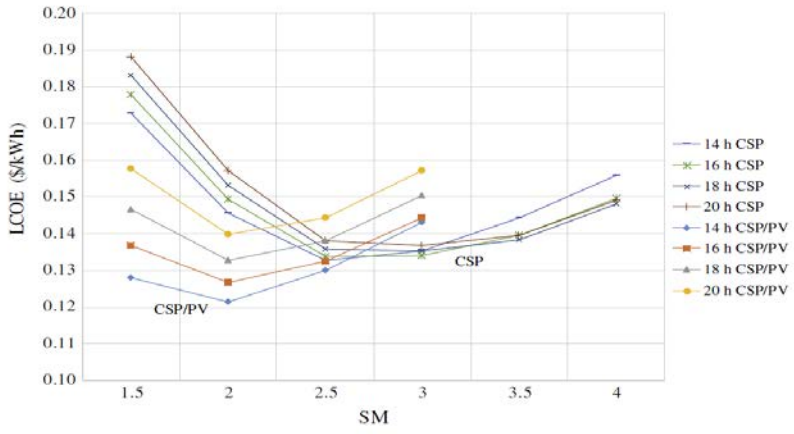

Figure 19: LCOE variation for different storage hour capacities and solar multiples, from [55]

The best configuration had a capacity factor of 92%, as shown in Fig.20. It was concluded that the best hybrid configuration has an LCOE of 0.133 $/kWh, which is 2.7% lower than a conventional CSP plant. Moreover, they explained how lower downtimes could result in an extended turbine lifetime and less maintenance costs, meaning again lower costs for the hybrid plant [55].

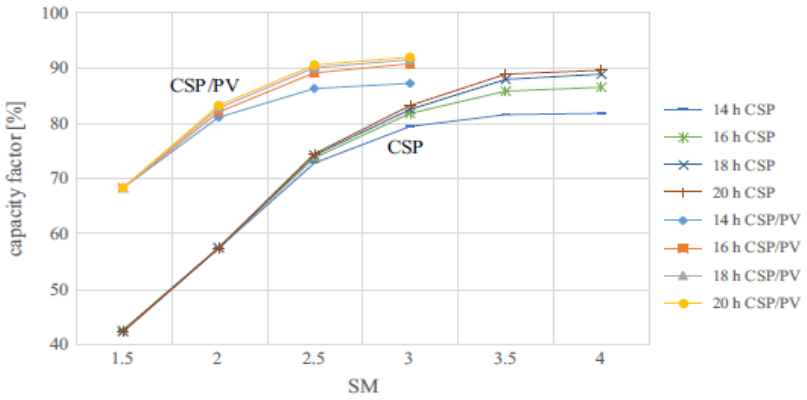

Figure 20: Capacity factor variation for different storage hour capacities and solar multiples, from [55]

Zaalouk [79] also studied the competitiveness of CSP and hybrid PV-CSP plants. He performed the simulations for the MENA region, specifically in the UAE. He concluded that in this region 11% reduction on the LCOE can be expected by using a hybrid configuration, as well as 40% reduction on CAPEX. Another aspect that has been studied is the optimum system configurations for PV in hybrid systems, in order to optimize the seasonal variation in power output. Green [80] showed that a higher tilt angle than the latitude angle maximizes the output in winter months. 45° is an optimum tilt angle to best utilize winter PV production when there is less CSP power available, without considerably reducing the total annual output.

Starke [81] studied the performance of different hybrid technologies of 50 MW in Chile, including parabolic trough and central receiver with PV both of them, as well as standalone technologies. The PV plant has the lowest LCOE of all plants (0.091 $/kWh), but a capacity factor of only 25%. The hybrid technologies (both parabolic trough and central receiver) have a capacity factor higher than 80%, and resulted slightly more cost-effective than their standalone counterparts.

Parrado [82] studied the economic aspects of the hybrid configurations and standalone systems for Chile. Three 50 MWe systems were compared: a fixed angle PV plant without storage, a 15 h TES parabolic trough and a hybrid plant enabling 24 hours dispatch: 20 MW fixed-angle PV and 30 MW parabolic trough with 15 h TES. To calculate the evolution for the next years Parrado used the two scenarios developed by the IEA: The Blue Map scenario and the Roadmap scenario. Here the roadmap scenario is more optimistic with regards to new solar installations worldwide, whereas the Blue Map scenario is a more conservative one.

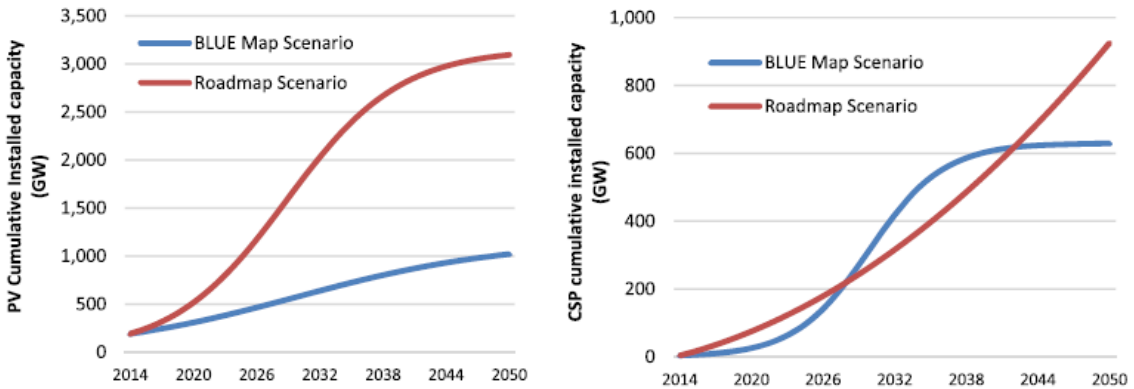

Figure 21: global PV and CSP installed capacity projection until 2050 [82]

Based on these two scenarios the LCOE evolution for all three solar technologies could look like in Fig.22 and 23:

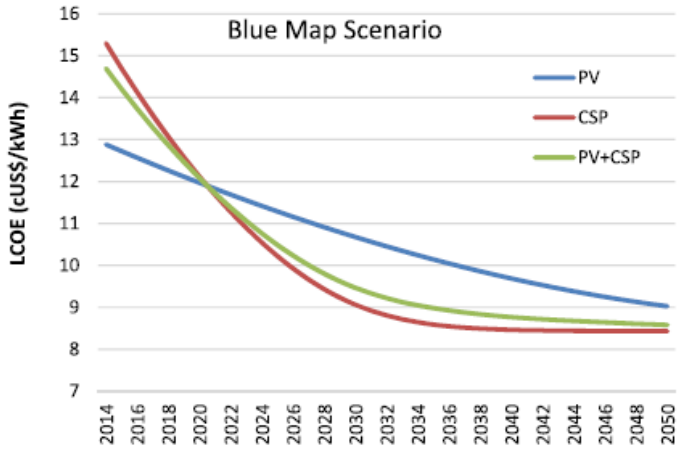

Figure 22: LCOE projection of PV, CSP and hybrid solar until 2050 under the Blue Map Scenario in Chile [82]

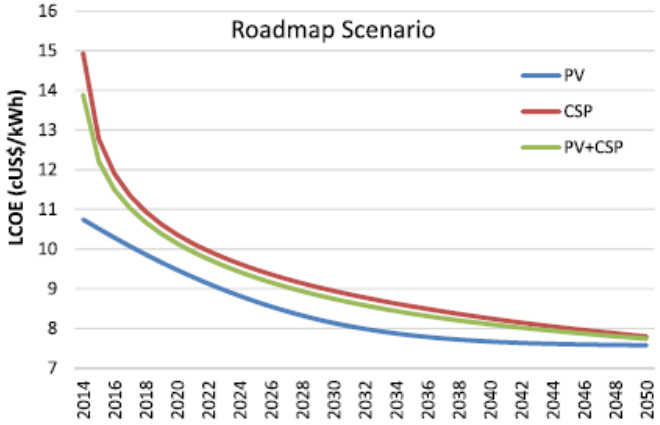

Figure 23: LCOE projection of PV, CSP and hybrid solar until 2050 under the Roadmap Scenario in Chile [82]

Finally, different system combinations were investigated in a study from 2016 [34], including a standalone CSP plant, a PV plant with battery and backup generator, as well as a CSP + PV + backup system (Gas turbine). The LCOE were calculated for different scenarios, including a baseload generation and a typical day load profile for locations in Morocco and Saudi Arabia. The results showed that in 2015 the CSP-PV hybrid system could supply electricity with the lowest LCOE out of these three variants. Solar towers were more favorable than parabolic trough plants with thermal oil, although by 2030 it was projected that PTC with salts as HTF will be highly competitive too. The hybrid configuration can supply electricity 24 hours long without using its backup generator during summer days. This configuration consisted of a 136 MWp PV plant with no integrated battery, a CSP plant with 2.5 SM and 17 h full load storage. During winter the backup generator is used since the TES could not be fully charged during the day. While PV reached its peak power at noon, the CSP plant was running at its lowest part load limit (around 25% load). For the year 2030, the system with the fastest LCOE reduction is the PV with battery and GT, due to the sinking battery and PV module costs. For 2030 it was suggested that this system would be as competitive as the CSP and hybrid CSP+PV. In must be noticed that these results are extremely dependent on the load requirements.

3 Photovoltaic Model Evaluation

3.1 PV model description

There are several ways to model the performance of PV modules in real life conditions. PV panels are tested at STC. For our application in *greenius* a model is required that accurately predicts stationary hourly power outputs with a limited number of input parameters, in order to keep the user interface simple. Therefore, before developing the battery model it has to be analyzed if the current PV model fulfills the requirements. In following, different modeling approaches are described and compared with *greenius*

3.1.1 3- coefficient Model in *greenius*

greenius predicts the output of the PV modules by calculating the real efficiency of the module as a function of the cell temperature and the irradiation [83]:

$$\eta(E,To) = \left[a_1 + a_2 \ln\left(\frac{E}{E_o}\right) + a_3\left(\frac{E}{E_o} - 1\right)\right] \cdot [1 + \alpha(T - T_o)] \quad (3.1)$$

With

- E_o : Nominal irradiation = 1000 W/m^2
- E : Current irradiation in W/m^2
- T_o : Nominal temperature = 25 °C
- T : Current temperature in °C
- α : Temperature coefficient in °C^{-1}

The term η is the efficiency at the maximum power point. The coefficient a_1 is equal to the nominal efficiency at STC. The second coefficient a_2 describes the part load behavior of the cell at lower irradiations and a_3 describes the behavior for concentrated PV cells. This approach has been used in other models such as Randall et al [84], Williams et al [85] and in the simulation software Polysun [86] [87]. To calculate the coefficient a_2 it is necessary to have at least two efficiency readings at two different irradiance conditions.

$$a_2 = \frac{\eta_{STC} - \eta_o}{ln\left(\frac{E_{STC}}{E_o}\right)} \quad (3.2)$$

The factor a_2 can be calculated with equation 2.2, where the index *o* represents the values from a second efficiency reading. Normally besides the STC values also the NOCT are given in datasheets, as well as the values for an irradiance = 200 W/m^2. Thus many different panels can be easily parametrized. For this reason this model has found its way into several applications.

3.1.2 5 Parameter Model

A series of different software tools use this model to perform their PV calculations, including PVSyst and SAM with its CEC Model [88] (also known as DeSoto Model [89]). Other papers analyzing the performance of PV modules like Ma et al [90] also made use of this approach.

PVSyst

The model used in the program PVSyst has been described by Mermoud et al [91]. It is based on the Shockley's simple one diode model, which is the most used standard equivalent circuit for PV cells found in literature [92] [90]. There exists another equivalent circuit model that uses two different diodes. However the single diode model is mostly used, due to simplicity [91].

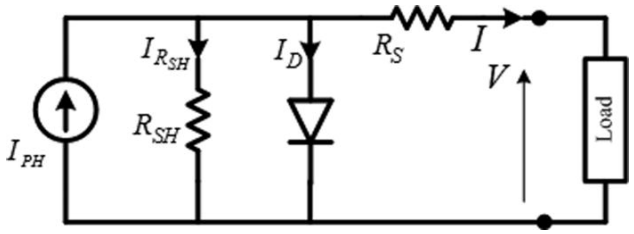

Figure 24: Standard single diode equivalent circuit for a PV cell. I_{ph} is the photocurrent (I_φ in the equations from PVSyst) [93]

The voltage and current delivered by the module is dependent on several factors, which are shown in equation 3.3.

$$I = I_{\boldsymbol{\varphi}} - I_o \left[e^{\left(q \frac{V + I \cdot R_S}{N_{cs} \cdot \gamma \cdot k \cdot T_c} \right)} - 1 \right] - \frac{V + I \cdot R_S}{R_{sh}} \tag{3.3}$$

The parameters of the single diode equation are listed in Table 3:

Table 3: Parameters for PV modeling in PVSyst

Parameter	Description	Unit
I	Current supplied by the module	A
V	Voltage at the terminals of the module	V
I_φ	Photocurrent, proportional to the irradiance E, with a correction as function of T_c	A
I_D	Diode current. Product of "$I_o\left[e^{(\ \ )} - 1\right]$"	A
I_o	Inverse saturation current, depending on the temperature	A
R_s	Series resistance	Ω
R_{sh}	Shunt resistance	Ω
q	Charge of the electron = $1.602e^{-19}$	C
k	Bolzmann´s constant = $1.381e^{-19}$	J/K
γ	Diode ideality factor, between 1 and 2	-
N_{cs}	Number of cells in series	-
T_c	Effective temperature of the cells	K

To determine all current and voltage values for any given condition it is necessary to firstly determine I_φ, I_o, γ, R_{sh} and R_s at STC. A PV manufacturer measures and provides information about I_{sc}, V_{mpp}, I_{mpp} and V_{oc} at STC for every produced cell or panel [91].

The electrical power generated by a photovoltaic cell is a function of both current and voltage, which depend on the load connected. During manufacturing different loads are connected to the cell in order to measure all currents for different voltages until the current reaches 0 A. The voltage at which this occurs is called the open-circuit voltage (V_{oc}). On the other hand, the PV current at which the voltage

is 0 V is called the short-circuit current (I_{sc}). The photovoltaic cell does not generate any power at any of these two points. The maximum generated power is at one specific point along this curve. The point at which this happens is the maximum power point (MPP). The current and voltage at the MPP point are the so-called MPP-current (I_{mpp}) and MPP-voltage (V_{mpp}). A complete typical I-V and P-V-curve are shown in Fig.25, as well as the parameters I_{sc}, V_{mpp}, I_{mpp} and V_{oc}.

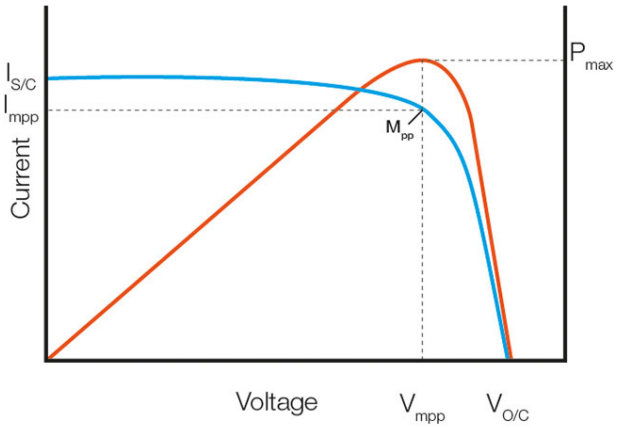

Figure 25: I-V curve of a PV cell in blue. P-V curve in red [94]

With the help of the I-V curve it is possible to determine the 5 parameters required for this model. The shunt resistance R_{sh} corresponds to the inverse of the slope around I_{sc}. When a measured I-V curve is provided from the manufacturer this can be done easily, but normally it is difficult to get all values of the curve. Therefore, an approximate value is calculated based on the points I_{sc}, I_{mpp} and V_{mp} with the equation 3.4.

$$R_{\mathrm{Sh}} = \left(C \cdot \left[\frac{I_{sc}+I_{mpp}}{V_{mpp}} \right] \right)^{-1} \tag{3.4}$$

The parameter C is a correction factor. With this equation the slope between the point at I_{sc} and I_{mpp} is calculated. This represents the maximum possible slope at the point I_{sc}. This is corrected and multiplied with an estimated coefficient C, since the slope at I_{sc} in a typical I-V curve is not so steep. The inverse of this slope is the value of R_{sh}.

The series resistance R_s can be found empirically. A default value for R_s has been used in the later versions of PVSyst, since it normally suits well the measured data. R_s can also be manually chosen from a set of values in order to find the one that best matches the I-V curve or to best match the temperature coefficient of the open circuit voltage if it is known. Up to a former version it was possible that the program selected a default γ, according to the cell type to find R_s, since they are both dependent on each other. This is the approach that was followed for the model comparison because a list of default values for γ is already documented in PVSyst [95].
The parameter γ is the diode ideality factor and is a measure of how well the diode follows the ideal diode equation.

After defining R_{sh} and γ, the three unknowns I_φ, I_o and R_s can be solved with equation 3.3 and three different data points (See Table 4). The values for current and voltage shown in Table 4 are taken from the manufacturer's data sheet.

Table 4: Set of known data points to determine the rest of parameters with eq. 3.3

	Current I	**Voltage V**
Data point 1	I_{sc}	0
Data point 2	I_{mpp}	V_{mpp}
Data point 3	0	V_{oc}

Correction for non-STC:

As already stated, a correction is needed for non-STC. The photocurrent and the diode saturation current depend on the irradiance and temperature at which they operate. Therefore additional equations are used to find all parameters for any given irradiance and temperature and subsequently to find the cell's power output.

$$I_{\varphi} = \left(\frac{E}{E_{STC}}\right) \cdot \left[I_{\varphi,STC} + \mu I_{sc} \cdot \left(T_c - T_{c,STC}\right)\right] \tag{3.5}$$

$$I_o = I_{o,STC} \left(\frac{T_c}{T_{c,STC}}\right)^3 \cdot e^{\left[\left(\frac{q \cdot \varepsilon_G}{\gamma \cdot k}\right)\left(\frac{1}{T_{c,STC}} - \frac{1}{T_c}\right)\right]} \tag{3.6}$$

The coefficient μI_{sc} is the temperature coefficient of I_{sc}. ε_G is the band gap of the material (1.12 eV for crystalline Si, 1.03 eV for CIS, 1.7 eV for amorphous Si, 1.5 eV for CdTe) [95].
This model fits really well the measured data from monocrystalline and polycrystalline-Si as well as CIS modules. But it needs adjusting for other thin film modules (a-Si). There are 3 corrections that are made in PVSyst [95]:

- R_{Sh} exponential correction: R_{Sh} is inversely proportional to the irradiance, as it tends to increase drastically in low irradiance regions.
- Recombination losses: It takes into consideration additional current losses inside the layers of the amorphous junctions.
- Spectral corrections: It takes into consideration the energy levels of the incoming solar radiation.

These corrections are explained in detail in [95]. However, they are too complex and are not implemented in other studies with the 5-parameter model. For this reason, this correction is not relevant for this study.

3.1.3 PVWatts

PVWatts is a tool developed by NREL. It is a simple model for applications that do not require much detail, e.g. when comparing the energy yield of a characteristic PV System between different locations. It is an adaptation of the Sandia PVForm algorithm [96]. It is based on the equation 3.7 [97]:

$$P = \frac{E}{1000} P_0 [1 + \alpha (T_{cell} - T_{STC})] \tag{3.7}$$

The power output P depends solely on the Irradiance E and the cell temperature T_{cell} and has a linear behavior. P_0 is the nameplate power rating and α is the temperature coefficient. The newest version of PVWatts (5^{th}) has been improved considerably since the first introduction of this tool. The inaccuracy

of the model was less than 2% for unshaded PV systems, when compared to measured data [97]. It is however, not recommended for thin film technologies [88].

3.1.4 SANDIA Model

This model, also called King Model was developed at Sandia laboratories and calculates all voltage and current values as a function of cell temperatures, irradiance and spectrum [98]. It needs however seven different coefficients, which have been found empirically after a several number of measurements. Even though this model can depict the whole I-V-Curve it is considered not suitable for *greenius* due to the complex parametrization.

3.1.5 Model comparison

A comparison between the PVWatts method, the 5 Parameter model – PVSyst [1] and *greenius* 3-coefficient method was carried out. All models were compared with the results from *greenius* software as a reference point.
The following modules were chosen:

- Schott Perform Poly 250 (polycrystalline)
- Shell Solar SQ175-PC (monocrystalline)
- GeneCIS-Solar 75 (CIS Thin film)

The location for the simulation was Almeria, Spain. Meteorological data is from *greenius* database. The plane tilt was 0°; hence the Global horizontal irradiance (GHI) could be used as the On-Plane irradiance. The inverter was not important for the calculation, since just the output from the module was discussed. The system consisted of only one module and no other losses were considered (Soiling, availability, etc.)

PVSyst model validation
In order to validate the 5-Parameter model used for the comparison, the coefficients used in this work were compared to the parameters for the Shell Solar SQ175-PC module found by Ma et al [90]. The first row in Table 5 contains the results from our model. The other 4 rows are taken from Ma et al.

Table 5: Parameter results from different models [90]

Method	I_{ph} [A]	I_o [A]	R_s [Ω]	R_{sh} [Ω]	γ [-]
5-Par. Model	5.454	0.55e-09	0.66	147.50	1.05
PVSyst software	5.430	2.00e-09	0.65	180.00	1.11
DeSoto model	5.457	0.05e-09	0.81	163.30	0.948
Tao Ma model	5.449	1.20e-09	0.70	196.20	1.086
INSEL software	5.43	-	0.71	171.06	-

[1] Due to the non-linear nature of this model, the simulations were performed in a dynamic simulation tool: No annual yield was calculated. Instead two characteristic days were simulated and compared to the other models. The other models were simulated with MS Excel.

R_s and I_{ph} show good accuracy compared to the results from PVSyst software. The parameter I_{ph} from our model is only 0.4% higher than PVSyst, whereas R_s is 1.5% higher.

R_{sh} in our model is determined with equation 3.4. The slope between the points at I_{sc} and I_{mpp} is calculated and a correction factor of 0.5 is used. However, due to the fact that PVSyst uses a multiplying factor that is not publicly available, R_{sh} is difficult to match with this first estimation. R_{sh} in our model has the value of 147.50 Ω. This is 19% lower than R_{sh} from PVSyst.

Even though R_{sh} is lower than the rest, the selection of γ has the highest influence on the final outcome. The chosen γ was 1.05 because it was the default value for monocrystalline silicon cells in the PVSyst manual. However, by setting γ to 1.11 in our model it was possible to match the diode saturation current I_o from PVSyst software (2.00e-09 A). The calculations for the 5 parameter model are therefore valid for further comparisons.

3.1.6 Results

The annual electricity yield results of the 3-coefficient (*greenius* Excel) and the PVWatts model are shown in Table 6, as well as the relative deviation compared to the results from the software *greenius*[2].

Table 6: Annual Electricity Yield

	***greenius* Software [kWh]**	***greenius* Excel [kWh]**	**Deviation [%]**	**PVWatts [kWh]**	**Deviation [%]**
Schott Perform Poly 250 (p-Si)	407.8	407.7	-0.04	434.1	6.44
Shell Solar SQ175-PC (m-Si)	286.3	286.5	0.06	303.8	6.12
GeneCIS-Solar 75 (CIS)	121.3	121.8	0.42	130.2	7.35

The annual yield from the *greenius* calculations in excel matched within a 0.42% deviation the results obtained in *greenius* software. Therefore the model built in excel is validated and can be compared to the other models. PVWatts, as expected delivered higher values than *greenius*, within a deviation of about 6%.

Due to the simple parametrization of the 3-coefficient and the PVWatts model, annual simulations are possible to be carried out. However, for the PVSyst model an MPP Tracker model would have to be simulated in order to automatically find the hourly maximum power output from the PV module. Since this is a preliminary evaluation a manual calculation of the maximum power output for two characteristic days is sufficient (A typical day in winter and in summer). The I-V curves for each hour are calculated with equations 3.3 - 3.5 and the maximum power output is then found for each hour. The results are shown in the next section.

Module performance in an hourly basis

For a specific day in winter (with the year's lowest temperatures) and a day in summer (with the year's highest temperatures) the daily DC power profile for the Schott Perform Poly 250 panel is calculated.

[2] Deviation: (Model value – Reference value)/ Reference value

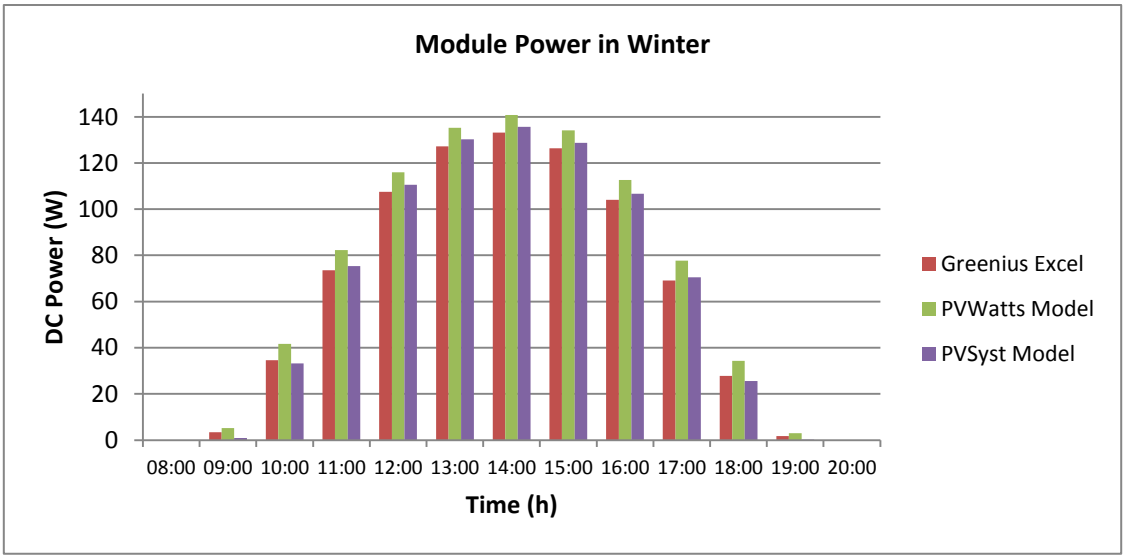

Figure 26: Module power in winter

Table 7: Daily results for a typical winter day

Schott Perform Poly 250 (p-Si)	*greenius*	PVWatts	Deviation [%]	PVSyst	Deviation [%]
Daily Electricity Yield [Wh]	808.6	883.0	9.2	817.4	1.1
Daily Power Peak [W]	133.2	140.8	5.7	135.6	1.8

The overall daily yield in winter is very accurate in both *greenius* and PVSyst models. The deviation between PVSyst and *greenius* is only 1.1%. PVWatts overpredicts the output, meaning that at its power peak the relative error between PVWatts and *greenius* is 5.7% and the daily energy yield differs by 9.2%. The reason for this is that PVWatts calculates the power output as a linear function of the irradiance, whereas in *greenius* the output sinks logarithmically at low irradiances.

In Fig.27 the hourly DC power output for a typical summer day from all models is shown.

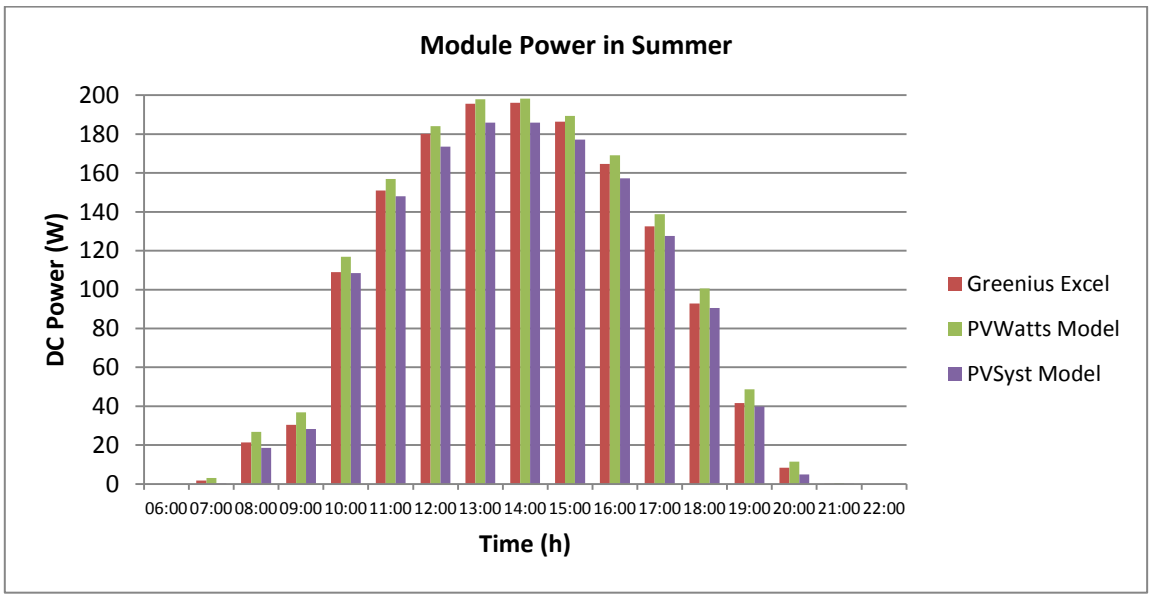

Figure 27: Module power in winter

Table 8: Daily results for a typical summer day

Schott Perform Poly 250 (p-Si)	*greenius*	PVWatts	Deviation [%]	PVSyst	Deviation [%]
Daily Electricity Yield [Wh]	1512.0	1579.0	4.4%	1446.6	-4.3%
Daily Power Peak [W]	196.0	198.3	1.2	186.0	-5.1

In summer the PVWatts results are closer to *greenius* than in winter, due to the higher irradiance values. The deviation is less than 1.2% at its power peak for PVWatts. The PVSyst model has an error of 5.1% for the power peak and 4.3% for the total daily energy yield. This occurs because the cell temperatures at this time are the highest in a year (> 50°C). A reason for the large deviation could be the high sensitivity of the PVSyst model to the changes in temperature. The correction equation for the temperature in the term I_{ph} uses the temperature coefficient of the short circuit current (μI_{sc}). (See equation 3.5)

The problem with using this model is that manufacturers sometimes include only the temperature coefficient for the MPP current and not the short circuit current [83]. Some others even prefer not to include any coefficient, such as for the second module from Table 6 (Shell Solar SQ175-PC). During the calculations it could be seen the large effect some small coefficient variations have on the maximum power. Vergura [99] and Quaschning [7, p. 192] claim that the increase in I_{mpp} can be calculated using the temperature coefficient for I_{sc}. However, King [100] investigated this behavior and during a measurement campaign it was found that there is a discrepancy between the coefficients for I_{sc} and I_{mpp}, including sometimes a difference in sign, as shown in Figure 28.

Module	dI_{sc}/dT (1/°C)	dI_{mp}/dT (1/°C)	dV_{oc}/dT (1/°C)	dV_{mp}/dT (1/°C)
ASE300, mc-Si	.00091	.00037	-.0036	-.0047
AP8225, Si-Film	.00084	.00026	-.0046	-.0057
M55, c-Si	.00032	-.00031	-.0041	-.0053
SP75, c-Si	.00022	-.00057	-.0039	-.0049
MSX64, mc-Si	.00063	.00013	-.0042	-.0052
SQ-90, c-Si	.00016	-.00052	-.0038	-.0048
MST56, a-Si	.00099	.0023	-.0041	-.0039
UPM880, a-Si	.00082	.0018	-.0038	-.0037
US32, a-Si	.00076	.0010	-.0043	-.0040
SCI50, CdTe	.00019	-.0012	-.0037	-.0044
$\pm U_{95}$ (%)	10	12	5	7

Figure 28: Temperature coefficients at STC conditions for different modules [100]

Therefore, a careful selection of the temperature coefficient has to be made in PVSyst to avoid errors.

3.2 PV Model conclusions

In the *greenius* model the efficiency and therefore the DC output of the module is calculated as a function of irradiance and temperature. It has been shown that all assumptions are valid and the results are highly accurate compared to the other software tools PVSyst and PVWatts (relative error <6% at power peak). The main disadvantage of using the 5 parameter model is the complex parametrization. All the different coefficients provided from the manufacturer have to be carefully analyzed before implementing. This can result in complications for the user. Thus, for the required application the currently used model in *greenius* proved to be suitable.

4 Battery Model Development

Several available battery models are discussed in this chapter. Subsequently, the most suitable option for *greenius* is selected and pre-evaluated before its implementation.

4.1 Electrochemical storage modeling

As it was already stated in chapter 2.4.2 the main battery types which are expected to dominate the electrochemical storage market are the lithium-ion and lead-acid batteries. These two battery types share similar physical effects and behavior. The main technical parameters to describe a battery are:

Depth of Discharge:
Batteries are not charged and discharged to their full capacity limits in order to maintain a longer lifetime. The percentage of the nominal capacity at which batteries are allowed to be discharged is called the depth of discharge (DOD). Some manufacturers recommend a DOD of 50% for stand-alone PV systems, although there is no consensus about what value is the optimum [101].

Battery temperature effect:
Temperature plays a major role for the battery operation. At high temperatures the battery's lifetime is shortened, whereas at cold temperatures its capacity diminishes [101] [102]. Batteries must always be placed in an insulated and vented area [103] [104].

Capacity:
The watt-hour capacity is a measure of the amount of energy that the battery can store or supply [105]. The capacity is a measure of the electric charge that the battery can take in or deliver [105]. It is measured in Ah. Even though a nominal capacity is given by the manufacturer, it also depends on several factors during operation conditions [102]. E.g. a battery with rated capacity C_{100} = 100 Ah indicates that 100 Ah are available when the battery is discharged during 100 h. In this example a faster discharge current of 8 A would cause that the cut off voltage is reached after 10 hours, meaning a capacity of only 80% C_{100} [7].
The capacity can deteriorate also due to aging. It is most commonly assumed that the end of life of a battery occurs when it reaches 80% of its nominal capacity [102]. Other few definitions claim that the end of lifetime is when the battery reaches 60% [32]. Normally a battery should be designed for 80% of its nominal capacity or however the end of lifetime is defined. Furthermore, it should be operated only within its limits, for instance 50% DOD. For this reason batteries are oversized during the design phase.

State of Charge:
The state of charge of a battery describes how much capacity is left after charging or discharging a battery. A way to estimate the SOC is the Coulomb counting. This method is used by Merei et al [106]. It measures the in-and-out current with the following equation:

$$SOC(t) = SOC_o + \int \left(\frac{I_{eff}(t)}{C(t)}\right) dt \tag{4.1}$$

With the following parameters:

- $SOC(t)$: Actual state of charge in %
- SOC_o : Initial state of charge in %
- $C(t)$: Actual battery capacity (dependent on aging) in Ah
- $I_{eff}(t)$: Effective charging/discharging current in A

Self-discharge:
Thermodynamically, the discharged state is the most stable state [29]. Therefore self-discharge is a natural process that happens in all types of batteries. Lead-acid batteries can have a monthly self-discharge rate less of than 5% [29].

Voltage:
Each cell has an own potential difference depending on the chemical reactions within [102]. Nonetheless, this value is not constant, as it depends on the operating conditions. At a low state of charge (SOC) the voltage drops steeply, e.g. to 10.8 V in a 12 V Lead-acid battery [102]. If the voltage drops to the lower limit it must be disconnected. The lower limit is called cut off voltage (See Fig.29). The battery voltage lies normally below the nominal PV module's voltage. If a PV module has a 16 V nominal rating, its operating voltage would probably lay in the range 14 to 16 V at lower irradiance levels and higher temperatures than STC. The battery must be designed accordingly to be supplied with a lower voltage than the PV MPP voltage, e.g. 12 V.
The nominal voltage according to one definition is "the reported or reference voltage of the battery, also sometimes thought of as the normal voltage of the battery" [107]. Another definition states that the nominal voltage can be measured at the mid part between the fully charged and discharged state of a battery [108]. Therefore, there is no agreed definition of the nominal voltage.

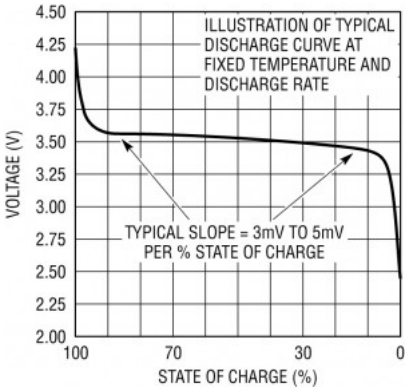

Figure 29: Typical voltage vs. SOC curve [108]

4.2 Battery layout and function

Lead-acid batteries

In charged state the positive electrode consists of PbO_2 and the negative electrode is made of Pb. The electrolyte is sulfuric acid H_2SO_4 [29]. Besides the main reactions, there are side reactions also occurring. An example is gassing, which is the production of hydrogen and oxygen when approaching the full state of charge. The battery terminal voltage is reduced during discharge and rises while it is charged. The gassing reaction takes place if the voltage exceeds the gassing voltage (2.39 V per cell) [29]. It is of uttermost importance to avoid this from happening continuously. This process is

irreversible and carries losses in the efficiency of the cells [19]. Voltage control can be done by measuring the state of charge of the battery.
Older lead-acid batteries showed low depths of discharge (< 20%), low cycle numbers (< 500) and lifetime of only 3 to 4 years [32]. More recent ones have a higher DOD and more cycles (>50% DOD with 2800 cycles) [32].

Lithium-ion batteries

The positive electrodes or cathodes can be made of $LiCoO_2$, $LiNiCoO_2$, $LiNiO_2$, $LiMn_2O_4$, among others [29]. The negative electrodes or anodes are formed with Graphite (nC) [7]. In regard to the electrolytes, there are different types, such as liquid, gel, polymer and ceramic electrolytes [29]. The majority of Li-ion electrolytes are nowadays the salt $LiPF_6$, due to its high ionic conductivity [29]. The DOD of a lithium-ion battery is between 60% and 100% according to multiple studies [22] [32] [106]. Li-ion batteries are ideal for short discharge cycles (< 4 h) [32] and have almost as twice cycle lifetime as lead batteries [35]. Li-ion batteries have also a higher energy density, meaning that less volume and weight is required to store the required amount of energy [109]. This is not only important in mobile applications and electric vehicles, but in utility-scale applications as well, where construction areas are limited.

4.3 Characterization of the battery models

In order to describe a battery's behavior is therefore required to model the most important parameters, such as capacity, state of charge or depth of discharge. There are many different approaches to model batteries. These are explained in this chapter.

4.3.1 Electrochemical and equivalent-circuit models

He et al [110] categorizes battery models used in the development of electric vehicles in mainly two groups: the electrochemical models and equivalent circuit battery models. Electrochemical models can describe quite accurately the chemical thermodynamic processes occurring within the battery and transpose this information into electrical quantities like voltage and current. The drawback however, is the large number of parameters required [110].

The equivalent-circuit models on the other hand, depict the battery as a circuit network with the use of electrical elements, such as resistors, capacitors and ideal voltage sources [110]. These models are summarized in the following figure from [110]:

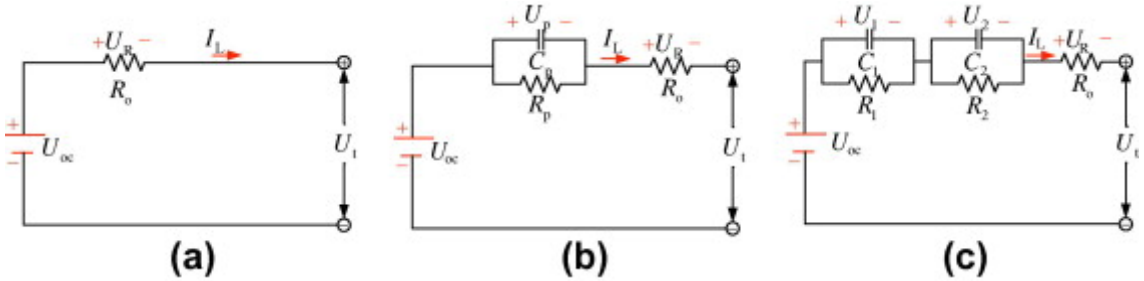

Figure 30: a) Rint model; b) Thevenin model; c) DP model. Modified from [110]

The Rint model is the most basic model with a single resistor. The Thevenin model connects parallel RC elements in series to describe the dynamic characteristics. The DP model is a more complex model with an additional RC network in series. These elements only describe the electrochemical

polarization of the battery. Therefore a higher degree of accuracy is achieved with the inclusion of chemical kinetics.

In another study [111] He et al shows a way to determine the parameters for a lithium-ion battery by an experimental approach. This procedure is quiet laborious. Even though He et al state that these models are for Li-ion batteries, Kai and Qifang [112] claim that these electrical models can be adapted to Lead-Acid batteries as well. Kumar presents another procedure to calculate the parameters of an electrical model [113] valid for Lead-Acid and Ni-Cd.
Kai [112] and Parthasarathy [114] also present additional models such as the impedance-based model, over-current battery model and a fourth-order dynamic model, each model depicting different battery types or applications.

4.3.2 CIEMAT model:

A model for lead-acid batteries was developed by CIEMAT and described by Copetti et al [115]. It is based on the Shepherd model [115], which is a simplified electrochemical model. It describes the battery's behavior in terms of voltage and current. The voltage equation depicts a simple equivalent circuit, just as the Rint model. The discharge voltage here depends on the temperature, the current and the state of charge. These equations are valid for a single-cell 2 V battery [115].

$$V = [2.085 - 0.12(1 - SOC)] - \frac{I}{C_{10}}\left(\frac{4}{1+I^{1.3}} + \frac{0.27}{SOC^{1.5}} + 0.02\right)(1 - 0.007 \cdot \Delta T) \quad (4.2)$$

The temperature variation is:

$$\Delta T = T - 25 \quad (4.3)$$

The state of charge:

$$SOC = 1 - \frac{Q}{C} \quad (4.4)$$

Q is the charge amount in the battery. The capacity C is limited by current and temperature:

$$\frac{C}{C_{10}} = \frac{1.67}{1+0.67\left(\frac{I}{I_{10}}\right)^{0.9}}(1 + 0.005 \cdot \Delta T) \quad (4.5)$$

For charging, the voltage equation looks somehow different:

$$V = [2 - 0.16 \cdot SOC] + \frac{I}{C_{10}}\left(\frac{6}{1+I^{0.86}} + \frac{0.48}{(1-SOC)^{1.2}} + 0.036\right)(1 - 0.025 \cdot \Delta T) \quad (4.6)$$

The SOC during charging is defined as follows:

$$SOC = SOC_o + \frac{\eta_c Q}{C} \quad (4.7)$$

With the term η_c defined as:

$$\eta_c = 1 - e^{\left[\frac{20.73}{\frac{I}{I_{10}}+0.55}(SOC-1)\right]} \quad (4.8)$$

This model provides a good understanding of the battery and the crossed-linked effects of voltage, SOC and current in a rather simple way. This model has also been used in [21] and mentioned in several other papers.

4.3.3 PVSyst

This model calculates the voltage as a function of the SOC, the internal resistance the battery's temperature. It is valid for Lead-Acid batteries.
The equation to calculate the battery voltage is the following:

$$V = V_{oc\ base} + \alpha \cdot SOC + \beta(T - T_{ref}) + R_i \cdot I \tag{4.9}$$

With the following terms:

- V : Battery terminal voltage.
- $V_{oc\ base}$: Intercept of the open circuit voltage linear part where SOC is 0.
- SOC : State of charge (between 0 and 1).
- α : Slope of the open-circuit line (depending on the chemical couple Pb-SO_4).
- T : Battery temperature.
- T_{ref} : Reference temperature (normally 20 °C).
- β : Temperature coefficient (between -5 and -6 mV/°C).
- R_i : Internal resistance (assumed to be constant).
- I : Battery current (charge > 0, discharge < 0).

The temperature dependence of the voltage is assumed to be linear for all operating conditions in this model. The SOC is determined via coulombic efficiency.

4.3.4 System Advisor Model (SAM)

The latest version of SAM includes models for Lead-Acid and Lithium-Ion batteries. These models are described by DiOrio et al [23]. The configuration is based on an AC-coupled battery system. SAM uses different models for the transient capacity and charge-transfer behavior in Lead-Acid batteries. Since Lithium-Ion batteries have a faster charge and discharge rate, a simple tank-of-charge model was used for this type [23]. Terminal voltage, battery charge/discharge cycles, cycling capacity fade and battery temperature are also modeled in SAM [23]. The performance of the chosen model for *greenius* is compared with SAM in chapter 4.5.

4.3.5 Charge balance model

Quaschning presented a model based on the charge balance of the battery [7]. For this model only few parameters are required to predict the battery's performance. The way it works is rather simple: The energy output from the PV module is stored in the battery until a previously defined limit, where it cannot be charged anymore. During the discharge process, the battery delivers back the stored energy into the system until a minimum state of charge that it must maintain. This model takes into account the self-discharge rate and a constant round-trip efficiency, which vary according to the battery type.

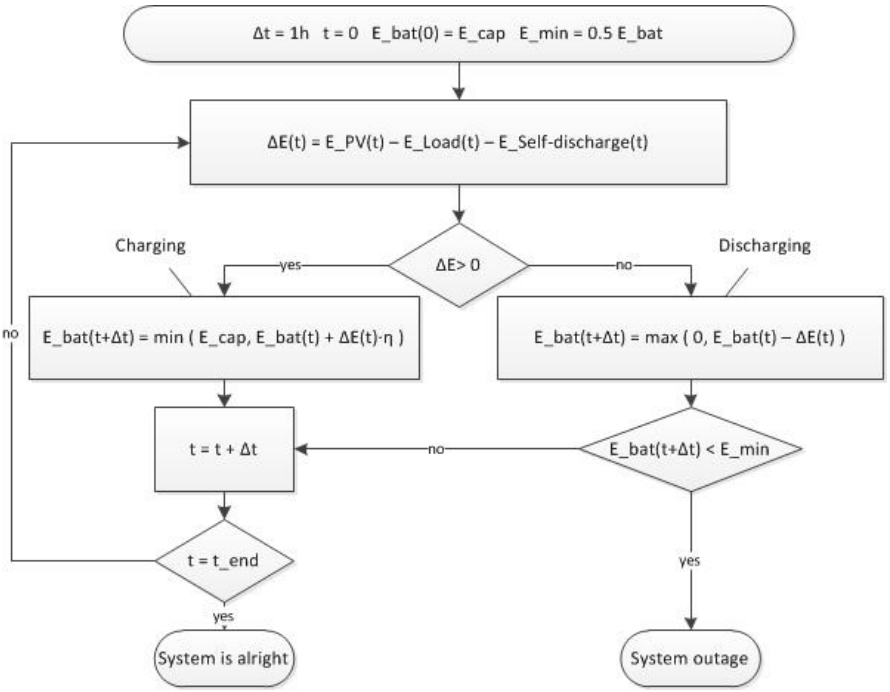

Figure 31: Charge balance model algorithm. Based on [7]

Although this model is rather simple, it represents an accurate depiction of the real behavior of the battery if more parameters are considered besides the efficiency and self-discharge; e.g. capacity degradation and allowed DOD.

4.4 Model selection and preliminary evaluation

The electrochemical models depend on several parameters, which makes them too complex for our application. The CIEMAT and PVSyst models are valid for lead-acid batteries only. They calculate the voltage as a function of SOC, current and temperatures. PVSyst requires the input of the internal resistance, open-circuit voltage and temperature coefficient of the battery. On the other hand, the CIEMAT model is already parametrized and is always valid for a 2 V cell. Other battery voltages and currents can be achieved by modelling the cells in arrays in series or parallel. The charge balance model is valid for all types of batteries and only few parameters are required. Therefore the charge balance model is considered for the preliminary evaluations, together with the CIEMAT model due to its simpler parametrization compared to PVSyst.

4.4.1 Battery dimensions

A Lead-Acid battery is tested for the Schott p-Si module already modeled in chapter 3. The PV module Schott p-Si 250 W is used for the location of Almeria, Spain. The results from the *greenius* Excel calculations shown in chapter 3.1.6 are used as PV output. The constant electric load is 100 W. When the PV panel power output is higher than 100 W, the exceeding energy is stored in the battery. During afternoon and night when the PV panel delivers less power than 100 W and the battery was charged, the battery could supply the difference. Thus the battery can dispatch the constant 100 W until it reaches the permitted DOD. The battery has the following boundary conditions:

- Round-trip efficiency: 80%
- Depth of discharge: 50%

- Nominal watt-hour capacity: 1.26 kWh
- Self-discharging rate: 5%/month (<0.01 %/h)
- Capacity deterioration: 0.37%/month (8 years until 70% capacity)

For the CIEMAT model additional battery parameters are needed, such as the nominal capacity in Ah. The data from a 50 Ah Fulmen EF2050 battery is used, same as in Copetti et al [115]. In order to have 1260 Wh the battery should consist of 12 Lead-Acid cells in series to have a total voltage of 24 V. The nominal capacity should be 52.5 Ah to reach the required 1260 Wh.
The PV module nominal voltage is 30.8 V; therefore 24 V is a first estimate for the battery. The PV panel should be able to supply the electricity needed to the battery even at low irradiances and high temperatures. The Fulmen EF2050 Battery has the following parameters according to its data sheet:

- 50 Ah nominal capacity
- Cut-off voltage at 1.6 V
- C_{10}: 55 Ah

Tension de fin de décharge 1,60 V

Eléments	Autonomie							
	15mn	30mn	1 h	2 h	3 h	5 h	8 h	10 h
EF 2050	60	42	27	17	13	9	6,2	5,5
EF 2075	90	63	40	25	19,5	13,5	9,3	8,2
EF 2100	120	84	54	34	26	18	12,5	11
EF 2150	180	126	81	51	39	27	18,7	16,5
EF 2200	240	168	108	68	52	36	25	22
EF 2250	300	210	135	85	65	45	31	27,5

Figure 32: Discharge current as function of discharge time for a Fulmen EF2050 Battery.

4.4.2 Charge balance model results

Quaschning's charge balance model is implemented in Microsoft Excel for the preliminary evaluation. The results for a typical day in summer are shown in Fig.33.

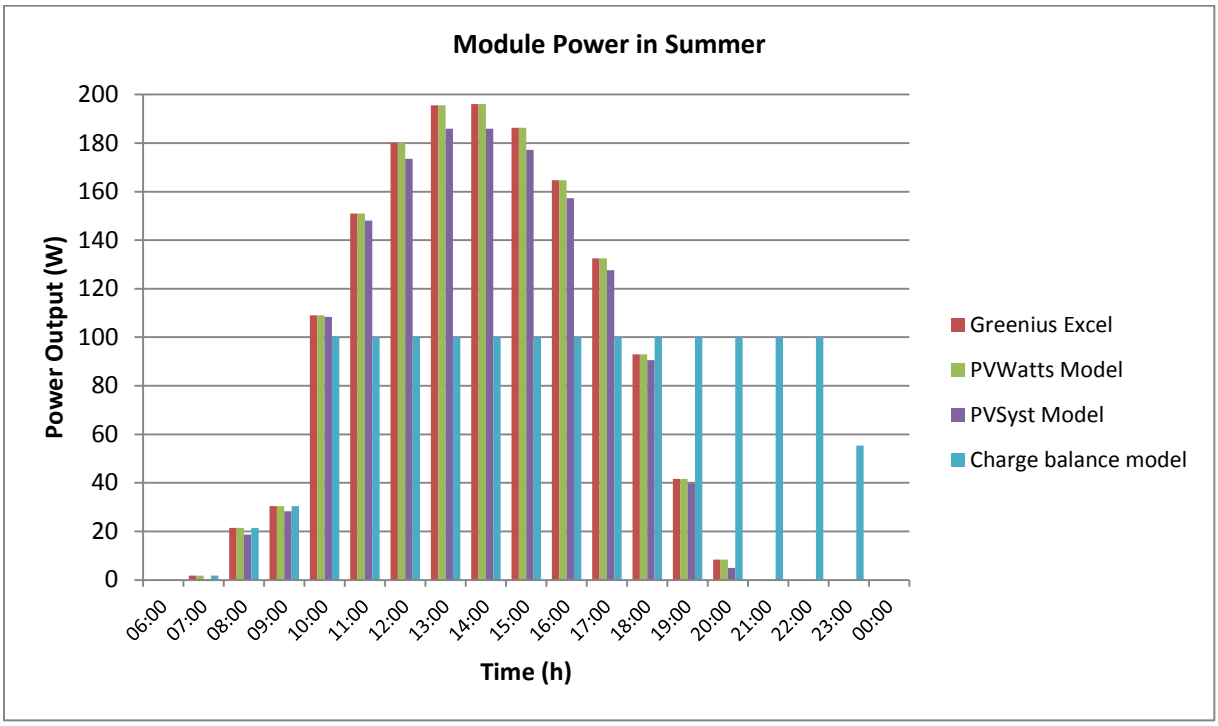

Figure 33: Oversized battery PV system with 6h storage on a typical summer day

For a constant 100 W dispatch and long supply time a big battery is needed that can account for the DOD. The maximum possible energy to be stored is 616 Wh (maximum excess energy from the PV module) and this is only possible with a battery with nominal rating > 1.25 kWh. As mentioned in chapter 4.1 the systems are usually oversized to account for the real DOD and capacity deterioration. Fig. 33 shows the results of using an oversized 1260 Wh battery. Thus with this battery selection, no electricity is dumped.

4.4.3 CIEMAT model

In order to investigate how the voltage and currents behave, the CIEMAT model is simulated. Its voltage is standard 2 V for a Lead-Acid cell. The voltage at the discharge and charge process was calculated with equations 4.2 and 4.6. The SOC was calculated using the Coulomb counting equation (eq. 4.1). The minimum SOC was set to 50%. For the total battery's voltage the cell's real voltage was multiplied by the number of cells.

Results

The results showed a SOC oscillating between 50% and 96.6%. This means a DOD of 46.6%, which is within the previously defined DOD of 50%. The cell's voltage varies between 1.91 V and 3.05 V. The lowest value causes no damage to the battery, since the cut-off voltage is 1.6 V. However, 3.05 V is higher than the gassing voltage, which is 2.39 V. These high voltages occur on June 19th between 15:00 and 16:00. In these two hours the following data is found:

Table 9: CIEMAT model results for two different time steps (June 19th)

Parameters	Time step 1	Time step 2
Time	15:00	16:00
Temperature	18°C	18°C
GHI	860 W/m^2	657 W/m^2
PV generation	200 W	152 W
Charging power	80 W	41 W
SOC	563 Wh (92%).	605 Wh (95%).

After Time step 2 the SOC reaches 96.6%, which is the maximum value for the whole year. This shows a high dependency from the voltage on the SOC. According to [29], the voltage of a lead-acid cell will always surpass the gassing voltage when approaching full charge, as almost all $PbSO_4$ has been turned into Pb or PbO_2. Hence, hydrogen will be produced and water will be lost [29]. Therefore, gassing during charging at high SOC is normal in a cell. Furthermore, the maximum battery voltage is 36 V. The panel is operating at a lower voltage than the battery voltage at this time. This means, that the PV module is not able to supply the whole amount of electricity demanded for the chosen battery voltage. Therefore a higher ratio between PV nominal voltage and battery voltage should be chosen during design.

Moreover, the discharging and charging current varies between -4.2 A and 4.5 A. These are suitable values for this battery type. As shown in Figure 32 the maximum discharging current is 5.5 A for 10h storage duration. Therefore discharging and charging rates are not a critical issue for the battery.

4.4.4 Model selection conclusions

The charge balance model is a suitable choice to simulate different types of batteries in a simple way. Therefore not only lead-acid batteries can be studied, but lithium-ion, zinc or sodium sulfur as well. The CIEMAT model cannot be used in the final model since it is only valid for a specific technology. This model was evaluated to compare the drawbacks and benefits compared to the charge balance model. One disadvantage of the CIEMAT model is that more parameters are needed, which must be carefully chosen, e.g. the voltage. If the battery voltage is not chosen properly the battery cannot operate when the PV module's voltage is too low. On the contrary, the dimensioning of the battery in the charge balance model is done according to the energy capacity [Wh].

The charge balance model is suitable for this type of applications (Stand-alone system) because the battery's charging and discharging rates are slow. For frequency control applications (transient simulations) other considerations would be necessary since discharging rates are faster, but this is not the case for *greenius*. The capacity deterioration, round-trip efficiency and depth of discharge are the most important distinguishable parameters for each battery type. The temperature could be kept constant, assuming that the battery is placed in a cooled store room.

4.5 Model comparison with other tools

The results of the charge balance model (which is called *greenius* model for further comparisons) are compared to a simulation in SAM for the same setup. The same reference module is used. No inverter losses are considered in order to ensure a simple result based on the PV module. Since there is only one panel there are no self-shading effects. The desired bank capacity is set to 1.42 kWh with a bank voltage of 24 V. The chosen battery type is Lead Acid Flooded and the cell capacity is 60 Ah. The SOC is limited between 45% and 95%. The meteorological data is taken from EnergyPlus (Almeria, Spain: Almeria 084870 (SWEC)). In SAM (Utilities model) it is only possible to select a manual dispatch controller based on hourly storage strategies. *greenius* covers firstly the load demand of 100 W before starting to charge the battery. This strategy is not available in SAM. Fig. 34 shows SAM manual dispatch model. The chosen hourly setup ensures discharge when the panel starts to decrease its electricity generation. Three different cases are modeled in SAM, as shown in Table 10.

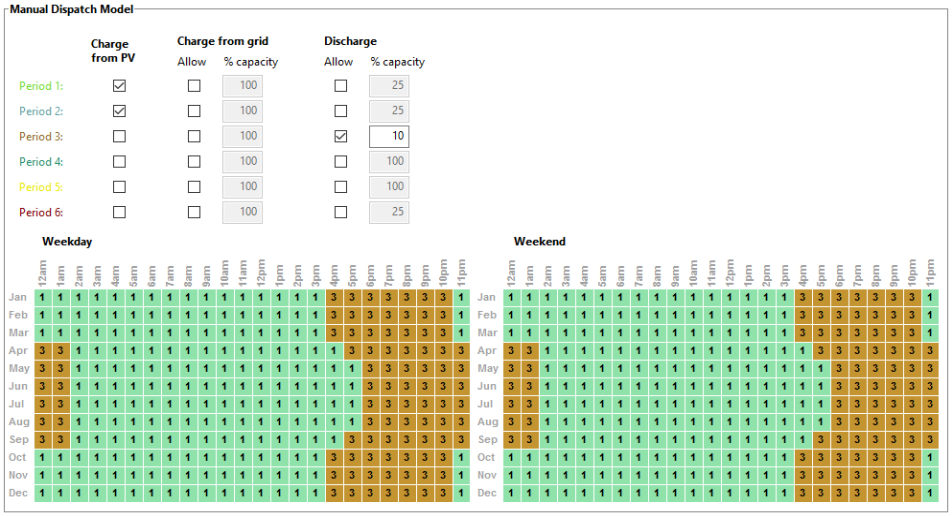

Figure 34: Dispatch control in SAM

Table 10: SAM Battery parameter variation

	Parameter Set A	Parameter Set B	Parameter Set C
Allowed capacity to be discharged (%)	10	20	10
Max C-rate of charge (%/hour)	0.3	0.3	0.1
Max C-rate of charge (A)	18	18	6

The allowed hourly discharge capacity was chosen between 10% and 20% of the nominal capacity, in order to prevent fast discharge rates. The max C-rate of charge for models A and B was left at the default value. Since in the preliminary evaluations it was shown that the maximum charge currents are smaller than 6 A, the max C-rate was reduced from 18 A to 6 A for model C.

4.5.1 Validation results

Table 11: SAM and *greenius* model annual results and SAM deviation compared to *greenius*.

	greenius	Parameter Set A	Deviation A	Parameter Set B	Deviation B	Parameter Set C	Deviation C
Battery efficiency (%)	80	83.5	4.4%	71.6	-10.5%	83.8	4.8%
Annual energy (kWh)	386	352	-8.8%	320	-8.8%	354	-8.3%
Annual energy without battery (kWh)	407	396	-2.7%	396	-2.7%	396	-2.7%

Table 11 shows that the energy generation in *greenius* is higher than SAM. The difference in the annual energy yield between both models was within 3% without battery and 8% with battery. A summer day (July 15th) with high irradiance was chosen for the analysis of the daily storage charging and discharging behavior of the systems.

Table 12: Comparison between models for one typical summer day and SAM deviation compared to *greenius*

	greenius	Parameter Set A	Deviation A	Parameter Set B	Deviation B	Parameter Set C	Deviation C
Daily produced energy (kWh)	1.663	1.615	-3%	1.496	-10%	1.628	-2%
Stored energy (kWh)	0.64	0.89	39%	0.92	44%	0.88	38%
Battery efficiency (%)	81	83.5	3%	70.8	-13%	84.70	5%

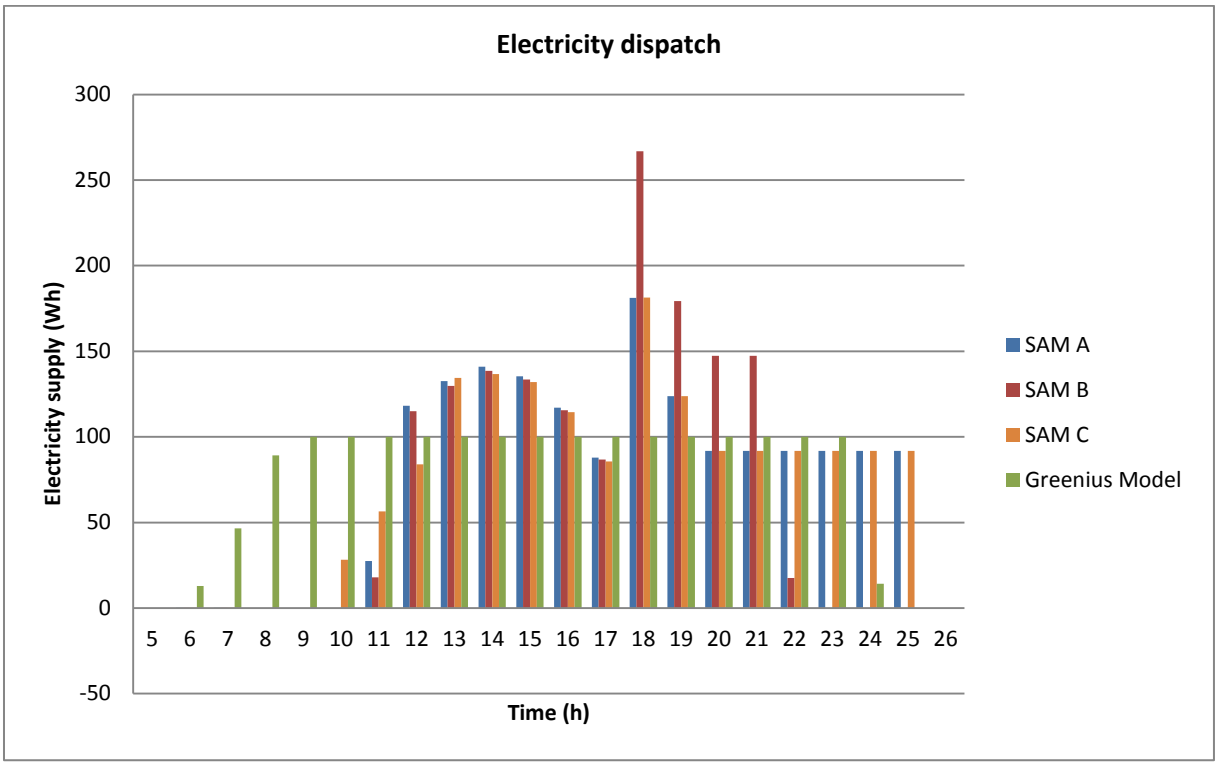

Figure 35: Electricity generation with different storage configurations

Although all 3 SAM simulations and *greenius* start generating power at 6:00, SAM is set to charge the battery first before supplying the load. At about 10:00 the three SAM models begin to supply electricity to the load and at 18:00 the battery starts discharging its energy, as specified in the operating strategy (See Fig. 34 and 35).

The daily battery efficiencies for Parameter Sets A and C are within 5% of *greenius* battery efficiency (See Table 12). The Parameter B configuration in SAM has the lowest efficiency of all configurations, with 70.8%. This is due to a higher allowed discharge rate. At high discharge rates the battery useful capacity decreases. This can be seen in Fig.35, where Parameter Set B discharge rates are higher than all other 3 simulations between 18:00 and 21:00.

The total energy being supplied on this day is similar among all simulations. Parameter Set C outcome is only 2% lower than *greenius* model according to Table 12. However, there are some disagreements between *greenius* model and SAM. These are presented in chapter 4.5.2.

4.5.2 Differences between SAM and *greenius* Model

The main difference with SAM is the stored energy. As shown in Table 12 the model in SAM can store up to 40% more than *greenius* (900 Wh), even though the maximal useful capacity was limited to 710 Wh (battery capacity = 1420 Wh and DOD = 50%). From the simulation results it is noticeable that the total electric charge reaches 63 Ah in some days, which is far off the input value (the minimum charge is 26 Ah and the maximum is 56 Ah). Moreover, the battery voltage increases to 31 V in several occasions in a year (See results for a typical summer day in Fig 36).
A possible reason for the battery to store more energy than specified is that the maximum capacity in SAM is wrongly calculated as the maximum voltage multiplied by the maximum electric charge.

A Lithium-ion battery (7 Lithium Manganese Oxide LMO cells) of the same size is also simulated with *greenius* and SAM models in order to compare both capacity and voltage models. In the *greenius* model the round-trip efficiency is changed to 90%. The DOD is kept constant. The voltage and capacity models have to be evaluated in order to understand the source of the deviations of the stored energy amount.

Problem 1: Capacity calculation

One reason for the strong capacity variation is the charge capacity calculation in SAM. The charge capacity model for Lithium-ion batteries is based on a simple tank model [23], just like in the charge balance model. The charge depends solely on the average charging and discharging current over a period of time Δt. However, for the lead-acid batteries the capacity is calculated using a different model (Kinetic Battery Model or KIBAM) [23]. This model depicts the battery as a two-tank system.

The li-ion battery in SAM is charged within its limits up to 56 Ah (95% SOC) as specified. Thus, our model matches with SAM for this battery type just as expected, since a charge balance model is used in SAM for Li-ion as well. However, the deviation in the stored energy amount between *greenius* and SAM is still considerably large, i.e. 28%. The main effect for the deviations between *greenius* and SAM is therefore the voltage model.

Fig.36 shows the voltage, electric charge and electricity dispatch from/to the battery for both battery types in SAM. The lead-acid total charge reaches 63.4 Ah and the lithium-ion reaches 56.5 Ah at 17:00. Moreover, it is shown how the voltage fluctuates during charging. Fig.37 shows only the voltage and electric charge for a better comparison between both battery types.

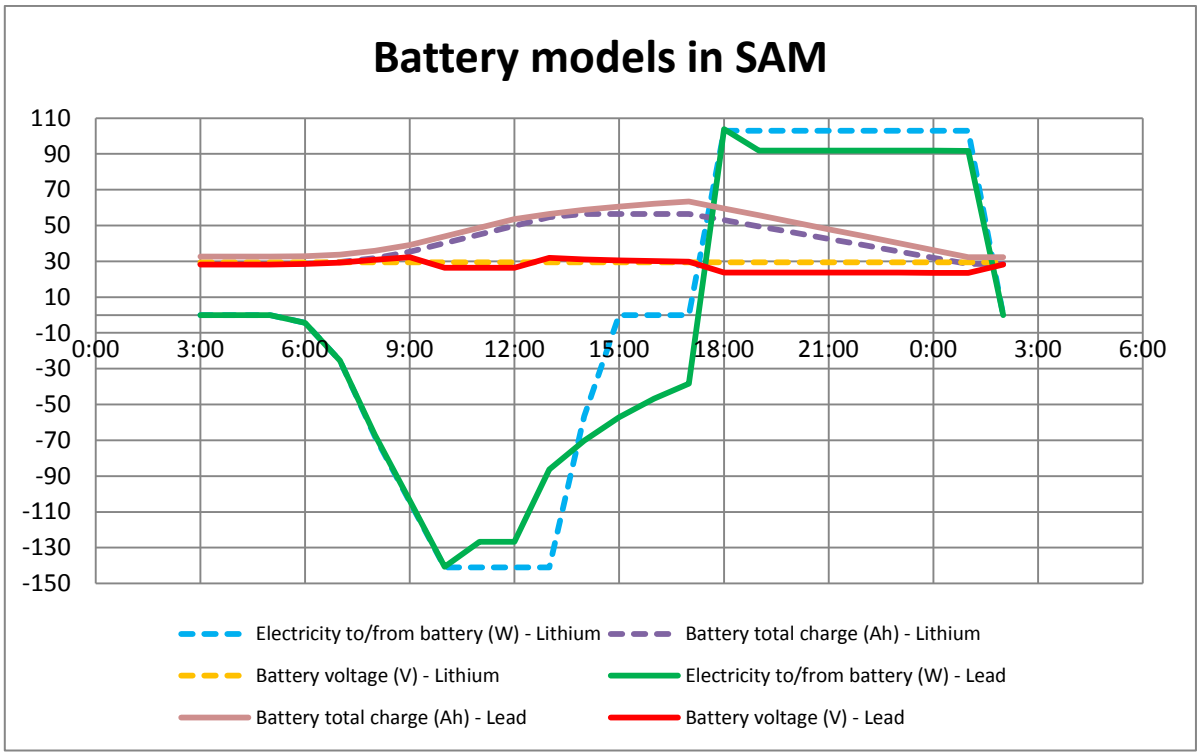

Figure 36: Voltage, Charge and Electricity Input/Output of Li-ion and lead battery in SAM for a typical summer day. Negative electricity values represent charging power and positive electricity values represent discharging.

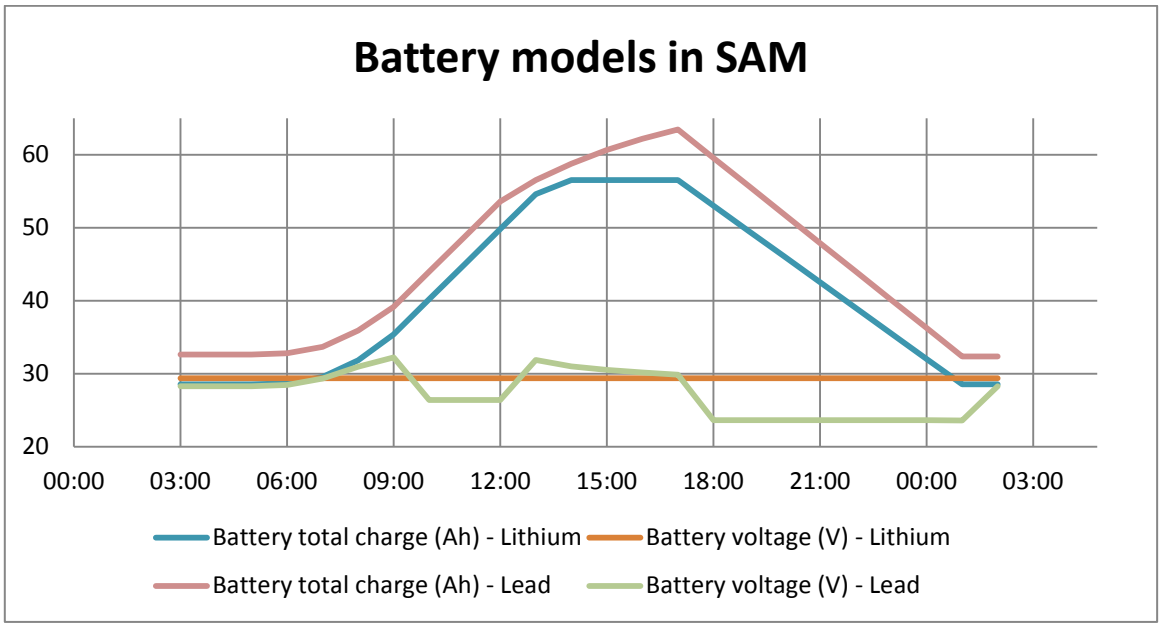

Figure 37: Voltage and Charge of Li-ion and lead battery in SAM for a typical summer day.

Problem 2: Voltage calculation

The voltage model for both battery types in SAM is a function of current, capacity, SOC and several other factors describing a voltage discharge curve [23]. The results showed that the lead-acid cells are not operating at the nominal point (24 V).

According to SAM, the nominal point for a flooded lead-acid battery is located at 10% SOC. As mentioned in Chapter 4.1 there is no agreed definition of the nominal voltage. Therefore the assertion of SAM could not be validated. For an SOC between 50% and 80% the lead-acid battery iss operating at a fully charged cell voltage of 26.4 V (See Fig.37 between 11:00 and 12:00). Below and above this range (9:00 and 13:00 to 15:00) the voltage increases abruptly to 31.3 V. This behavior does not match with a typical voltage – SOC curve. Instead, the voltage should decrease at low SOC values, as pointed out in chapter 4.1.

On the other hand, the li-ion battery results show a constant 29.4 V (See Fig.37), thus contradicting the voltage model presented in [23]. 29.4 V is the fully charged voltage of this lithium battery. This value is constant over the whole year, meaning that even during discharge times the voltage is kept at the fully charged power point, hence completely neglecting the nominal region.

The high voltages in both battery types are the main reason for the deviation in the stored amount of energy between *greenius* and SAM, since the battery capacity in SAM is calculated with the maximum voltage instead of the nominal battery voltage.

4.5.3 Model evaluation conclusions

The discrepancies between the Lithium-ion and the lead-acid battery in regard to the voltage are the reason SAM could not be used to completely validate our model.

As a relatively simple tool with focus on annual yield calculations *greenius* should keep the nominal voltage constant over the specified SOC range. The SOC range for both types of batteries is chosen accordingly to avoid problems with high voltage fluctuations and capacity deterioration, as seen in Figure 38. It is therefore assumed that the nominal voltage is constant on the specified operating range of the battery. The higher voltage needed for charging is well depicted in our model by using the round-trip efficiency value on top of the discharge curve; i.e. all efficiency losses are subtracted during charging. Therefore the energy stored and available to be discharged is already less than the energy required to charge the battery. Thus, our model is a simple but sufficiently accurate representation of the storage capabilities of a battery.

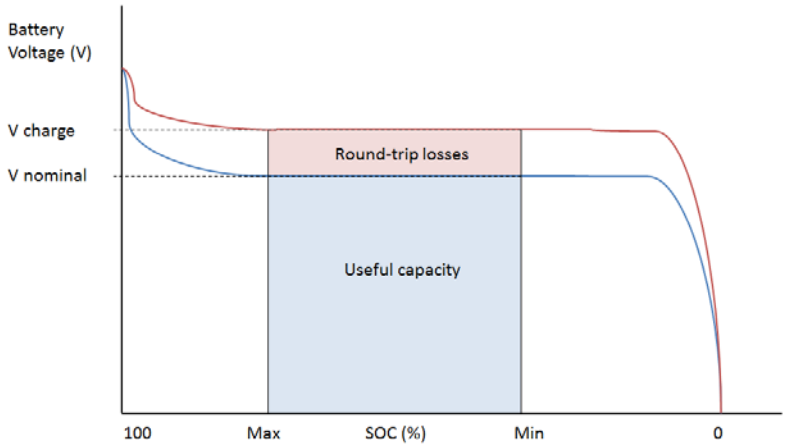

Figure 38: *greenius* model assumptions

4.6 Model Implementation

4.6.1 Software preparation

For a CSP plant in *greenius*, the energy dispatch system is done through a central control element. This distributor has the task of controlling the heat flows from the different sources and consumer elements. The sources are the solar field, burner and thermal storage. The consumers are the power block as well as the storage during charging mode. Analogously, an electricity distribution matrix was implemented using an AC topology for the battery element (See Fig. 39).

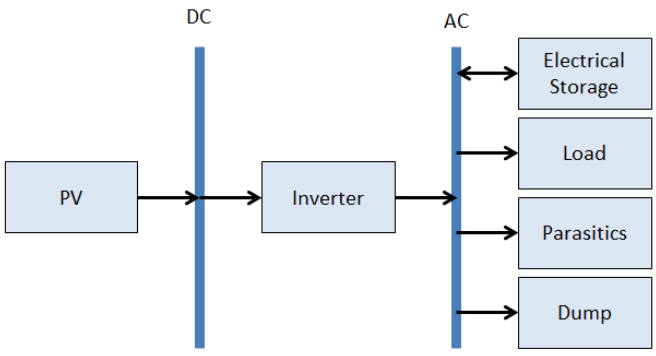

Figure 39: PV-Battery topology

The implemented central control element is shown in Fig. 40. With this configuration, it is possible for the PV generator and battery to supply electricity for the consumer (Load) with a flexible operation strategy. The electrical storage element implemented is described in Chapter 4.6.2.

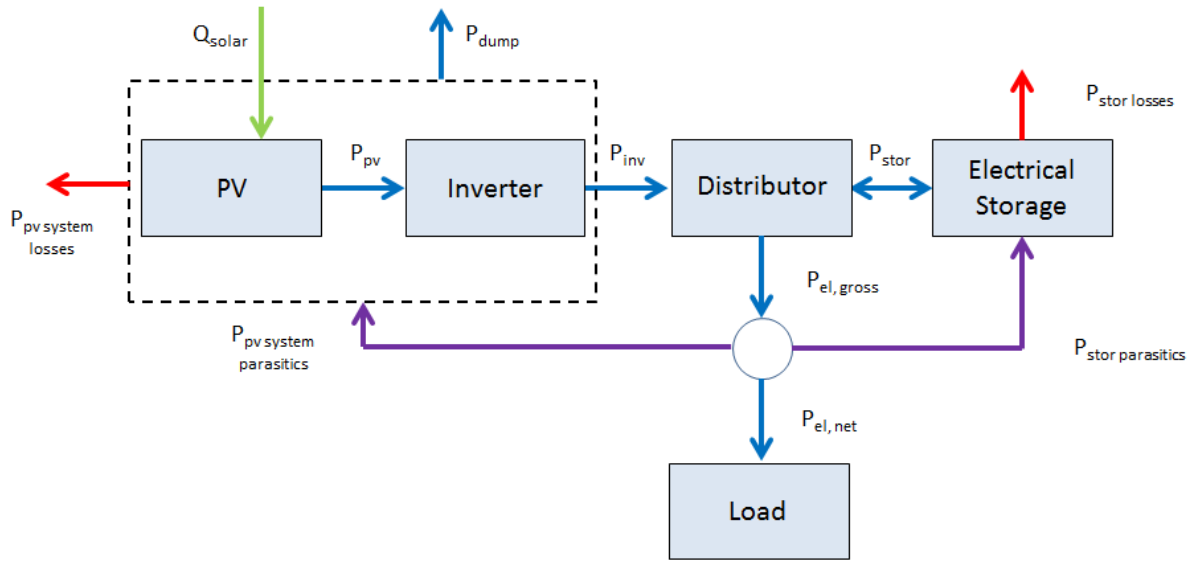

Figure 40: Central control element for electrical energy transfer

4.6.2 Final implementation

The electrical storage element was implemented based on the existing thermal storage element. It was configured to be a part of the PV technology type (See Fig. 41). The main difference is the capacity input. In the thermal storage model the net capacity is entered, whereas for the battery model the input value is the nominal capacity. The main advantage of defining the nominal capacity instead of the net capacity is that many different batteries with the same nominal rating can be compared by adjusting their allowed DOD, storage efficiency and self-discharge losses. Moreover, the specific battery costs provided from manufacturers are always given in €/kWh$_{Nominal}$. The net capacity is calculated as the nominal capacity minus the minimal content. The resulting net number of full load hours can be seen in the GUI (See Fig.42).

An additional annual capacity degradation feature was implemented. The total capacity loss over the battery lifetime is defined as the difference between the nominal capacity and the allowed residual capacity. The annual capacity degradation is calculated dividing the total capacity loss by the lifetime. In order to keep a constant DOD over the lifetime, the minimal content is also reduced by the same degradation factor each year of the project.

Due to the fact that batteries have a shorter lifetime than thermal energy storage, an additional element was included in the cost sheet in order to include the replacement costs at any year during the project's lifespan.

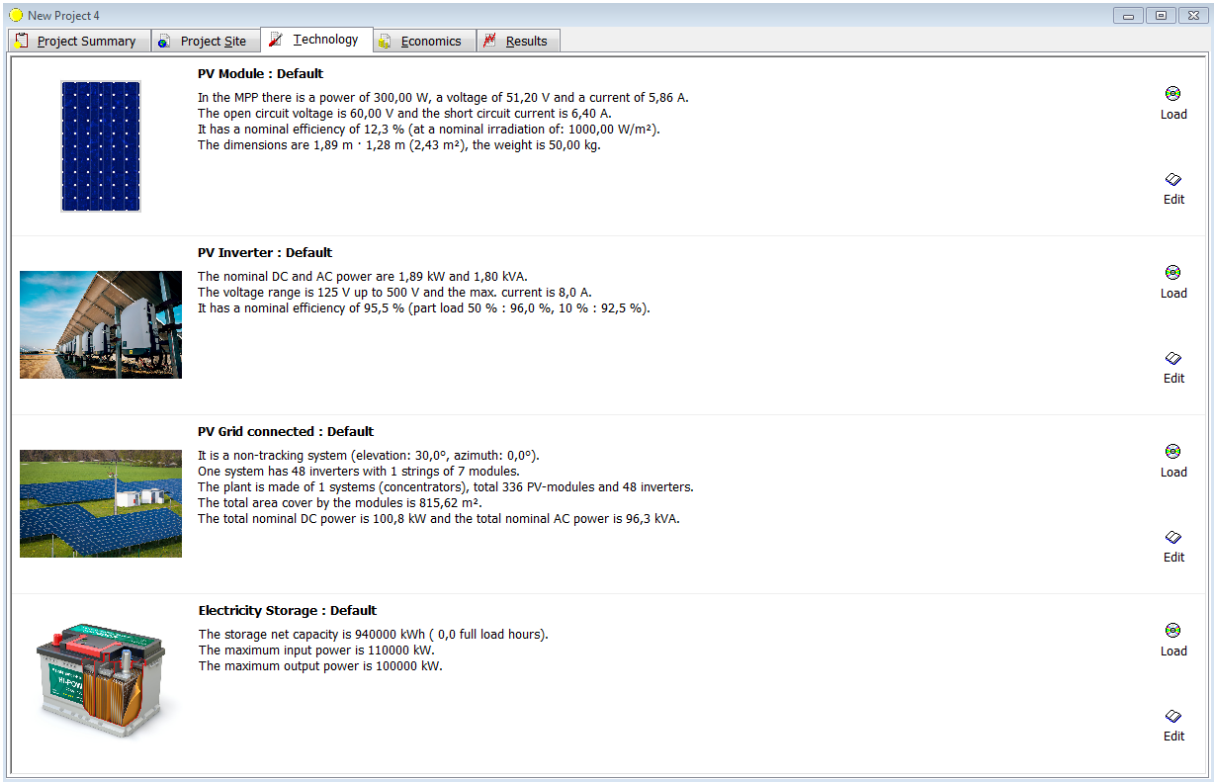

Figure 41: PV technology GUI

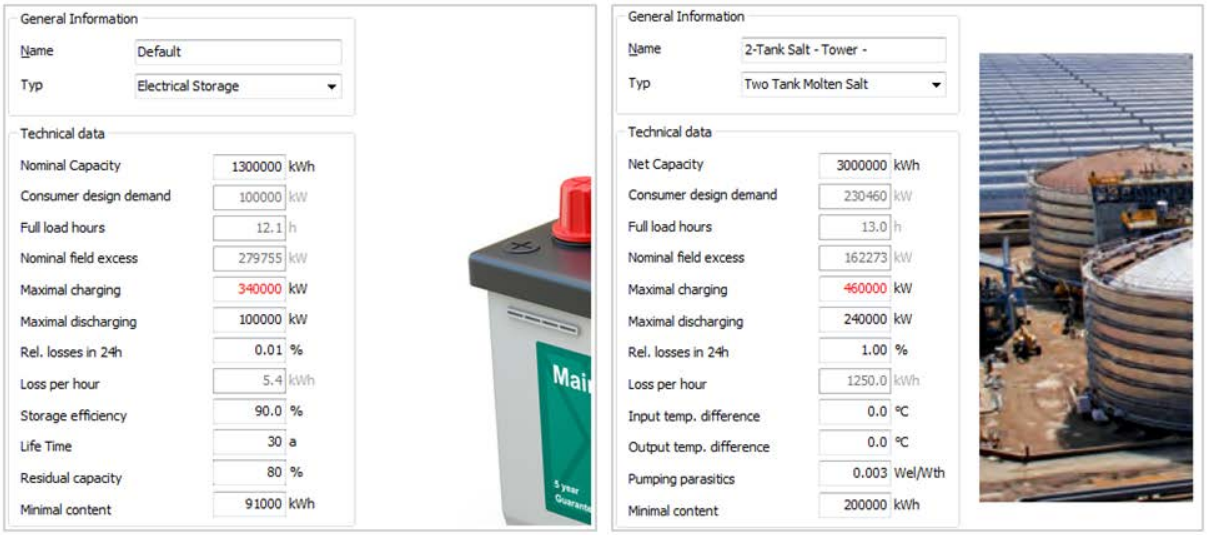

Figure 42: Comparison between thermal energy storage and electric storage in *greenius*.

Battery costs are commonly separated in energy costs and power costs but for the program a single specific cost value should be inserted. This is calculated with equation 4.10:

$$K_{spec} = \left[K_{E,spec} + \frac{P}{c_{DOD}} \cdot K_{p,spec}\right] \tag{4.10}$$

With:

- K_{spec} : Unified specific capacity and power costs in €/kWh
- $K_{E,spec}$: Specific nominal capacity costs in €/kWh

- $K_{p,spec}$: Specific power costs in €/kW
- P : Battery maximum power in kW
- C_{DOD} : Nominal capacity in kWh

The upgraded PV model with battery is used in the following chapter for the techno-economic analysis of hybrid PV/CSP systems.

5 Techno-economic evaluation of a hybrid PV/CSP plant

The aim of this chapter is to model and optimize a hybrid PV/CSP for a location with high irradiation levels. The main optimization criterion is minimizing the LCOE. Capacity factors of at least 90% are sought. The capacity factor is defined as the ratio of actual electrical energy output over a period of time (e.g. a year) and the maximum possible electrical energy output over this period of time at a certain power. The maximum possible energy output is defined as the resulting energy yield of the plant operating continuously at full nominal power. To analyze its financial feasibility the hybrid solution is compared with a PV system with electric batteries and CSP plant with the same capacity factor.

The cost assumptions are shown in chapter 5.1. The plants designed in this chapter are based on the hybrid plant Cerro Dominador in Chile. The plant's specifications are shown in chapter 5.2. As a first step, both PV and CSP part of Cerro Dominador are simulated in order to calculate the maximum power output without any load constraint. This is useful to validate the model, since the results can be compared to the PPA from Cerro Dominador. If there are no load constraints there is a power peak during daytime when both plants can generate electricity, followed by a night dispatch from the CSP plant. However, as explained in chapter 2.5.1 PV power is saturating the grid in northern Chile by day, therefore CSP offers high value for the grid due to its capability to dispatch power at night. A CSP/PV hybrid dispatch mode could reduce the power costs during daytime generation compared to a standalone CSP plant, therefore reducing costs altogether. Meanwhile the CSP/PV hybrid dispatch could extend the number of annual full load hours compared to a CSP plant.

In chapter 5.3 an optimization is carried out to find out the standalone plant variations that could compete with the hybrid configuration. In chapter 5.4 the hybrid solution is designed and subsequently all configurations are analyzed. The complete technical and financial parameters used for the simulations in this chapter are found in the annex A1-3.

5.1 Cost assumptions

The specific costs for PV are updated to 2017. For a one-axis tracked 100 MW plant the costs are 1110 US$/kWp or 1041.8 €/kWp [116].[3] The average LCOE for a 100 MW PV plant between 2010 and 2017 and a cost projection for 2025 from [11] are plotted in Fig.43. With the help of this graph, a cost assumption for 2032 is made in order to evaluate the costs of PV for the future as well. The results are shown in Table 13.

Table 13: Cost assumptions for the PV plant

PV Costs	Unit	2017	Cost Reduction	2025	Cost Reduction	2032
Specific Investment Costs	**€/kW**	1042	-31%	730	-14%	630

[3] Based on the average exchange rate of the first quarter of 2017: 1 US$ = 0.93856 € (https://www.oanda.com/lang/de/currency/average)

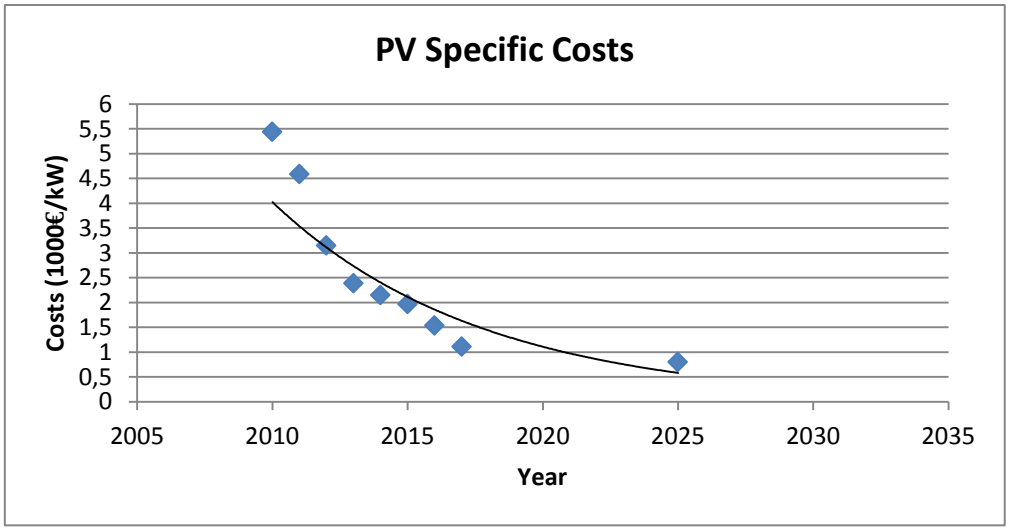

Figure 43: Average PV specific costs between 2010 and 2017 from [116]. Projection for 2025 from [11]

The costs for 2025 decrease by 31% compared to 2017. For 2032 a conservative assumption is made, since the learning curve is reaching its asymptote after 2025. The costs for 2032 are estimated at 630 €/kW. The battery costs are also estimated. According to the information presented in Chapter 2.4.4 all battery performance indicators from [109], [32], [34], [35] and [117] are analyzed in order to have standardized values for the cost evaluation. The sources provided different information and projections from 2013 to 2030. The values for efficiency, DOD, lifetime, self-discharge and costs were plotted against their reference year and the trend lines were identified. From these trend lines standardized values for 2017, 2022 and 2032 were selected and summarized in Table 14. For data series with high dispersion or no representative information, the parameters were chosen according to the most recent values. This was the case for lead-acid batteries (efficiency, DOD and self-discharge), where some of the data from the sources was outdated. The energy cost trend line is shown in Fig. 45 as an example of how the trend lines were made. All values from the reference studies are shown in the annex A4.

Table 14: Battery parameters summary

Parameter	**Units**	**Lead-acid**			**Lithium-ion**		
		2017	**2022**	**2032**	**2017**	**2022**	**2032**
Round-trip efficiency	**%**	80	80	80	90	91	93
DOD	**%**	50	70	80	93	95	98
Lifetime	**a**	12	14	17	14	18	23
Self-discharge	**%/month**	4	3	2	4	1	1
Energy capacity costs	**€/kWh**	155	110	68	391	254	157
Power costs	**€/kW**	152	129	83	161	131	72

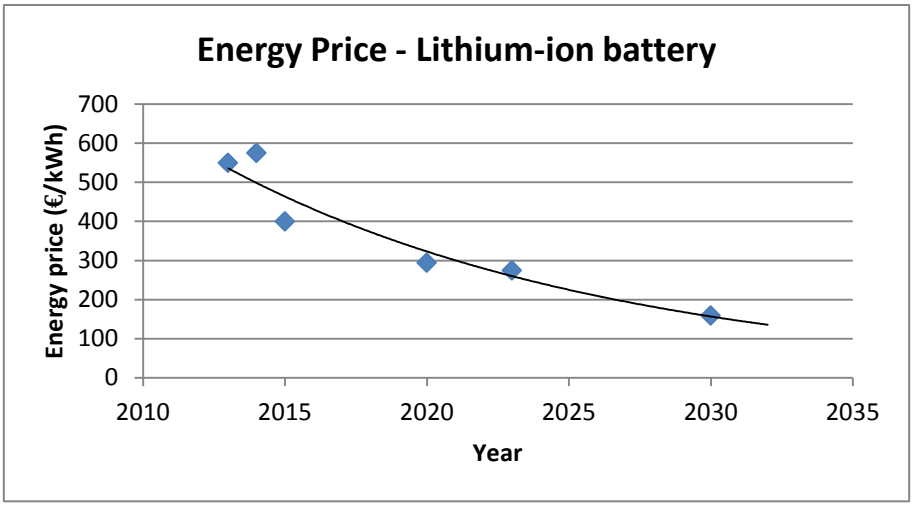

Figure 44: Lithium-ion battery cost evolution (Specific energy capacity costs).

Additionally, the CSP costs are summarized in Table 15. The specific costs for 2017 are the default values from *greenius*. They lie between the values of two studies from 2016 [118] [119]. The projected CSP cost reduction between 2015 and 2025 is described in [118]. Heliostat costs should decrease by 28%, whereas receiver and tower costs sink by 20%. The power block and storage costs decrease by 13% and 15% respectively.

Table 15: Cost assumptions for the CSP plant

CSP Costs	Unit	2017	Cost Reduction[4]	2025	Cost Reduction[5]	2032
Heliostat field	**€/m²**	150	-28%	108	-19%	87
Central receiver	**€/kW**	131	-20%	105	-14%	90
Tower	**€/m**	94000	-20%	75200	-12%	66000
Power block	**€/kW**	1328	-13%	1150	-7%	1065
Thermal Storage	**€/kWh**	27	-15%	23	-12%	20

A study from IRENA shows a cost breakdown for a 100 MW net plant for 2012 [120]. However, single component costs such as for the central receiver or tower are not listed. Since not enough information about all these single costs before 2015 was available, it was not possible to find a characteristic cost function. Therefore a simplified approach was used:

There are two extreme cases for the cost evolution that can happen until 2032. The costs could either continue decreasing linearly or the learning curve is at its end in 2025 and the costs do not longer change. Both cases are not exactly realistic, therefore a conservative scenario is chosen by selecting a middle value between these two cases. Fig.47 shows an example, where the heliostat field costs are depicted.

[4] The cost reduction values are from Dieckmann et al. [118].
[5] The cost reduction between 2025 and 2032 are calculated as the relative change between the costs for 2025 and the extrapolated costs for 2032. See explanation in pages 48- 49 and Fig.47-48.

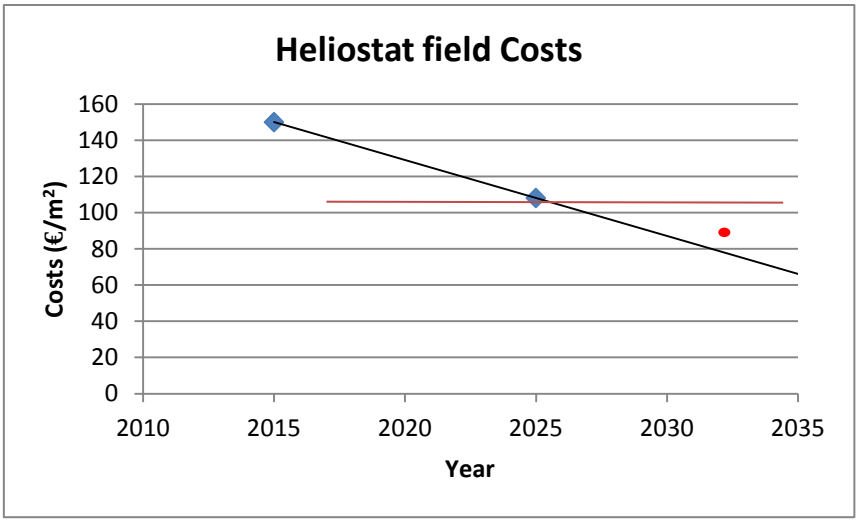

Figure 45: Heliostat cost reduction between 2015 and 2025 from [118] and possible scenarios until 2035 (Red line: constant costs; Black line: linear cost reduction; red circle: chosen value).

This simplified approach was compared with the data from Vallentin and Viebahn [121], where the investment cost projection for CSP between 2005 and 2050 was modeled. The results show that the projected value from the learning curve for 2032 can be easily calculated using this approach. This is shown in Fig.46.

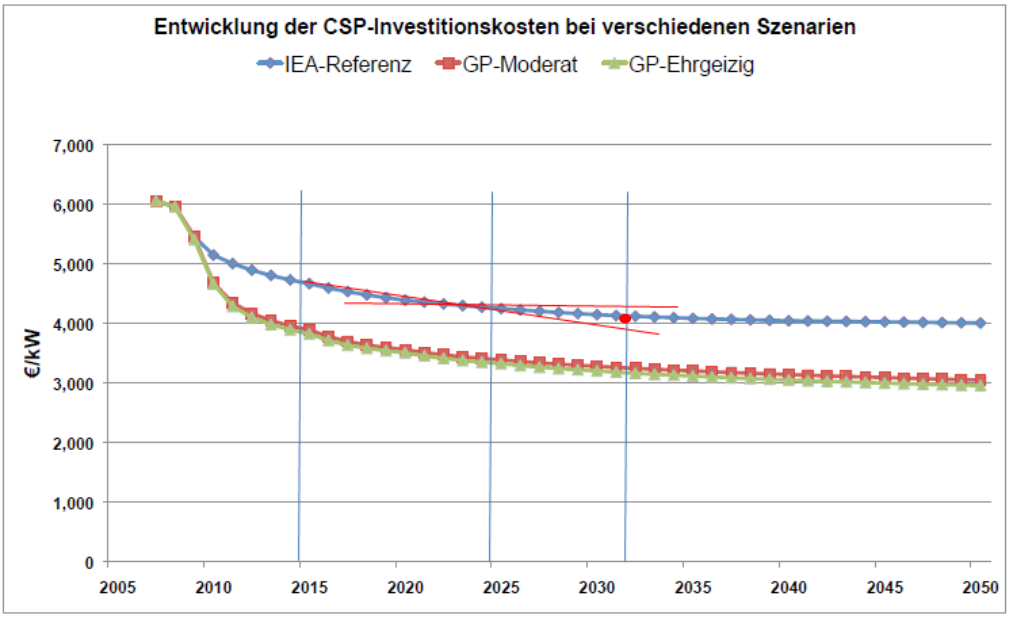

Figure 46: CSP investment cost reduction between 2005 and 2050, modified from [121].

The two red lines show a linear cost reduction between 2015 and 2025 extending to 2032 and a constant cost projection between 2025 and 2032. It can be seen that the middle value between these two scenarios (linear and constant value scenarios) for the year 2032 matches very precisely the projected value from the learning curve in blue, based on the conservative Blue Map scenario from the IEA [121]. Therefore this cost reduction assumption was used for all CSP components and the resulting values for central receiver, tower, power block and thermal storage are summarized in Table 15.

5.2 Reference plant Cerro Dominador

5.2.1 Plant specifications

Figure 47: Cerro Dominador solar tower being under construction [51]

Cerro Dominador is located at -22.77°N -69.48°E. Local weather measurements from Diego de Almagro, Chile (-26.33°N -69.98°E) are used for the simulation. It is approximately 300 km from the exact location. The climate conditions are however very similar with desert conditions. The elevation differs by approximately 500 m but the irradiance values match the typical values found for Chile's desert (up to 3800 kWh/m^2) [49]. The annual sum of the DNI is 3477 kWh/m^2 and GHI is 2449 kWh/m^2.

CSP Tower plant

A tower system with molten salts is selected. The HTF temperatures are 290 °C and 565 °C on the cold and hot side. The power block has a net output of 110 MWe. The aperture area is 1,484,000 m^2. The 2-tank salt storage is designed with 4.45 GWh capacity to achieve 17.5 full load hours.

PV plant

The nominal AC power for this plant is 100 MW. It has 392,000 crystalline modules rated at 305 Wp each [122]. A generic polycrystalline panel implemented in *greenius* is used. It is rated at 300 Wp. The plant's inverters are rated at 1000 kW$_{AC}$ [122]. A generic inverter with 1000.1 kVA and 97% nominal efficiency is used for the simulation. The optimal configuration for the chosen modules and inverters are 15 modules/string and 250 strings/inverter. There are in total 92 inverters. Thus, the total power is 100.4 kVA.

5.2.2 Results

Table 16: Cerro Dominador Plant single simulation results

Parameter	Unit	Single CSP Plant	Single PV Plant
Nominal power	**MW**	110.1	100
Annual net output	**GWh/a**	857.79	271.69
Full load hours	**h/a**	7788	2717
Capacity factor	**%**	89.02	31.0
LCOE	**€/kWh**	0.0871	0.0441
PPA @ IRR = 12%	**€/kWh**	0.127	0.066
CAPEX	**Million €**	713.97	123.41

The CSP plant with 17.5 hours TES provides a high capacity factor (89.02%) at a cost of 0.0871 €/kWh. The PV plant has 31% capacity factor, which is considerably high and is due to the one-axis tracking. As explained in Chapter 2.5.1 Cerro Dominador has a PPA agreement to sell 950 GWh/a for 15 years. Without any constraints to the energy dispatch of both plants the total annual energy yield is 1120 GWh/a. The real PPA price of the plant is 0.114 $/kWh (0.1026 €/kWh) [6]. In our simulations, the PPA for a CSP plant is 0.127 €/kWh and 0.066 €/kWh for PV at an internal rate of return (IRR) of 12%. The IRR of the CSP project is 7.45% if the energy is sold at 0.1026 €/kWh. The modeled plants can thus be validated because the sum of the energy generated is > 950 GWh/a and both CSP and PV plant make profit for a PPA price of 0.1026 €/kWh.

In order to understand how this plant could be operated in hybrid dispatch mode, the following case is analyzed: Both plants supply a constant 100 MWe load and PV has dispatch priority while the CSP storage is charged by day and the power block runs at night. The results indicate that the PV plant covers 31% of the total annual supply and the solar tower with storage covers 66.7%. As a result the sum of the energy output from both plants represents a capacity factor of 97.7%. Under these conditions the LCOE of the CSP plant rose to 0.1265 €/kWh due to the high amounts of dumping (32.5%). For an optimal hybrid power plant a smaller heliostat field is required to avoid large dumping losses. The energy output is 855.5 GWh. Thus, it is not possible to comply with the existing PPA with such a constant load.

Therefore the real supply profile of Cerro Dominador has to be somewhat different than a constant 100 MW load. An option could be to supply a constant 110 MW load, but this means that at day time the PV cannot supply the load completely by itself and the CSP power block would have to be operated at part load with significant efficiency losses. A solution for this problem could be to supply a lower load by day and higher at night with an additional increase in the power block capacity.

Since there is no published information about the load requirements for this plant, an optimization for four power plants with constant load of 100 MW is carried out in the following chapters (CSP-only, PV-only, PV with batteries and CSP+PV).

5.3 Plant optimization

To identify what are the optimal plant configurations for a standalone CSP plant, a standalone PV plant with and without battery storage and a hybrid CSP+PV plant it is necessary to optimize their field aperture and storage capacity in regard to their capacity factor and LCOE.

5.3.1 CSP Plant

Figures 48-50 show the LCOE and capacity factor for different TES capacities and heliostat field sizes of CSP with 100 MWe net power.

[6] Based on the average exchange rate between 2015 and 2017: 1 US$ = 0.90036 €
(https://www.oanda.com/lang/de/currency/average)

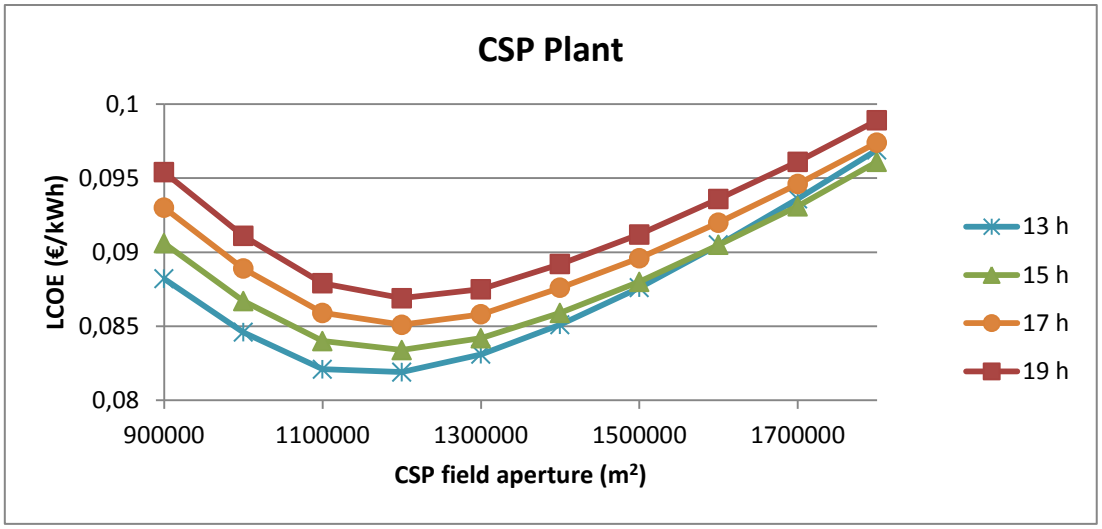

Figure 48: LCOE for varying heliostat field size and TES capacity

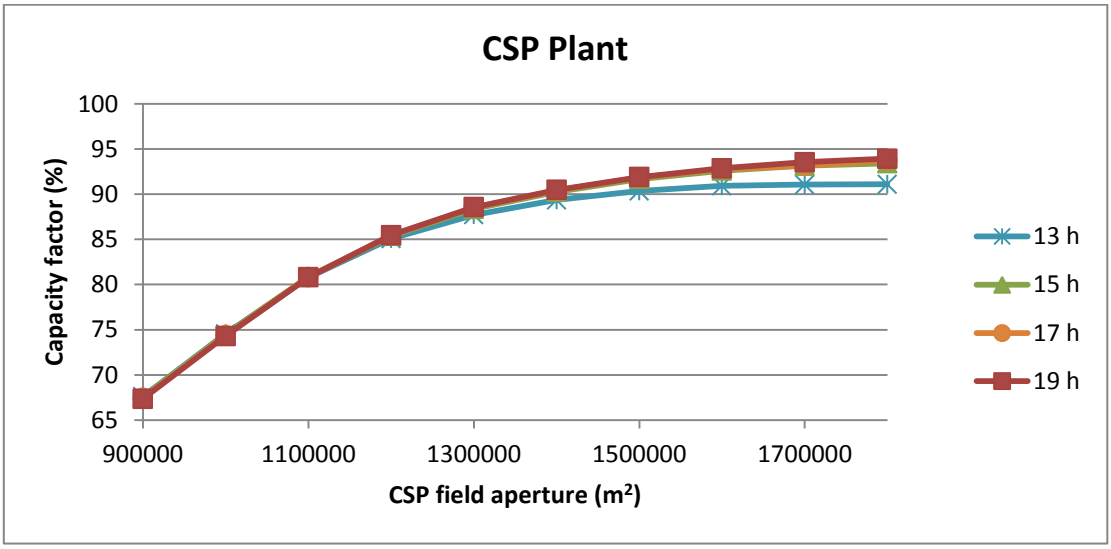

Figure 49: Capacity factor for varying heliostat field size and TES capacity

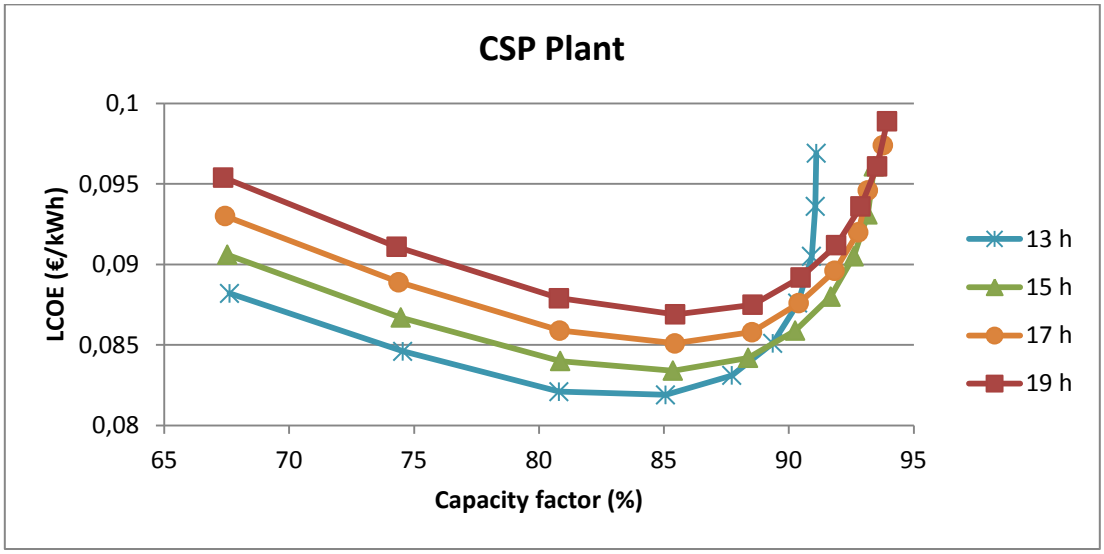

Figure 50: LCOE in relation to capacity factor with varying heliostat field size and TES capacity

The LCOE is the lowest for a plant with an aperture area of 1,200,000 m^2 and 13h TES. The capacity factor for this configuration is 85%. However, for baseload operation a higher capacity factor is needed. A larger capacity factor is bonded with higher LCOE. Therefore the optimum configuration is a trade-off between these 2 parameters. The results show that the most cost-efficient configuration with 90% capacity factor has 15h storage capacity and 1,400,000 m^2 heliostat field aperture. This corresponds to a solar multiple (SM) of 2.8. The SM is defined as the receiver power output divided by the nameplate thermal power input of the power block at design conditions. The LCOE for this plant is 0.0859 €/kWh. Higher capacity factors are only possible with exponentially increasing LCOE.

5.3.2 PV Plant

5.3.2.1 Plant without electrical storage

A PV plant without storage is simulated and the total installed AC power is varied to identify the optimal PV size for a 100 MW constant load.

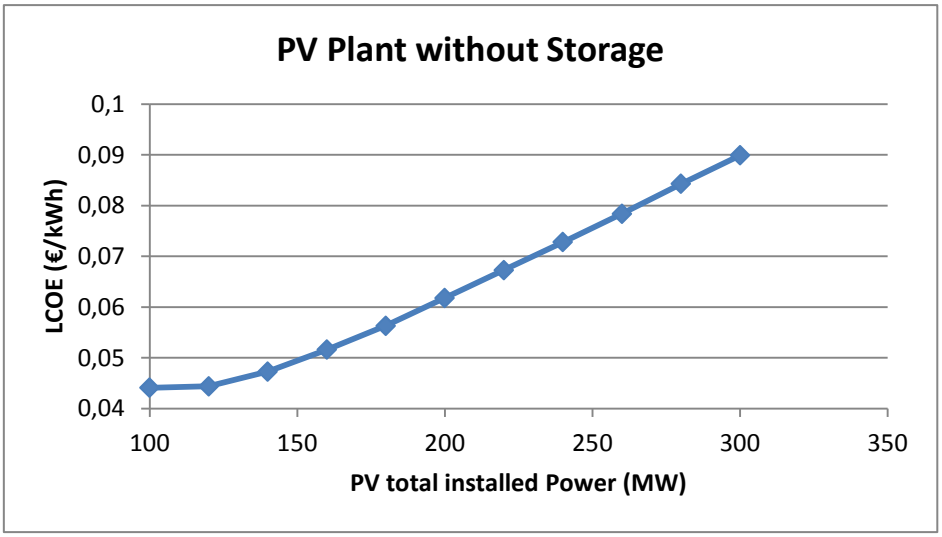

Figure 51: LCOE in relation to total installed power for a PV plant without electrical storage

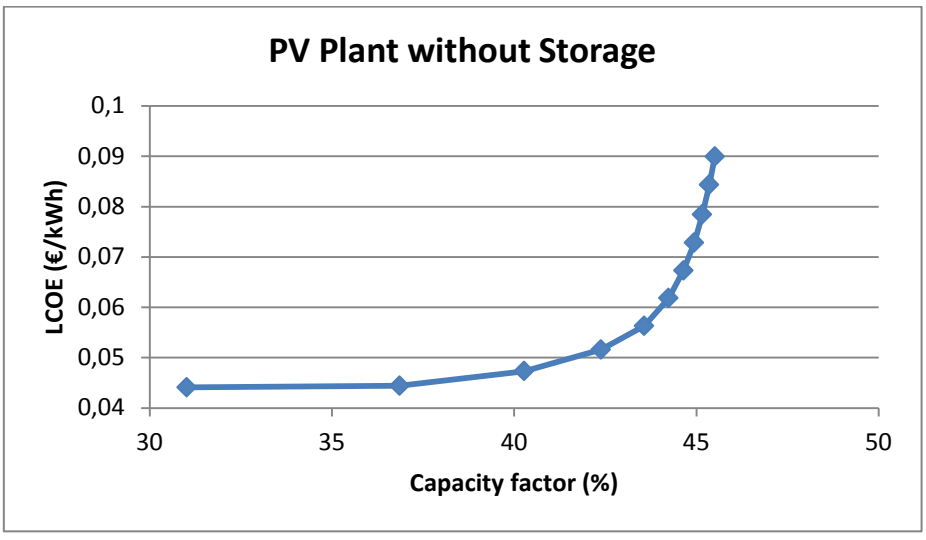

Figure 52: LCOE in relation to capacity factor for a PV plant without electrical storage

The PV plant with the lowest LCOE has 100 MW_{AC} installed power. The LCOE for this plant is 0.0441 €/kWh. There is a capacity factor increase of 19% for a plant with 120 MW_{AC} installed power, whereas the LCOE increases only by 0.7%, i.e. the LCOE increases to 0.444 €/kWh and capacity factor to 36.8% (See Fig.52).

For a 140 MW_{AC} plant the relative increase of the capacity factor is 29.7%, whereas the LCOE rises by 7% compared to the 100 MW_{AC} plant, meaning that the LCOE is 0.0473 €/kWh. In chapter 5.4 it is explained why the configuration with 140 MW_{AC} is chosen as the most suitable for the hybrid operation.

5.3.2.2 Plant with electrical storage

Moreover, a range of PV plants with different lithium-ion battery sizes and varying total installed AC power are simulated. The aim is to analyze the LCOE for capacity factors > 65%. The technical and financial parameters for lithium-ion batteries for 2017 were used in the simulation, as described in chapter 5.1. The results are shown in Fig.53-55.

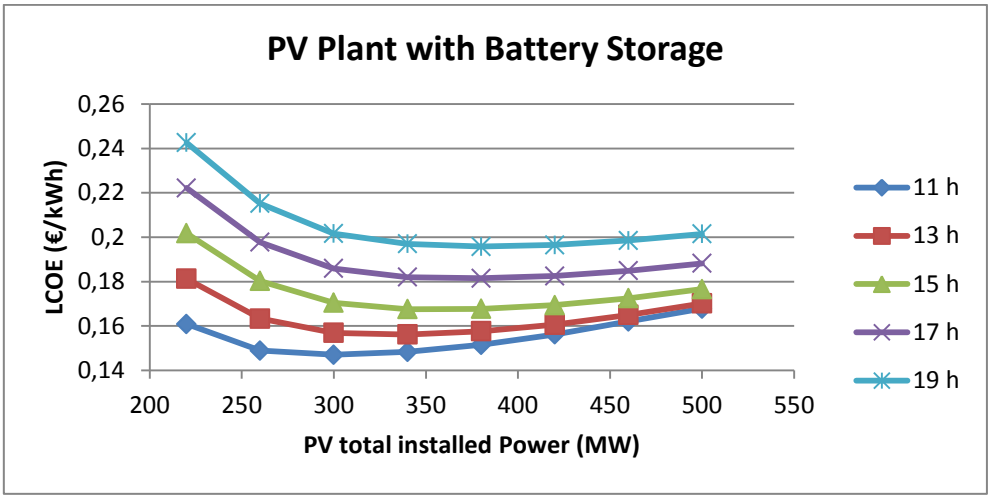

Figure 53: LCOE for varying peak power and electric storage capacity

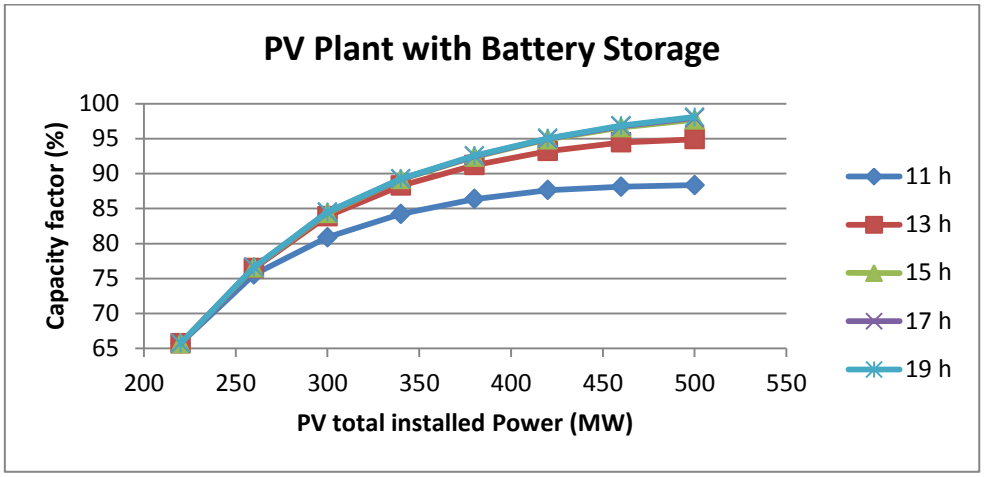

Figure 54: Capacity factor for varying installed peak power and electric storage capacity

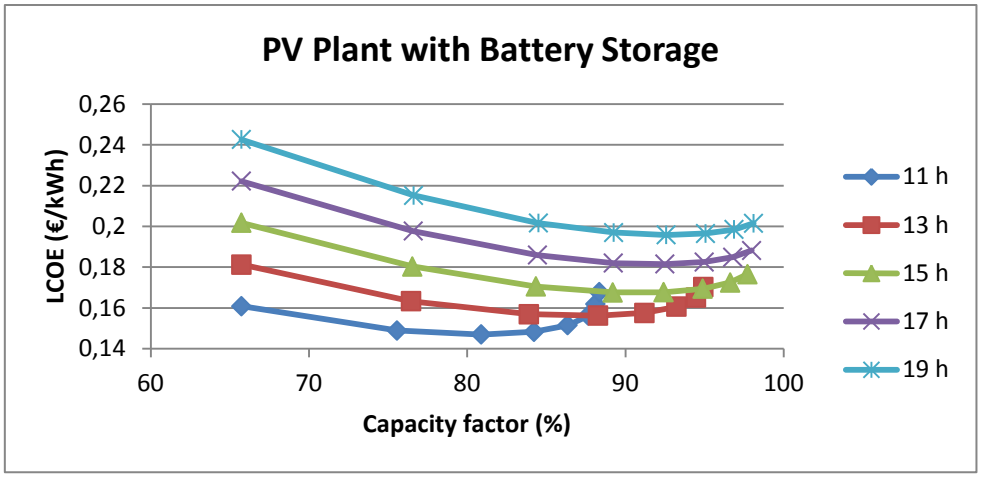

Figure 55: LCOE in relation to capacity factor for varying peak power and battery size

Fig.55 shows that the optimum storage size for a capacity factor = 90% is 13h, which corresponds to a nominal capacity of 1300 MWh. The plant must have a peak power of 340 MW in order to store the required energy in the batteries by day. The LCOE for this option is 0.1748 €/kWh, meaning that the investment costs for this plant configuration are almost four times as high as for a PV plant without any electrical storage.

5.4 Hybridization

The simulation for the hybrid power plant is done in two steps: Firstly, the PV plant is simulated and the power output is recorded. The values from the constant load curve and the PV power output are subtracted and then entered in *greenius* as the load curve for the CSP plant. Fig.56 shows the ideal load-supply curve for the hybrid operation.

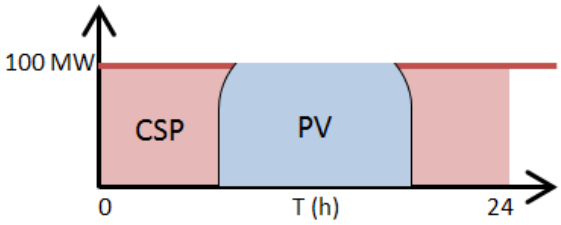

Figure 56: Ideal load curve during hybrid dispatch for a typical sunny day

5.4.1 PV Dimensioning

In chapter 5.3.2.1 it was found that a PV plant with peak power of 140 MWp has an LCOE of 0.0473 €/kWh. This configuration with 40% oversized PV field carries some advantages for the hybrid application: The PV field alone can supply constant 100 MWe in summer days for 10 hours straight (See Fig.57). This means that the power block in the CSP does not run during these 10 hours. Otherwise if the PV plant has a 100 MWp rating it rarely reaches its peak power. Therefore in such case the turbine on the CSP side has to constantly work at part load to supply the small difference needed by day. This produces higher efficiency losses. Moreover, frequent turbine startups and shutdowns increase thermal stresses and thus accelerate the material fatigue, leading to a sooner turbine replacement. Therefore the option with 140 MW installed power not only provides benefits on

the PV side alone with low LCOE and high capacity factors, but it brings economic benefits to the CSP plant as well.

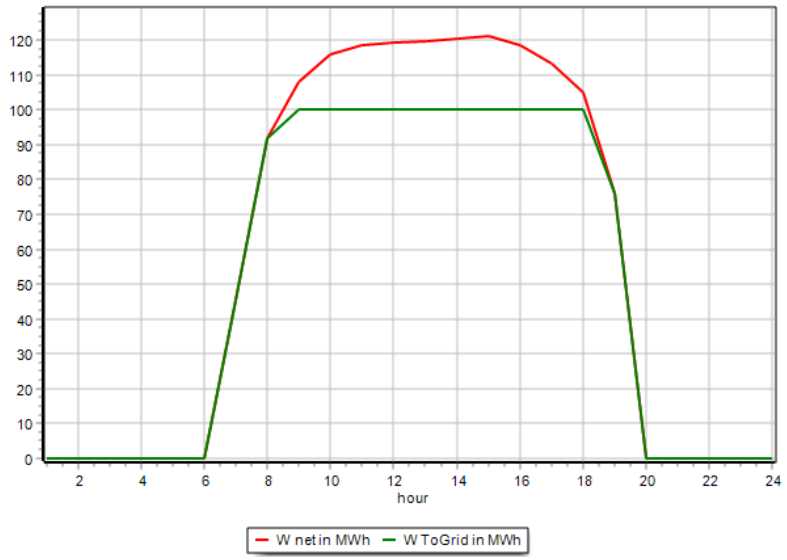

Figure 57: 140 MW PV plant daily electricity generation. Red line: Net PV system output; Green line: PV following the load.

5.4.2 Hybrid PV/CSP Optimization

After defining the PV plant size, the annual energy generation profile from the 140 MW PV plant was used to create the load curve for the hybrid CSP. The CSP plant should cover the remaining load requirements of the total 100 MW. The CSP field aperture and storage size are optimized to achieve the lowest LCOE, just as previously evaluated in chapter 5.3.1 for a CSP plant without PV. Different configurations are simulated with the storage size ranging between 13h and 19h capacity. The CSP aperture area is modified between 400,000 m^2 and 1,800,000 m^2. The results are shown in Fig.58-60. The shown capacity factors are the sum of the energy produced by both the PV plant (31%) and the CSP divided by the maximum possible delivered energy (876 GWh). The weighted average of the PV and the CSP plant's LCOE is calculated with the following equation:

$$LCOE_{Hyb} = \left[\frac{(LCOE_{CSP} \cdot E_{CSP}) + (LCOE_{PV} \cdot E_{PV})}{(E_{CSP} + E_{PV})}\right] \quad (5.1)$$

With:

- $LCOE_{CSP}$: Levelized cost of electricity of the CSP plant in €/kWh
- E_{CSP} : Annual energy generation of the CSP plant in kWh
- $LCOE_{PV}$: Levelized cost of electricity of the 140 MWp PV plant in €/kWh
- E_{PV} : Annual energy generation of the 140 MWp PV plant in kWh

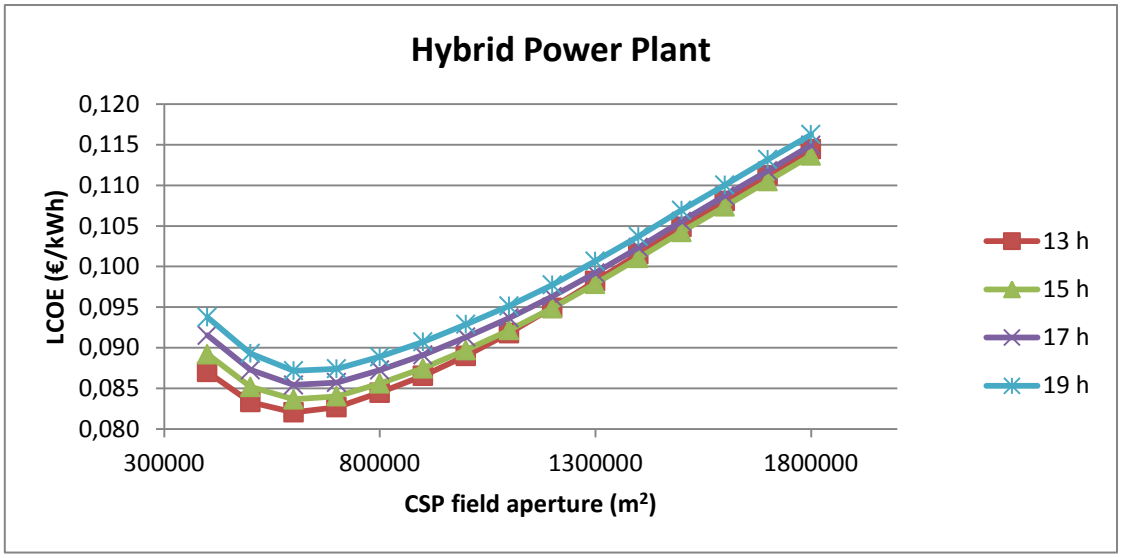

Figure 58: LCOE for varying heliostat field size and TES capacity

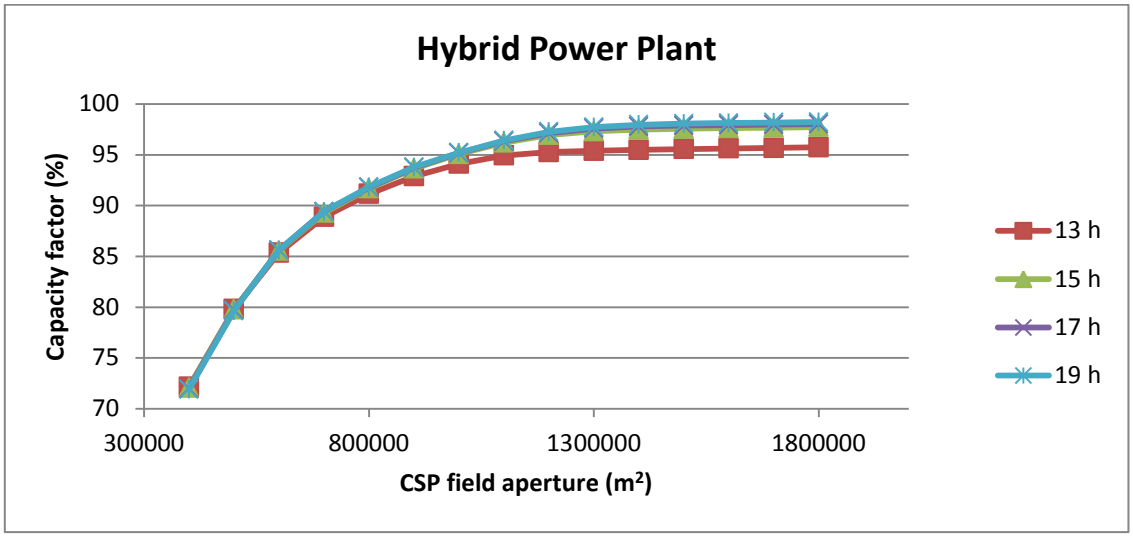

Figure 59: Capacity factor for varying heliostat field size and TES capacity

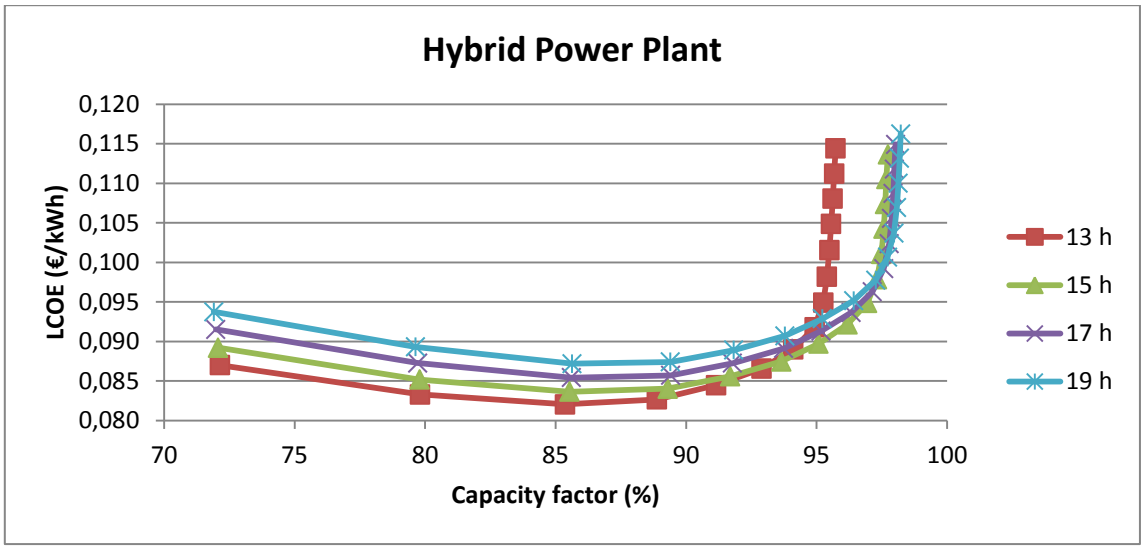

Figure 60: LCOE in relation to capacity factor with varying heliostat field size and TES capacity

Fig.59 and Fig.60 show that the most cost-efficient CSP plant with PV that can achieve 91% capacity factor has an LCOE of 0.0845 €/kWh. This plant has a TES with 13h capacity and CSP aperture of 800,000 m^2, which corresponds to a SM = 1.7. The heliostat field aperture is thus reduced by 43% compared to the CSP plant without PV and the required TES is 13% smaller. Therefore dumping in the CSP part in this case is only 22.7%, meaning a 10% reduction compared to the original design of Cerro Dominador CSP plant (See chapter 5.2.2).

Furthermore, capacity factors up to 96% which cannot be achieved with a non-hybrid plant become available with a 15h TES. In this case the optimal SM is 2.3. The CSP aperture is 1,100,000 m^2 and the LCOE for this configuration is 0.0922 €/kWh. Fig.61 and 62 show the LCOE curves of the CSP and PV/CSP plant for a better comparison.

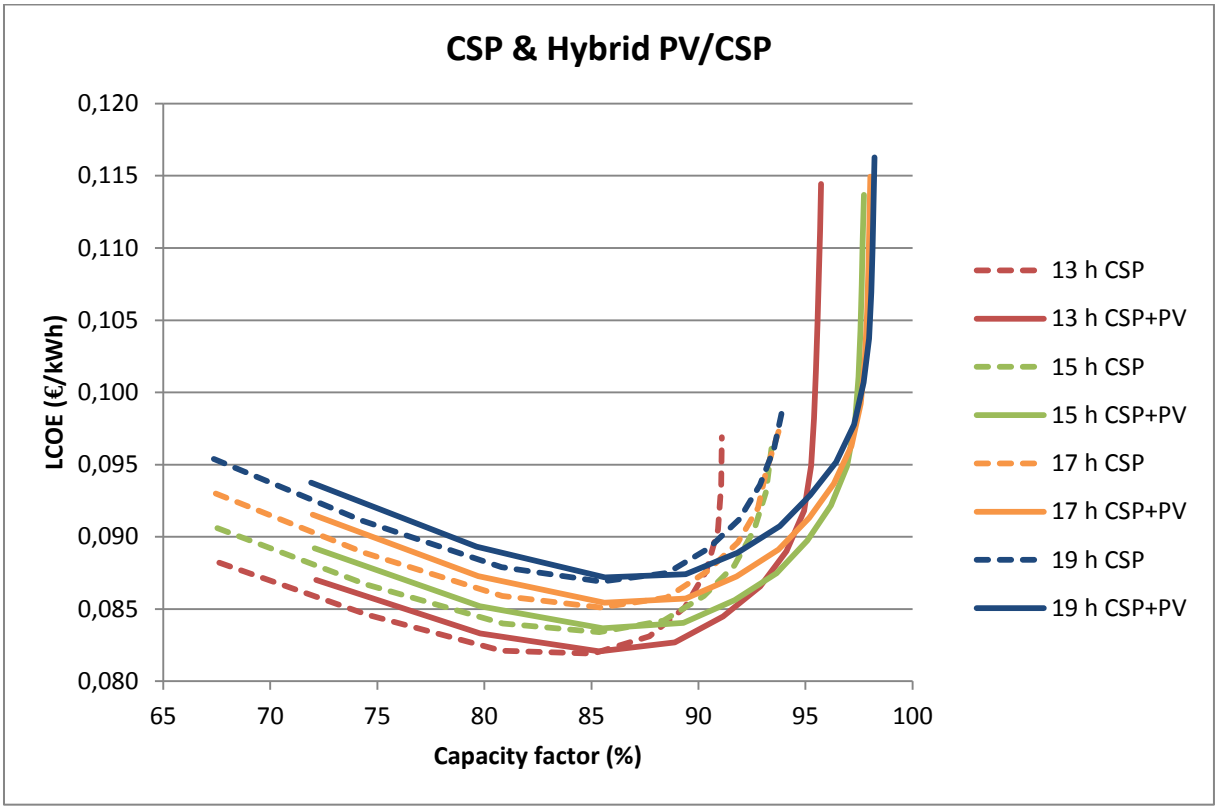

Figure 61: LCOE in relation to capacity factor for a CSP plant and a CSP+PV plant

The dotted lines represent the CSP without PV and the solid lines the hybrid power plant. Fig. 62 shows that integrating a PV plant could reduce the CSP aperture area by 38% at the same LCOE. For example a CSP plant with 15h TES and 1,600,000 m^2 aperture area has an LCOE = 0.09 €/kWh and the capacity factor is 92.6%. A CSP plant with 15h TES and PV needs only to have 1,000,000 m^2 aperture area to reach the same LCOE. As a consequence the capacity factor increases to 95.1%.

This means that the capacity factor increases by 3.5% for the CSP+PV combinations with the same LCOE (See Fig.61). Additionally, CSP plants without PV cannot reach capacity factors > 95%. The highest capacity factor achieved with CSP+PV is 98.2%, meaning downtimes of only 6.5 days a year.

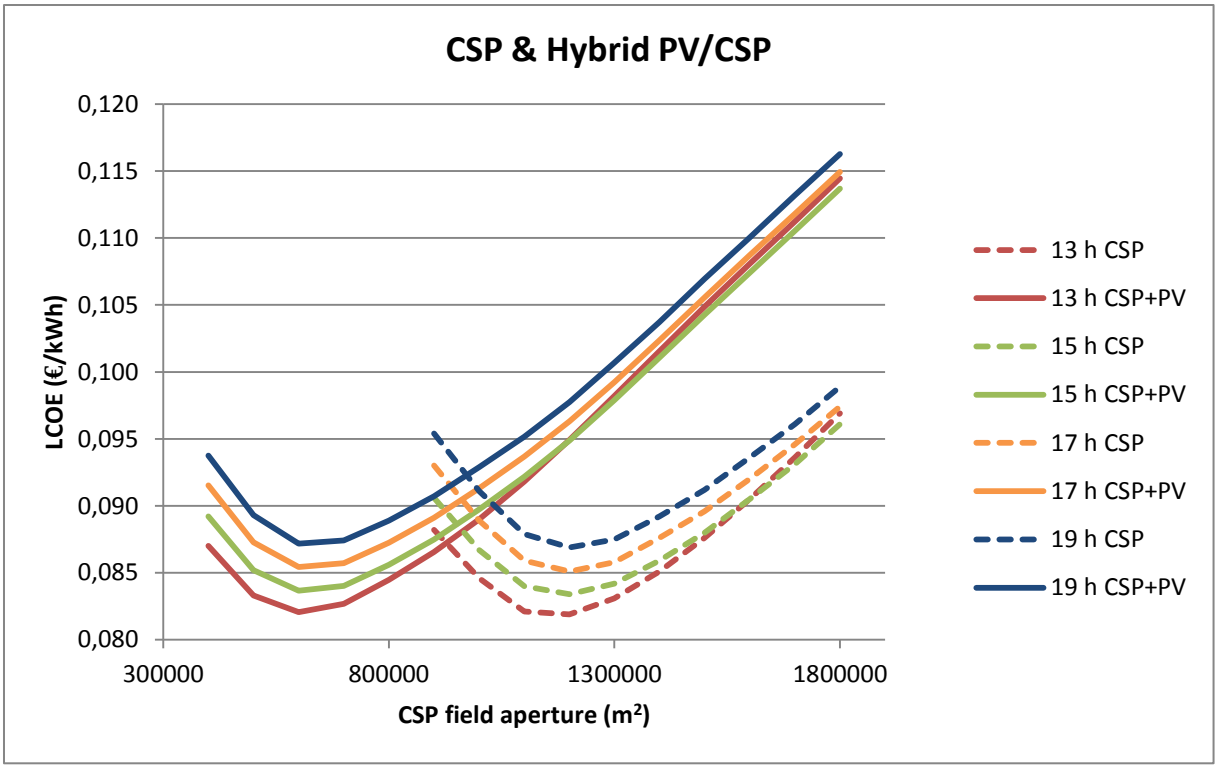

Figure 62: LCOE in relation to CSP field aperture for a CSP plant and a CSP+PV plant

5.5 Results discussion

The LCOE of the two optimized hybrid configurations with 91% and 96% capacity factors are shown in Fig.63. The optimized CSP without PV is compared to these two alternatives. The PV option with storage is too expensive (0.1748 €/kWh), therefore it is not included in the comparison.

The LCOE for the optimized hybrid PV/CSP configuration is 1.7% lower than the standalone CSP and the plant has 1% higher annual energy generation. However, the main advantage of integrating PV in a CSP plant is that higher capacity factors can be achieved while keeping low LCOE values. For a CSP plant it was not possible to have a capacity factor > 95%.

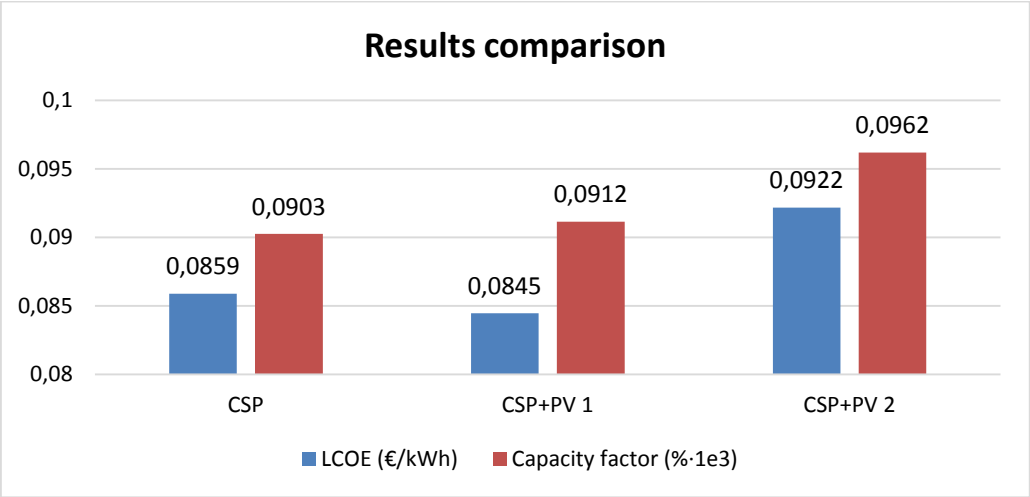

Figure 63: LCOE and capacity factors for optimized CSP and CSP+PV (CSP+PV configurations with different capacity factors)

With hybrid power plants, capacity factors > 97% with LCOE below 0.10 €/kWh are possible. The LCOE for an optimal hybrid CSP/PV plant with 96% capacity factor is 0.092 €/kWh. Although the LCOE in this case is 6% higher than the CSP plant option the total annual energy generation increases also by 6%.

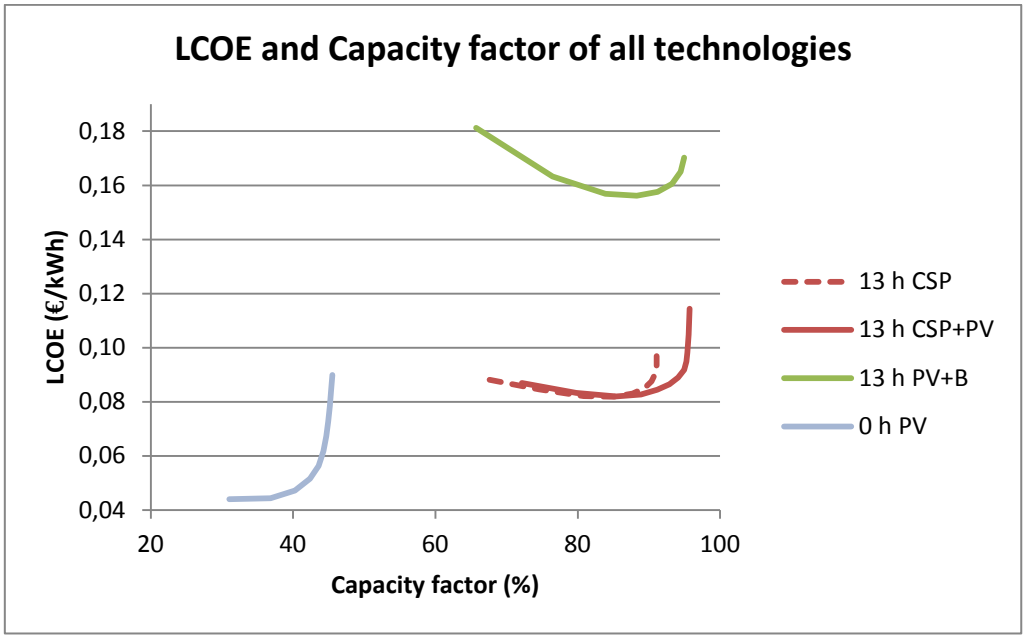

Figure 64: LCOE vs Capacity factor for CSP only, CSP+PV, PV with battery and PV only.

Fig. 64 shows all 4 different technologies and their LCOE and capacity factors for 13h electrical energy storage. The battery has 13h gross capacity. The TES has 13h net capacity and the PV-only option has no battery. It can be seen that when large capacity factors are not required (< 50%) PV remains as the cheapest solar energy alternative among all technologies. However, for larger capacity factors CSP plants are the most cost-efficient option. Even though CSP plants cost around 90% more than PV plants without batteries, they cost about half the price of PV systems with electrical storage. For even larger capacity factors the combination of CSP and PV is the best choice at the moment, being able to annually generate up to 4% more energy than CSP-only at a similar LCOE.
Such high capacity factors can only be achieved in regions where the annual DNI sum is as high as in Chile (>3400 kWh/m^{2}a). No other place on Earth has irradiances as high as Chile's desert. However, Australia has also a DNI of around 3000 kWh/m^{2}a. Therefore hybrid CSP/PV power plants might be also the most cost-efficient alternative for high capacity factor supply in Australia. In other regions near the equator, such as Central Africa, India or Central America the annual DNI sum is lower than the GHI, which is favorable for PV plants. In these cases the hybridization of CSP with PV could help lower the LCOE by more than 2% as in the case for Chile.

Coincidentally, the minima of both curves CSP and CSP+PV for the location in Chile lie at about the same LCOE for the same storage size, as shown in Fig.64. In a study from Pan and Dinter for a location in South Africa [55], the minimum LCOE value for CSP+PV is 0.015 $/kWh lower than the minimum LCOE of CSP-only, as shown in chapter 2.5.2. This confirms that a larger relative reduction of CSP costs by means of PV hybridization could be achieved in countries with lower DNI than Chile, since the LCOE for CSP in a country like Chile is already the lowest in the world.

Further investigation has to be made in other regions with DNI of 2000 – 2400 kWh/m^{2}a, such as Morocco or some parts of China. These countries are especially interesting because of their major policies fostering CSP power plants.

Future LCOE evaluation

A hybrid power plant proved to be the cheapest and most reliable source of power among all evaluated alternatives. An additional investigation is made on the feasibility of PV plants with batteries for the future. The projected battery performance indicators and costs for 2022 and 2032 summarized in chapter 5.1 are used for the calculations. The battery technical details are updated as well as the specific costs. The specific costs for PV plants and CSP are updated for 2025 and 2032 according to the cost reduction assumptions presented also in chapter 5.1. The O&M annual costs of all technologies are modified with the same rate as the specific investment costs reduction. The results are shown in Fig.65 and Table 17.

.

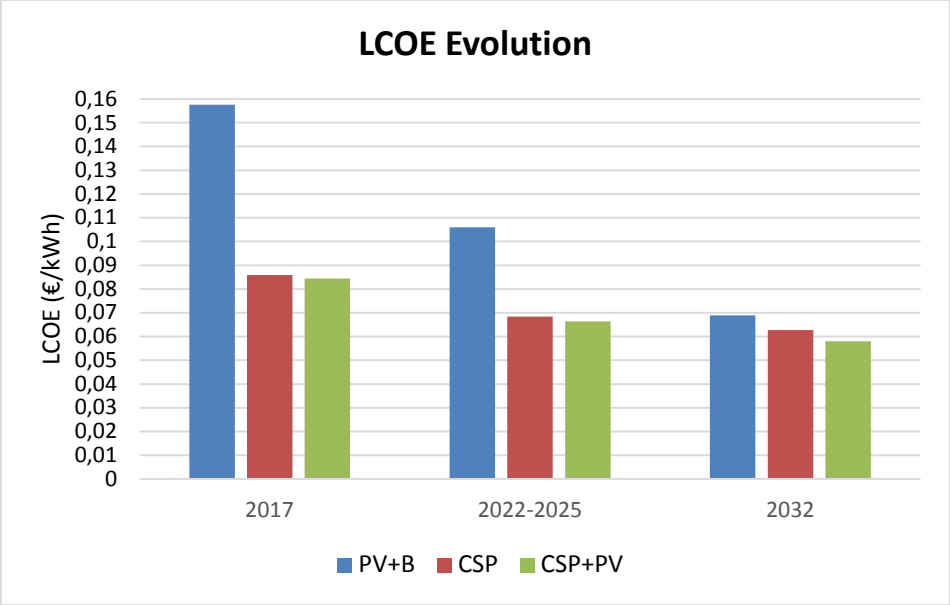

Figure 65: LCOE evolution for CSP, PV and CSP+PV with 90% capacity factor

Table 17: LCOE Evolution for all three plants with 90% capacity factor

Year	PV+B	CSP	CSP+PV
2017	0.1576	0.0859	0.0845
2022-2025	0.106	0.0684	0.0664
2032	0.0689	0.0627	0.0580

The LCOE of PV plants with batteries sinks by 40% from 2017 to 2022-2025. For the next 15 years CSP+PV and CSP are expected to be the most cost-efficient alternative, although PV with batteries become also extremely cheap as they cross the 0.10 €/kWh line by 2032. PV and battery costs have the steepest price drop from all alternatives. Therefore all three power plants could deliver energy at approximately the same price in 2032. The difference is about 0.01 €/kWh. These results show agreement with the previous Thermvolt study by DLR and partners [34], as described in Chapter 2.5.2. The location used was Morocco and Saudi Arabia. The combined CSP+PV plant from that study consisted of a 136 MWp PV plant with no battery (limited at 75 MW) and a 100 MWe CSP Tower

with SM = 2.5 and 17h TES. An additional PV plant with 291 MWp installed power, 750 MWh battery park and 150 MW gas turbine was evaluated. The results showed that the CSP+PV alternative was the most cost-efficient in most of the simulated cases. For a baseload scenario the LCOE of the CSP+PV plant was slightly cheaper than the CSP option and PV+B was the most expensive alternative. For a baseload scenario in 2030, the LCOE of all three plants were close to each other. Therefore it was not possible to define the optimal option. In some scenarios it was shown that a PV plant with battery even had slightly lower LCOE than CSP and CSP/PV combinations in 2030. This key finding matches with the results from this master thesis.

Additionally, it is investigated what the battery costs should be for the PV alternative in 2017 to have the same LCOE as CSP (0.0859 €/kWh). It is found that as of 2017 the specific lithium-ion battery costs should be 100 €/kWh in order for a PV plant to be competitive with CSP and TES. The only system currently close to that price is the Eos Aurora Zinc-air battery, being offered at 160 $/kWh (144 €/kWh). Eos battery systems have supposedly an efficiency of 75%, which is lower than in lithium-ion batteries. The Tesla Powerpack costs 445 $/kWh (400 €/kWh) at the moment. Therefore it can be concluded that until 2030 a hybrid CSP with TES and PV is the most cost-efficient alternative to supply near baseload operation, unless major technological breakthroughs bring battery costs further down.

6 Conclusions and Future Work

In the present work, a new battery model for the software *greenius* was further developed. The investigations on the existing 3- coefficient efficiency PV model showed that this is a simple yet very precise model to describe photovoltaic modules based only on few parameters from manufacturer's common datasheets. The comparison with other models such as the 5-parameter model used in other commercial tools showed a maximum relative error of 5.1% during peak power time. The drawbacks of such complex photovoltaic models are the longer simulation times and the difficulty for the end user to correctly assess the validity of all different parameters required, e.g. the module's temperature coefficients.

The battery model implemented in *greenius* is based on a charge balance model. This model proved to be suitable for our application, since stationary simulations are sufficient for techno-economic analyses. One of the advantages of this approach is that I-V curves from the PV module are not required. The results from the model showed discrepancies with SAM but the model in SAM could not be used for reference because of unrealistic voltage values as explained in chapter 4.5.2.

After implementing the new battery-feature for PV an exemplary techno-economic analysis of the Cerro Dominador hybrid power plant in Chile was performed leading to several general findings regarding hybrid PV/solar thermal plants. The cheapest overall option for Chile's northern region is a photovoltaic system without battery with LCOE = 0.0441 €/kWh. The drawback of this system is its low capacity factor of 31%. This system can only generate full load power for 2300 h/a. At the moment photovoltaic energy is overloading Chile's northern grid because there is more installed power than demand during peak times. This problematic occurs because there is a limited powerline infrastructure between Chile's northern and central grid. Therefore it is not possible to transmit this excess energy to Chile's central and southern regions. Therefore PV without storage is not the best solution.

All hybrid and standalone solutions with 90% capacity factor were compared, which seems to be a reasonable high capacity factor without incurring into too high LCOE. Upon comparison it was shown that the hybrid PV/CSP plant does indeed reduce the overall LCOE by almost 2% compared to the standalone CSP (0.0859 vs. 0.0845 €/kWh). The optimum hybrid configuration has 13h thermal storage and SM = 1.7, whereas the standalone CSP optimum design has 15h and SM = 2.8. The main advantage of hybrid CSP/PV plants is that combining both technologies is the only possible way to reach capacity factors > 95% at a cost lower than 0.10 €/kWh. Improvements in capacity factors up to 4% were achieved at the same LCOE with the hybrid solution.

The storage size needed for a PV plant to reach 90% capacity factor is 1.3 GWh nominal capacity, which exceeds the order of magnitude of the largest battery parks being built today as shown in chapter 2.4.2. The LCOE of a PV plant with li-ion battery park this large is 0.1748 €/kWh. However, in 2032 the LCOE are expected to drop to 0.0689 €/kWh and can be competitive with CSP and CSP/PV hybrid systems. The difference in LCOE among the three alternatives is only 0.01 €/kWh. Until then it is expected that CSP remains as a more cost-efficient alternative than PV with electric batteries.

There are many improvements that can be carried out in *greenius* in future works. An additional inter-row PV shading setting can be implemented to account for additional losses. This way the accuracy of the PV model can be further improved. In this work the procedure to simulate the hybrid configurations was done manually in two steps but it can be optimized to reduce calculation times and effort. A common distributor model for both thermal and electrical energy can be implemented in the software to automatically create the load curves for both PV and CSP plants in a hybrid configuration for future projects.
The cost evolution for CSP and PV was made according to the information from a study from IRENA, where the cost evolution between 2016 and 2025 was presented. The assumptions in this work for the further cost evolution until 2032 were very conservative, so they must be carefully examined in future works.

Since the hybrid power plant is the most cost-efficient alternative for desert regions with high annual irradiances, such as Chile or Australia, more analyses are desirable for other regions with lower DNI, such as China or Morocco. In such countries there are many plans to foster the CSP technology. Therefore the profitability of CSP/PV plants in those countries can be really important to develop new projects.

Bibliography

[1] PBL Netherlands Environmental Assessment Agency and European Commission, Joint Research Centre (EC-JRC), „Trends in global CO2 emissions: 2016 Report,“ The Hague, Netherlands, 2016.

[2] REN21, „Renewables Global Futures Report - Great debates towards 100% renewable energy,“ 2017.

[3] EASE, EERA, „European Energy Storage Technology Development Roadmap Towards 2030,“ 2013.

[4] U.S. Energy Information Administration, International Energy Outlook, 2016.

[5] World Energy Council, World Energy Resources - Solar 2016, 2016.

[6] EU - European Commission, "Concentrated Solar Power - "What is Concentrated Solar Power (CSP)?"," 2016. [Online]. Available: http://s3platform.jrc.ec.europa.eu/concentrated-solar-power. [Accessed 12 07 2017].

[7] V. Quaschning, Regenerative Energiesysteme, 7. Hrsg., Berlin, Germany.

[8] V. Siva Reddy, S. Kaushik, K. Ranjan and S. Tyagi, "State-of-the-art of solar thermal power plants - A review," *Renewable and Sustainable Energy Reviews 27*, pp. 258-273, 2013.

[9] R. Pitz-Paal, S. Giuliano and M. Wittmann, "Concepts for Cost Reduction in CSP Power Plants," 2015.

[10] C. Ho, "Advances in central receivers for concentrating solar applications," *Sol. Energy*, 2017.

[11] IRENA, „The Power to Change: solar and wind cost reduction potential to 2025,“ 2016.

[12] IEA, „Energy Technology Perspectives: Scenarios & Strategies to 2050,“ 2010. [Online].

[13] IEA, „Solar Photovoltaic Roadmap,“ 2010.

[14] J. Arp and F. Schmidt, "Leistungs- und Ertragsmessung von Solarmodulen und Modultests," Bonn, Germany, December 2009.

[15] SMA Solar Academy, "Planning and Design," [Online]. Available: https://www.sma.de/fileadmin/Partner/Solaracademy/Downloads/EN/Planning%20and%20Design%20for%20small%20and%20medium%20PV-Plants_EN-123610_web.pdf.

[16] International Finance Corporation (IFC) - World Bank Group, „Utility-Scale Solar Photovoltaic Power Plants - A project developer's guide,“ Washington, USA, 2015.

[17] Solar Power World, "Solar inverters and clipping: What DC/AC inverted load ratio is ideal?," 2016. [Online]. Available: https://www.solarpowerworldonline.com/2016/07/solar-inverters-clipping-dcac-inverter-load-ratio-ideal/. [Accessed 28 08 2017].

[18] Alternative Energy Tutorials, "Grid Connected PV System," [Online]. Available: http://www.alternative-energy-tutorials.com/solar-power/grid-connected-pv-system.html. [Accessed 17 07 2017].

[19] D. U. Sauer, „Untersuchungen zum Einsatz und Entwicklung von Simulationsmodellen für die Auslegung von Photovoltaik-Systemen,“ Freiburg, 1994.

[20] Northern Arizona Wind & Sun, "Solar-Electric - All About Maximum Power Point Tracking (MPPT) Solar Charge Controllers," [Online]. Available: https://www.solar-electric.com/learning-center/batteries-and-

charging/mppt-solar-charge-controllers.html. [Accessed 29 05 2017].

[21] D. Parra, G. Walker and M. Gillott, "Modeling of PV generation, battery and hydrogen storage to investigate the benefits of energy storage for single dwelling," *Sustainable Cities and Society*, 2013.

[22] J. Weniger, T. Tjaden and V. Quaschning, "Sizing of residential PV battery systems," *8th international renewable energy storage conference and exhibition*, 2013.

[23] N. DiOrio, A. Dobos, S. Janzou, A. Nelson and B. Lundstrom, "Technoeconomic Modeling of Battery Energy Storage in SAM," 2015.

[24] J. Weniger, T. Tjaden, J. Bergner and V. Quaschning, "Emerging Performance Issues of Photovoltaic Battery Systems," *32nd European Photovoltaic Solar Energy Conference and Exhibition 2016*, 2016.

[25] EnergieAgentur.NRW, „Photovoltaik und Batteriespeicher: Technologie, Integration, Wirtschaftlichkeit," 2015.

[26] pv-magazine, ""Mexico signs lowest-price solar contracts to date"," 2017. [Online]. Available: https://www.pv-magazine.com/2017/02/06/mexico-signs-lowest-price-solar-contracts-in-the-world-to-date/. [Accessed 12 07 2017].

[27] IEC Market Strategy Board (International Electrotechnical Commision), „White Paper: Electric Energy Storage," 2011.

[28] A. Gil, P. Arce, I. Martorell, M. Medrano and L. F. Cabeza, "State of the art of high temperature storage in thermosolar plants," 2010.

[29] D. Linden und T. B. Reddy, Handbook of Batteries, 3rd Hrsg., McGraw-Hill, 2001.

[30] N. DiOrio, A. Dobos and S. Janzou, "Economic Analysis Case Studies of Battery Energy Storage with SAM," November 2015. [Online]. Available: http://www.nrel.gov/docs/fy16osti/64987.pdf.

[31] World Energy Council, „World Energy Resources - E-Storage 2016," 2016. [Online]. Available: https://www.worldenergy.org/wp-content/uploads/2017/03/WEResources_E-storage_2016.pdf.

[32] IRENA - International Renewable Energy Agency, Battery Storage for Renewables: Market status and technology outlook, 2015.

[33] The Boston Consulting Group, Batteries for Electric Cars - Challenges, Opportunities, and the Outlook to 2020, 2010.

[34] DLR, Fichtner, M+W, Lappeenranta University of Technology, „THERMVOLT - Systemvergleich von solarthermischen und photovoltaischen Kraftwerken für die Versorgungssicherheit - Schlussbericht," Germany, December 2016.

[35] AGORA Energiewende, „Stromspeicher in der Energiewende," 2014.

[36] Batteries International, ""German Utility buys UK lead acid/lithium firm for solar and storage"," 2017. [Online]. Available: http://www.batteriesinternational.com/german-utility-buys-uk-lead-acidlithium-firm-for-solar-and-storage/. [Accessed 14 07 2017].

[37] CleanTechnica, "Tesla Powerwall & Powerpack Per-kWh Lifetime Prices vs Acquion Energy, Eos Energy, & Imergy," 2015. [Online]. Available: https://cleantechnica.com/2015/05/09/tesla-powerwall-powerblocks-per-kwh-lifetime-prices-vs-aquion-energy-eos-energy-imergy/. [Accessed 14 07 2017].

[38] TeslaMag.de, ""Tesla reduziert Preis des Powerpack um 5%, Wechselrichter sogar um 19%"," 2016. [Online]. Available: http://teslamag.de/news/tesla-reduziert-preis-des-powerpack-um-5-wechselrichter-sogar-um-19-9554. [Accessed 14 07 2017].

[39] North American Clean Energy, ""Eos Energy Storage Now Taking Orders at $95/kWh for the Eos Aurora DC Battery System"," 04 2017. [Online]. Available: http://www.nacleanenergy.com/articles/26342/eos-energy-storage-now-taking-orders-at-95-kwh-for-the-eos-aurora-dc-battery-system. [Accessed 14 07 2017].

[40] Tesla, "Powerpack Technical Details," [Online]. Available: https://www.tesla.com/de_DE/powerpack.

[41] Siemens, ""Siemens und AES gründen Fluence, ein neues weltweit operierendes Unternehmen für Energiespeichertechnologien"," [Online]. Available: https://www.siemens.com/press/de/feature/2017/corporate/2017-07-fluence.php?content[]=Corp&content[]=EM.

[42] SolarReserve, "Baseload Solar-Power - Improving Mining Economics with Predictable Energy Costs (Mining Brochure)," 2014. [Online]. Available: http://www.solarreserve.com/en/solutions/mining-industry.

[43] CSP Plaza, ""Chile - The leading market of PV/CSP hybrid plants"," 14 08 2015. [Online]. Available: http://en.cspplaza.com/chile-the-leading-market-of-pvcsp-hybrid-plants.html. [Accessed 26 06 2017].

[44] Energia Limpia XXI, ""En Chile dos plantas de energía solar más grandes del mundo"," 24 02 2017. [Online]. Available: https://energialimpiaparatodos.com/2017/02/24/fmx-enty/. [Accessed 2017 06 26].

[45] SolarReserve, „SolarReserve receives environmental approval for 260 megawatt baseload solar plant in Chile,“ Santiago, Chile, 2015.

[46] CleanTechnica, ""Solar Reserve bids 24-hour solar at 6.3 cents in Chile"," 13 03 2017. [Online]. Available: https://cleantechnica.com/2017/03/13/solarreserve-bids-24-hour-solar-6-3-cents-chile/. [Accessed 2017 06 26].

[47] NewEnergyUpdate:CSP, ""SolarReserve eyes Chile CSP wins as surplus PV disrupts markets"," 06 2016. [Online]. Available: http://analysis.newenergyupdate.com/csp-today/markets/solarreserve-eyes-chile-csp-wins-surplus-pv-disrupts-markets. [Accessed 26 06 2017].

[48] SolarReserve, "CSP Project Overview," [Online]. Available: http://www.solarreserve.com/en/global-projects/csp/redstone. [Accessed 26 06 2017].

[49] HeliosCSP, "How to achieve US$63MWh in a CSP tower project with storage," 25 09 2016. [Online]. Available: http://helioscsp.com/how-to-achieve-us63mwh-in-a-concentrated-solar-power-tower-project-with-storage/. [Accessed 26 06 2017].

[50] ABENGOA Solar Chile, "Proyecto Planta Solar Cerro Dominador Atacama 1 - Presentación cuenta regresiva hacia la COP21 Desafíos actuales," 2015. [Online]. Available: http://conferencias.cepal.org/alto_nivel2015/Ppt/04%20Roberto%20Marcos.pdf. [Accessed 27 06 2017].

[51] Cerro Dominador Concentrated Solar Power, "Complejo Solar Cerro Dominador Planta termosolar," [Online]. Available: https://cerrodominador.com/wp-content/uploads/2016/12/termosolar2.pdf. [Accessed 27 06 2017].

[52] Cerro Dominador, ""Proyecto solar Cerro Dominador conecta a la red eléctrica sus primeros 62 MW"," [Online]. Available: https://cerrodominador.com/noticias/proyecto-solar-cerro-dominador-conecta-a-la-red-electrica-sus-primeros-62-mw/.

[53] Electricidad - la revista energética de Chile, ""Planta termosolar de proyecto Cerro Dominador entraría en

operaciones en 2019"," 14 03 2017. [Online]. Available: http://www.revistaei.cl/2017/03/14/planta-termosolar-de-proyecto-cerro-dominador-entraria-en-operaciones-en-2019/#. [Accessed 26 06 2017].

[54] K. Larchet, „Solar PV-CSP Hybridisation for Baseload Generation: A Techno-economic Analysis for the Chilean Market - M.Sc. Thesis,“ Stockholm, Sweden, 2015.

[55] C. A. Pan and F. Dinter, "Combination of PV and central receiver CSP plants for base load power generation in South Africa," South Africa, 2017.

[56] F. Dominio, „Techno-Economic Analysis of Hybrid PV-CSP Power Plants: Advantages and disadvantages of intermediate and peak load operation - M.Sc. Thesis,“ Stockholm, Sweden.

[57] ACWA Power Africa Holdings - Golder Associates, „Draft Scoping Report: Proposed Solar Power Development on the Remaining Extent of Farm Bokpport 390, Northern Cape,“ South Africa, 2015.

[58] ARCUS, "Bokpport II Solar Farm," [Online]. Available: http://arcusconsulting.co.za/projects/bokpoort-ii-solar-farm/. [Accessed 26 06 2017].

[59] Brightsource, ""Brightsource and Alstom win tender for 121 Megawatt solar thermal power plant in Israel"," 19 11 2012. [Online]. Available: http://www.brightsourceenergy.com/brightsource-and-alstom-win-tender-for-121-megawatt-solar-thermal-power-plant-in-israel#.WVDzWU0Uncs. [Accessed 26 06 2017].

[60] BN americas, ""Argentina planea proyecto solar híbrido de US$740mn"," 05 02 2016. [Online]. Available: https://www.bnamericas.com/es/noticias/energiaelectrica/argentina-planea-proyecto-solar-hibrido-de-us740mn. [Accessed 26 06 2017].

[61] EnerNews, ""GigaWatt Global acordó la Termosolar de Mendoza"," 05 02 2016. [Online]. Available: http://www.enernews.com/nota/293633/gigawatt-global-acordo-la-termosolar-de-mendoza. [Accessed 26 06 2017].

[62] European Investment Bank, "Morocco-Rabat: EIB - Design, construction, operation, maintenance and financing of a 300-380 MW solar power installation programme 2016/S 141-254260," 18 06 2016. [Online]. Available: http://ted.europa.eu/udl?uri=TED:NOTICE:254260-2016:TEXT:EN:HTML. [Accessed 27 06 2017].

[63] MASEN, „Call for expression of interest for first phase of NOOR Midelt complex development project(s), in the framework of the moroccan solar plan, NOOR,“ Morocco, 2015.

[64] HeliosCSP, ""Morocco to launch Midelt Concentrated Solar Power tender by start of 2017"," 04 12 2016. [Online]. Available: http://helioscsp.com/morocco-to-launch-midelt-concentrated-solar-power-tender-by-start-of-2017/. [Accessed 27 06 2017].

[65] MASEN, „Call for expression of interest - NOOR Midelt - NOOR Midelt solar complex: launching of phase I,“ Rabat, Morocco, 2015.

[66] SolarReserve & ACWA Power, „South Africa Department of Energy awards 100 MW solar thermal project to consortium led by SolarReserve and ACWA Power,“ Johannesburg, South Africa, 2015.

[67] Portal Minero, "Complejo solar Cerro Dominador (ex Atacama 1)," 21 03 2017. [Online]. Available: http://www.portalminero.com/display/serv/Planta+Solar+Cerro+Dominador. [Accessed 27 06 2017].

[68] SolarReserve, "PV Projects Overview," [Online]. Available: http://www.solarreserve.com/en/global-projects/pv. [Accessed 27 06 2017].

[69] CSPWorld, "Planta Solar Cerro Dominador (Atacama 1)," [Online]. Available: http://cspworld.org/cspworldmap/planta-solar-cerro-dominador. [Accessed 27 06 2017].

[70] NewEnergyUpdate:CSP, ""Chile: a sun mine about to be exploited"," 10 10 2014. [Online]. Available: http://analysis.newenergyupdate.com/csp-today/markets/chile-sun-mine-about-be-exploited. [Accessed 27 06 2017].

[71] NREL, "Concentrating Solar Power Projects," 2015. [Online]. Available: http://www.nrel.gov/csp/solarpaces/. [Accessed 27 06 2017].

[72] Servicio de Evaluación Ambiental, II Región de Antofagasta, "Declaración de Impacto Ambiental "PLANTA SOLAR CERRO DOMINADOR"," 22 04 2014. [Online]. Available: http://seia.sea.gob.cl/expediente/ficha/fichaPrincipal.php?modo=ficha&id_expediente=2128879352. [Accessed 27 06 2017].

[73] Cerro Dominador Concentrated Solar Power, "Complejo Solar Cerro Dominador Planta Fotovoltaica," [Online]. Available: https://cerrodominador.com/wp-content/uploads/2016/12/tabloide-hoja-2.pdf.

[74] El Mostrador - BLOOMBERG, ""Elefante blanco solar de Chile podría emerger del desierto"," 27 01 2017. [Online]. Available: http://www.elmostrador.cl/mercados/2017/01/27/elefante-blanco-solar-de-chile-podria-emerger-del-desierto/. [Accessed 27 06 2017].

[75] renewable-technology-com, "Jasper Solar Power Plant, Northern Cape, Kimberley, South Africa," [Online]. Available: http://www.renewable-technology.com/projects/jasper-solar-power-plant-northern-cape-kimberley/. [Accessed 27 06 2017].

[76] GRS, "Engineering, Procurement and Construction. Photovoltaic power projects in South Africa," [Online]. Available: http://grs.energy/projects/south-africa/epc-services/. [Accessed 27 06 2017].

[77] U.S. DOE, "Global Energy Storage Database," [Online]. Available: http://www.energystorageexchange.org/projects/global_search?q=atacama. [Accessed 27 06 2017].

[78] L. Castillo, "Techno-economic Analysis of Combined Hybrid Concentrating Solar and Photovoltaic Power Plants: a case study for optimizing solar energy integration into the South African electricity grid - M.Sc. Thesis," Stockholm, Sweden, 2014.

[79] O. A. Zaalouk, „Identifying opportunities for developing CSP and PV-CSP hybrid projects under current tender conditions and market perspectives in MENA - benchmarking with PV-CCGT - MSc Thesis,“ Universitat Politecnica de Catalunya, Spain, 2016.

[80] A. Green, C. Diep, R. Dunn and J. Dent, "High Capacity factor CSP-PV hybrid systems - SolarPACES 2014," *Energy Procedia 69*, pp. 2049-2059, 2015.

[81] A. R. Starke, J. M. Cardemil, R. A. Escobar and S. Colle, "Assessing the performance of hybrid CSP + PV plants in northern Chile," *Solar Energy Vol. 138*, pp. 88-97, 2016.

[82] C. Parrado et al, „2050 LCOE (Levelized Cost of Energy) projection for a hybrid PV (photovoltaic)-CSP (concentrated solar power) plant in the Atacama Desert, Chile,“ *Energy Vol.94*, pp. 422-430, 2016.

[83] DLR, *Greenius Manual - Version: Release 4.3.2.2*, Köln, Germany, 2016.

[84] J. Randall and J. Jacot, "Is AM1.5 applicable in practice? Modelling eight photovoltaic materials with respect to

light intensity and two spectra," *Renewable Energy 28*, 2003.

[85] S. Williams, T. Betts and T. Helf, "Modelling Long-Term Module Performance Based on Realistic Reporting Conditions with Consideration to Spectral Effects," *3rd World Conference on Photovoltaic Energy Conversion*, 2009.

[86] VelaSolaris, *Polysun Simulation Software User Manual*, 2017.

[87] H. G. Beyer et al, "Identification of a general model for the MPP performance of PV-modules for the application in a procedure for the performance check of grid connected systems," 2000.

[88] N. J. Blair, A. P. Dobos and P. Gilman, *Comparison of Photovoltaic Models in the System Advisor Model*, NREL, Ed., 2013.

[89] W. De Soto et al, "Improvement and validation of a model for photovoltaic array performance," *Solar Energy 80*, 2005.

[90] M. Tao, Y. Hongxing and L. Lin, "Development of a model to simulate the performance characteristics of crystalline silicon photovoltaic modules/strings/arrays," *Solar Energy 100*, 2013.

[91] A. Mermoud and T. Lejeune, "Performance Assessment of a Simulation Model for PV Modules of any available technology".

[92] S. Pukhrem, „A photovoltaic panel model in matlab/simulink,“ Augut 2013.

[93] A. M. Eltamaly, "Performance of smart maximum power point tracker under partial shading conditions of photovoltaic systems," 2015.

[94] Seaward, "Curve Tracing," [Online]. Available: http://www.seawardsolar.com/userfiles/curve-tracing.php. [Accessed 18 10 2017].

[95] PVSyst, "PVSyst Help Contents - PVsyst 6.62," 18 05 2017. [Online]. Available: http://files.pvsyst.com/help/.

[96] N. J. Blair, A. P. Dobos und P. Gilman, *Comparison of Photovoltaic Models in the System Advisor Model*, NREL, Hrsg., 2013.

[97] A. P. Dobos, *PVWatts Version 5 Manual*, 2014.

[98] D. King et al, "Photovoltaic Array Performance Model," Albuquerque, New Mexico, 2004.

[99] S. Vergura, „A Complete and Simplified Datasheet-Based Model of PV Cells in Variable Environmental Conditions for Circuit Simulation,“ 2016.

[100] D. L. King, J. A. Kratochvil and W. E. Boyson, "Temperature Coefficients for PV Modules and Arrays: Measurement Methods, Difficulties and Results," 1997.

[101] Sun Xtender - Concorde Battery Corp., "Battery Sizing Tips for Stand Alone PV Systems," [Online]. Available: http://ecee.colorado.edu/ecen4517/components/sunextenderbatterysizingtips.pdf. [Accessed 30 05 2017].

[102] IEA International Energy Agency, „Lead-Acid Battery Guide for Stand-Alone Photovoltaic Systems,“ 1999.

[103] SEIAPI Sustainable Energy, IRENA, NORTHREP, "SEIAPI PPA Install Off Grid Connect Guidelines," [Online]. Available: https://www.irena.org/DocumentDownloads/events/2013/March/Palau/9_SEIAPI_PPA_OffGrid_Install_Guidelines.pdf. [Accessed 30 05 2017].

[104] S. McCluer, "Battery Technology for Data Centers and Networks Rooms: Ventilation of Lead-Acid Batteries.," Schneider Electric.

[105] ITACA, "A Guide to Lead-Acid Batteries," [Online]. Available: http://www.itacanet.org/eng/elec/battery/battery.pdf. [Accessed 05 07 2017].

[106] G. Merei, J. Moshövel, D. Magnor and D. U. Sauer, "Optimisation of self-consumption and techno-economic analysis of PV-battery systems in commercial applications," *Applied Energy*, 2016.

[107] MIT Electric Vehicle Team, "A Guide to Understanding Battery Specifications," 2008. [Online]. Available: http://web.mit.edu/evt/summary_battery_specifications.pdf. [Accessed 28 08 2017].

[108] BIXmart, "Nominal Voltage of Lithium Ion Batteries," [Online]. Available: http://www.bixmart.com/nominal-voltage-of-lithium-ion-batteries_ep_54-1.html. [Accessed 05 07 2017].

[109] EASE, EERA, „European Energy Storage Technology Development Roadmap Towards 2030 - Technical Annex," 2013.

[110] H. He, R. Xiong, H. Guo and S. Li, "Comparison study on the battery models used for the energy management of batteries in electric vehicles," 2012.

[111] H. He, R. Xiong and J. Fan, "Evaluation of a Lithium-ion battery equivalent circuit models for state of charge estimation by an experimental approach," 2011.

[112] S. Kai and S. Qifang, "Overview of the Types of Battery Models," *Proceedings of the 30th Chinese Control Conference*, 2011.

[113] A. Kumar, „Battery Modeling and its Dynamics for the application in Renewable Energy Systems - Thesis," Rourkela, Odisha, India, 2014.

[114] N. Parthasarathy, "Adaptive Battery Monitoring Using Parameter Estimation - Thesis," 2009.

[115] J. B. Copetti, E. L. Pigueiras and F. Chenlo, "A general battery model PV system simulation," *Progress in Photovoltaics Research and Applications*, 1993.

[116] R. Fu, F. D. Chung, R. Margolis, M. Woodhouse and K. Ardani, "U.S. Solar Photovoltaic System Cost Benchmark: Q1 2017 - NREL," 2017.

[117] U. Sauer, „Marktanreizprogramm für dezentrale Speicher insbesondere für PV-Strom," Aachen, 2013.

[118] S. Dieckmann, J. Dersch, S. Giuliano, M. Puppe, E. Lüpfert, K. Hennecke, R. Pitz-Paal, M. Taylor and P. Ralon, "LCOE Reduction Potential of Parabolic Trough and Solar Tower CSP Technology until 2025," 2016.

[119] S. Dieckmann and J. Dersch, "Simulation of Hybrid Solar Power Plants," in *SolarPaces*, 2016.

[120] IRENA, "Renewable Energy Technologies: Cost Analysis Series - Concentrating Solar Power," 2012.

[121] D. Vallentin und P. Viebahn, „Ökonomische Chancen der deutschen Industrie resultierend aus einer weltweiten Verbreitung von CSP (Concentrated Solar Power)- Technologien," 2011.

[122] ABENGOA SOLAR, "Declaración de Impacto Ambiental - Proyecto "Planta PV Cerro Dominador" (EIA PV Cerro Dominador Plant)," 2015. [Online]. Available: http://seia.sea.gob.cl/expediente/ficha/fichaPrincipal.php?modo=ficha&id_expediente=2130634551.

Annex

A1 General information and cost overview

Table A1.1: Project general specifications

Description	Value	Unit
Location	-26.33°N -69.98°E	
DNI	3477	kWh/m^2
GHI	2449	kWh/m^2
Project discount rate	6.00	%
Land costs	1	€/m^2

Table A1.3: CSP Economic data

Financial specifications	Value	Unit
HELIOSTAT FIELD		
Specific investment costs	150	€/m^2
Specific O&M Costs	3	€/m^2·a
Replacement costs	0.5	%/a
Insurance costs	1	%/a
RECEIVER[7]		
Specific investment costs	131	€/kW
Specific O&M Costs	2.50	€/kW ·a
Replacement costs	1	%/a
Insurance costs	1	%/a
TOWER		
Specific investment costs	94100	€/m
Specific O&M Costs	900	€/m^2·a
Replacement costs	1	%/a
Insurance costs	1	%/a
POWERBLOCK		
Specific investment costs	1328	€/kW
Specific O&M Costs	2.50	€/kW ·a
Replacement costs	0.20	%/a
Insurance costs	1	%/a
THERMAL STORAGE		
Specific investment costs	27	€/kWh
Specific O&M Costs	0.20	€/kWh ·a
Replacement costs	0.20	%/a
Insurance costs	1	%/a

Table A1.2: PV Economic data

Financial specifications	Value	Unit
PV SYSTEM		
Specific investment costs	1041.8	€/kWp
Specific O&M Costs	10	€/kWp·a
Replacement costs	0.2	%/a
Insurance costs	1	%/a
BATTERY		
Energy capacity costs	391	€/kWh
Power costs	161	€/kW
Replacement costs after 14 a	157	€/kWh

[7] Receiver costs must be calculated with the field intercept power

A2 Technical details overview of single operation power plants

Table A2.1: Technical details of optimal single PV configuration

Technical specifications	Value or Definition	Unit
PV SYSTEM		
Total nom. DC power	391,500	kWp
Total nom. AC power	379,755	kVA
Photovoltaic module	Canadian Solar Quartech CS6X-300W	
Inverter	Dasstech DSP-M331000K	
No. modules/string	15	
No. strings/inverter	250	
No. of parallel inverters	348	
Availability	99	%
Cleanliness	95	%
Shadowing factor	90	%
BATTERY		
Gross capacity	92	MWh
Efficiency	90	%
Self-discharge	0.01	%/day
DOD	93	%
Capacity degradation limit	80	%
Lifetime	30	a

Table A2.2: Technical details of optimal single CSP configuration

Technical specifications	Value or Definition	Unit
HELIOSTAT FIELD		
Intercept power	743	MW
Clean mirror reflectivity	94	%
Average cleanliness	95	%
Field availability	99	%
Total reflective area	1400336	m^2
Number of heliostats	11544	
RECEIVER		
Fluid type	Solarsalt	
Design inlet temperature	292	°C
Design outlet temperature	565	°C
THERMAL STORAGE		
Net Capacity	3450	MWh
Rel. losses in 24h	1	%
Minimal Content	200	MWh

A3 Technical details overview of hybrid operation power plant

Table A3.1: Technical details of optimal hybrid configuration (PV)

Technical specifications	Value or Definition	Unit
Total nom. DC power	103500	kWp
Total nom. AC power	100395	kVA
Photovoltaic module	Canadian Solar Quartech CS6X-300W	
Inverter	Dasstech DSP-M331000K	
No. modules/string	15	
No. strings/inverter	250	
No. of parallel inverters		
Availability	99	%
Cleanliness	95	%
Shadowing factor	90	%

Table A3.2: Technical details of optimal hybrid configuration (CSP)

Technical specifications	Value or Definition	Unit
HELIOSTAT FIELD		
Tower field intercept power	449	MW
Clean mirror reflectivity	94	%
Average cleanliness	95	%
Field availability	99	%
Total reflective area	800124	m^2
Number of heliostats	6596	
RECEIVER		
Fluid type	Solarsalt	
Design inlet temperature	292	°C
Design outlet temperature	565	°C
THERMAL STORAGE		
Net Capacity	3450	MWh
Rel. losses in 24h	1	%
Minimal Content	200	MWh

A4 Battery technical and financial parameter details (From Chapter 5.1)

Table A4.1: Technical details of lead-acid battery

Source	Reference Year	Lifetime (years)	Efficiency (%)	Power Price (€/kW)	Energy Price (€/kWh)	O+M Costs (%)	Allowed DOD (%)	Self-discharge (%/month)
EASE, EERA [109]	2013		78					
Thermvolt [34]	2015							
Thermvolt [34]	2020							
Thermvolt [34]	2030							
AGORA [35]	2014	8	80	160	200			
Handbook of Batteries McGraw [29]	2001							5
IRENA [32]	2015	17					50	
Sauer [117]	2013	10	73	175	175		70	4
Sauer [117]	2023	14	76	125	100		80	3

Table A4.2: Technical details of lithium-ion battery

Source	Reference Year	Lifetime (years)	Efficiency (%)	Power Price (€/kW)	Energy Price (€/kWh)	O+M Costs (%)	Allowed DOD (%)	Self-discharge (%/month)
EASE, EERA [109]	2013		93					
Thermvolt [34]	2015		91	200	400	0.025	85	
Thermvolt [34]	2020		92	147	294	0.025	95	
Thermvolt [34]	2030		93	80	159	0.025	97	
AGORA [35]	2014	12	90	160	575			
Handbook of Batteries McGraw [29]	2001							4
IRENA [32]	2015						90	
Sauer [117]	2013	13	83	175	550		100	4
Sauer [117]	2023	18	88	125	275		100	1